Supervised data-driven approach

to early kick detection during drilling operation

by

© Somadina Innocent Muojeke

A Thesis submitted to the

School of Graduate Studies

in partial fulfillment of the requirements for the degree of

Master of Engineering

Faculty of Engineering and Applied Science

Memorial University of Newfoundland

October – 2020

St. John's, Newfoundland and Labrador, Canada.

1 Abstract

The margin between pore pressure and fracture gradient in new offshore discoveries continues to get narrower. This poses greater risks and higher cost of ensuring safety of lives, facilities, and the environment. The 2010 Macondo blowout has fueled increased interests in monitoring downhole parameter for early kick detection. Early detection of kick is important part of the process safety. It provides opportunity to activate safety measures. However, after an extensive literature search, certain gaps were identified in early kick detection research. This ranged from limited availability of downhole drilling data from oil fields with downhole pressure and flow measurements for research purposes to limited modelling efforts that applies machine learning to downhole measurements in the area of early kick detection. Leveraging machine learning is crucial because of the tremendous advancements in artificial intelligence and information technology. This research provides a simple design approach to build machine learning kick detection models. In the absence of field data, we collect data from existing and new experiments that records downhole measurements. A simple model is rewarding when data processing is done downhole. The hardware used is typically battery powered. Simpler and fewer software operations will lead to less power consumption, smaller memory and simpler cooling requirements. This will lead to an increase battery run time, miniaturized designs/reduced bulk size, reduced maintenance frequency for such hardware, improved response time and lower costs.

In this thesis, we investigate the simplest supervised neural network-based machine learning kick detection system to ensure high reliability using experimental data. Building upon previous kick experiments conducted using a Small Drilling Simulator (SDS), we present a detailed design of a new kick experiment setup that uses a Large Drilling Simulator (LDS) and synthetic rock

samples. We also provide a detailed design of synthetic rock sample with geometrical capability to trap high-pressure formation fluid within. The experiment setup produces new set of data from downhole parameter monitoring that will be used in testing the machine learning model. Parameters such as mud flow-out rate, conductivity, density, and downhole pressure from two previous drilling experiment that monitored downhole parameters are combined to build a data-driven model for early kick detection. This model combines an Artificial Neural Network (ANN) with a binary classifier at its output. Several input combinations are trained and tested. The model can be scaled to capture other types of drilling problems such as lost circulation and also applied in the LDS system. The model was tested and evaluated with data from the SDS system, SDS system with faulty conductivity data and different experimental drilling system. Abnormal pressure and flow regimes in the wellbore provide early warnings and are shown to be more significant parameters than others; however, solely relying on them can increase susceptibility to false alarm.

2 Acknowledgements

My profound gratitude goes to God Almighty for the gift of life, good health and connecting me to be refined by renowned supervisors. I would like to express my sincere gratitude to my supervisors, Dr. Ramachandran Venkatesan and Dr. Faisal Khan for their continuous support, insightful comments, and for sharpening my research skills from various perspectives.

My sincere appreciation goes to Dr. Stephen Butt, who provided me the opportunity to join his team with access to the Drilling Technology Laboratory and research facilities. I would like to thank team member Nhat Minh for his excellent team play, Augustine Osarogiagbon, DTL team members Mohammed Said, Abdelsalam Abugharara, Jeronimo De Moura, Idris Sule, Olalere Oloruntobi and Justin Royce for assistance during the design, development of experimental setup and conducting the experiments. I would also like to thank Technical Services team Dennis Cramm, David Snook, Ken, Aaron and Shawn Organ of the Concrete laboratory.

I would like to thank my family: my parents, siblings, godparents, and friends for supporting me throughout my research and my life in general. Special appreciation to Archbishop Martin Currie, Fr. Joe Mroz, SJ, Presentation Sisters and the Sisters of Mercy for immense spiritual support. I also appreciate the Public Service Alliance of Canada for rich extracurricular learning and volunteering experience which included an oversea trip as a delegate on a Social Justice mission to Guatemala and participation in conferences and convention.

I thankfully acknowledge the financial support provided by the Natural Sciences and Engineering Research Council of Canada (NSERC) and the Canada Research Chair (Tier I) Program in Offshore Safety and Risk Engineering.

3 Table of Contents

4 List of Figures

5 List of Tables

6 List of Abbreviations

1. ANFIS – Adaptive Neuro Fuzzy Inference System
2. ANN – Artificial Neural Network
3. ASIC – Application-Specific Integrated Circuit
4. CFD – Computational Fluid Dynamics
5. DAS – Data Acquisition System
6. DBN – Dynamic Bayesian Network
7. DMA – Divergence of Moving Average
8. DMSA – Divergence of Moving Slope Average
9. DPG – Drilling Parameter Group
10. FPG – Flow Parameter Group
11. FPGA – Field Programmable Gate Array
12. FNR – False Negative Rate
13. FPR – False Positive Rate
14. GRU – Gated Recurrent Unit
15. KIS – Kick Injection System
16. KRI – Kick Risk Index
17. LDS – Large Drilling Simulator
18. LSTM – Long Short-Term Memory Network
19. LWD – Logging While Drilling
20. MEMS – Micro-Electro-Mechanical Systems
21. MLP – Multi Layer Perceptron
22. MWD – Measurement While Drilling

23. NPV – Negative Predictive Value

24. PPV – Positive Predictive Value

25. RNN – Recurrent Neural Network

26. ROP – Rate of Penetration

27. RPM – Revolutions per minute

28. SoC – System-on-Chip

29. SDS – Small Drilling Simulator

30. SMOTE - Synthetic Minority Over-sampling Technique

31. TOB – Torque on Bit

32. TNR – True Negative Rate

33. TPR - True Positive Rate

34. WOB – Weight on Bit

1 Introduction

1.1 Background of study

A kick is an undesirable event during drilling, workover, and completion operations, which can compromise the safety of rig workers, the environment, and associated assets. It is simply an influx of formation fluid into the wellbore when the pore pressure exceeds the bottom-hole pressure [1]. This situation occurs due to: sudden abnormality in pore pressure, hitting abnormal geological conditions such as faults, salts, charged zones, over pressured shale, depleted zones and anticlines while drilling, failure of pump, drop in equivalent circulating density, swabbing/surging while tripping, loss of casing back pressure, gas, oil or water cuts in drilling mud.

Gas kicks occur as a coupled dynamic and transient process involving gas migration through porous and permeable formation from the underlying reservoir and multiphase flow in the wellbore. This dynamically dampens the bottom-hole pressure initiating a positive mass transfer rate from the reservoir into the wellbore. Consequent response of other drilling parameters include increase in flow-out rate from the annulus, quadratic increase in pit gain, drop in standpipe pressure, decreased equivalent circulating density, increase in the rate of penetration caused by reduced compaction strength and improved drilling of a porous/permeable formation [2]. It is important that the formation fluids have a low viscosity to permit flow. Early detection can be useful in implementing the appropriate well control strategy to manage kick situations [3]. Delay in detecting kick events allows for magnification of the pressure associated with the influx thus increasing the kill pressure required to control the situation [4], [5] and a blow-out if not properly managed.

Early detection of kicks is facilitated with the availability of downhole measurements, efficient communication of data to the processing devices and accurate processing of the data to identify anomalies. The development and adaptation of downhole monitoring and data-driven approaches are being seriously considered for field application. One such effort is led by a major oil and gas company, Total S.A. to address the three crucial areas that facilitate early detection. The first part is to develop miniaturized sensors that are easier to integrate to the bit/bottom-hole assembly and the drill-string to measure bottom-hole and annular flow. The second part is the development of wireless technology to efficiently transmit large amounts of data to the surface. The third part is to leverage on analytics and artificial intelligence to process the large amount of data and get the correct information out of them [6].

Given the limited availability of downhole data from the field, The Centre for Risk, Integrity and Safety Engineering (CRISE) at Memorial University of Newfoundland is building on research efforts over the last four years that focus on design and conducting of laboratory experiments that monitor downhole drilling parameters for early kick detection.

The pilot experiment in this research was conducted by Nayeem et al. [7]. They developed a downhole sensor assembly and kick injection setup that was integrated to a Small-scale Drilling Simulator (SDS). The setup was used to study relative changes in pressure, drilling fluid density, conductivity, and mass flow rate downhole when a kick occurs. Their work aimed to identify the most sensitive parameters to an influx and experimentally verify the expected behavior of monitored parameters during an abnormal well condition. They concluded that downhole monitoring could improve kick detection with a difficult-to-achieve precision when compared to surface monitoring.

Then Islam et al. [8] using the experimental setup in [7], experimentally tested and validated kick detection using a risk assessment model. Multiple downhole parameters such as fluid conductivity, fluid density, downhole pressure and mass flow rate were combined in different logical combination to assess kick occurrence and the associated risk of a blowout and it was concluded that a combination of flow rate and any other parameters provides very reliable basis for detecting kicks and estimating the likelihood of blowout.

Sule et al. [9] explored the effect of a gas kick on different downhole drilling parameters using the laboratory scale drilling rig in [7] with the addition of sensors measuring bit vibrations. They reported the dampening effect of drilling vibrations due to a kick which became evident after performing frequency analysis on the axial bit-rock displacement. The rock sample drilled was a completely pre-drilled synthetic rock of medium compressive strength. This was proposed to be a potential new kick indicator upon further field investigations.

Previous experiments in [7] and [8] involved circulation of drilling fluid through the experimental set up only. Actual drilling was not performed; drilling fluid (water) was circulated through the drill string. Kick was initiated by opening the valve of an air injection system at the bottom of the pressured drilling cell (wellbore) to allow air influx into the drilling cell during circulation. However in [9], drilling was performed on a synthetic rock sample. Yet still, kick was initiated by opening the valve of an injection system at the bottom of the pressured drilling cell while drilling through the rock sample. The experiments in [7], [8] and [9] were conducted using the same laboratory scale drilling setup.

Table 1-1: Differences in kick detection experiments using downhole parameter monitoring reported in [6], [7], [8] and the current work.

	Nayeem et al. [7]	**Islam et al.** [8]	**Sule et al.** [9]	**Current work**
Design of experimental setup	Yes	No	No	Yes
Modification to experiment	-	No	Included vibration sensors	New drilling system, synthetic rock geometry
Downhole monitoring	Yes	Yes	Yes	Yes
Drilling fluid circulation	Yes	Yes	Yes	Yes
Drilling of synthetic rock sample	No	No	Yes	Yes
Manner of kick initiation	Manually opening valve of air injection system	Manually opening valve of air injection system	Manually opening valve of air injection system	Drilling into high pressure fluid zone
Parameters monitored	Downhole pressure, drilling fluid density, conductivity, and mass flow rate	Downhole pressure, drilling fluid density, conductivity, and mass flow rate	Downhole pressure, drilling fluid density, conductivity, mass flow rate, weight on bit, rotary speed, drill bit vibrations, torque, rate of penetration, choke pressure	Downhole pressure, drilling fluid density, conductivity, mass flow rate, weight on bit, rotary speed, torque on bit,
Frequency analysis	No	No	Yes	Yes
Machine learning modeling	No	No	No	Yes

1.2 Problem Statement (Research motivation)

There have been numerous efforts in early kick detection including those that use machine learning (neural network, decision tree, logistic regression etc.) together with monitoring of surface drilling parameters. There has been a relatively little effort in monitoring downhole drilling parameters. This is because current downhole monitoring is done with bulky and expensive Measurement While Drilling (MWD) and Logging While Drilling (LWD) tools. These tools and data are not always readily available to researchers in the academia. With rapid advancements in the fields of Micro-Electro-Mechanical Systems (MEMS), wireless communications, information technology and emphasis on digitalizing the oilfield, there is need to leverage massive computing power that will be made available from digitalization with the investigation of machine learning and monitoring of downhole drilling parameters for early kick detection. The gaps identified in early kick detection research include the following:

1. There are limited modelling efforts that apply machine learning to downhole measurements in the area of early kick detection.
2. There is limited availability of downhole drilling data from oil fields with downhole pressure and flow measurements. As a result, data will have to be collected from existing and new experiments that records downhole measurements.
3. Kick experimental setup described in previous publications simulates kick by manually opening an air influx system connected to the bottom of a drilling cell while circulating or drilling through a completely predrilled rock sample. There exists the need to improve laboratory kick simulation that involves drilling into an overpressure formation. This requires the replication of kick-prone rock formation. There are designs for synthetic rock formation with similar geological properties but limited knowledge on the geometric

design of such rock samples to enable them to contain trapped high-pressure kick fluids within.

1.3 Research Objectives

This research aims to investigate the capabilities of supervised machine learning for early kick detection using data from existing and new kick experiments. The new kick experiment simulates drilling into an overpressure formation and monitoring of downhole drilling parameters to generate downhole measurements.

1.4 Scope of research

The proposed research is an advancement of earlier efforts. The scope of the present work to achieve the research goals entails:

1. The designing and casting of synthetic rock samples with similar geological properties to those bearing hydrocarbon and geometrical capability to contain a zone of trapped high-pressure formation fluids at its bottom. The rock sample will be confined and held in place for drilling by a pressured drilling cell.
2. Scaling-up of the kick experimental setup design proposed in [7] using a larger drilling system. This involves:
    a. Replacing the Small Drilling Simulator (SDS) system used in in [7], [8] and [9] with a Large Drilling Simulator (LDS) system.
    b. The design and fabrication of a pressured drilling cell to hold the synthetic rock sample in place for drilling.
    c. Integrating the LDS system, pressured drilling cell and kick injection system.

    d. Instrumentation of the downhole sensor assembly (for downhole monitoring) and kick injection system for measurements.
    e. Wiring of the sensors and transmitters to the Data Acquisition system to record process data.
3. Developing experimental methodology to collect downhole data in the laboratory using the scaled-up experimental setup and the synthetic rock samples.
4. Developing data-driven modelling methodology that leverages on machine learning
    a. Comparison of several neural network architectures for building supervised machine learning-based kick detection models.
    b. Building of ANN-based kick detection models with downhole data.
5. Performing frequency analysis of new experimental data before and during the occurrence of kick using digital signal processing techniques.
6. Testing and evaluating developed data-driven model with data from the SDS system, SDS system with faulty conductivity data and the LDS system.

1.5 Fundamental Assumptions

The following assumptions have been made in conducting this research:

1. A conventional overbalanced drilling scenario is investigated wherein the bottom hole pressure is expected to always exceed the pore pressure.
2. Water is used as drilling fluid. This is due to availability and ease of cleanup.
3. Air is used as formation fluid that will cause a kick. This is to mitigate risks associated with handling other kinds of gases in the laboratory. Air is pressurized using a compressor to attain a predefined pore pressure value and channeled to the bottom of the wellbore using a pneumatic kick injection system.

4. Kick occurs near the drill bit. Kicks that occur due to a previously depleted zone was not covered

1.6 Research Outcome

This research employs an experimental methodology that relies on collecting downhole data in a laboratory and a data processing methodology that leverages on machine learning. The expected outcome of this research includes the following:

1. A detailed design of synthetic rock sample with geometrical capability to trap high-pressure formation fluid within.
2. A detailed design of a new kick experiment setup that uses a Large Drilling Simulator (LDS) and synthetic rock samples.
3. New set of experimental data from downhole parameter monitoring.
4. A data-driven model for early kick detection that employs neural network-based supervised machine learning using historical drilling data from drilling systems with downhole monitoring capabilities.
5. Results from testing and evaluating the performance of the data-driven model with data from the SDS and the LDS drilling system.

1.7 Thesis structure

The rest of this thesis document is organized as follows. Chapter 2 provides review of research articles that use a variety of methods for kick detection. This chapter segments the articles by type of parameter monitoring vis-a-vis surface or downhole then provides general thoughts that lead to designing the experiment for the current work. Chapter 3 presents the design of synthetic rock samples for drilling experiments, rock geometry design to facilitate trapping of high-pressure fluids, rock materials design, mixing, casting, and curing procedures. Chapter 4 discusses the new experimental system, system setup and the experimental methodology. Chapter 5 presents the proposed data-driven model development methodology. This chapter discusses the sources of data and the data processing procedures such as machine learning problem formulation, selecting training, validation and test datasets, preprocessing, comparison of several neural network architecture, ANN architecture design, parameter significance, model training, testing and evaluation. It also presents the technology stack employed in processing the data. Chapter 6 provides detailed results from testing the three trained models. Results include values of training features for each model and their corresponding label, plot from testing with data from SDS system, plot from testing with data from SDS system that includes faulty conductivity data, plot from testing with data from LDS system and model evaluation metrics for all three test cases. Chapter 7 provides a brief discussion of the current work. Finally, Chapter 8 provides conclusions and presents recommendations for the possible future extensions of the current work.

1.8 List of Publications

1.8.1 Journal Publications

1. S. Muojeke R. Venkatesan, and F. Khan, "Supervised data-driven approach to early kick detection during drilling operations," *Journal of Petroleum Science and Engineering, 2020*.
2. A. Osarogiagbon, S. Muojeke, R. Venkatesan, and F. Khan, "A new methodology for kick detection during petroleum drilling using long short-term memory recurrent neural network," *Journal of Process Safety and Environmental Protection, 2020*.

1.8.2 Conference Proceedings

1. S. Muojeke, "Spatiotemporal analysis of fibre optic sensor data for pipeline leak detection," in Proceedings of IEEE Newfoundland Electrical and Computer Engineering Conference, (NECEC), St. John's, November, 2018.

1.9 Co-authorship statement

Drs. Faisal Khan and Ramachandran Venkatesan proposed the idea of this work. The candidate (Somadina Muojeke) has implemented the idea through numerical modelling and also experimental testing. The candidate has developed the numerical presented in the thesis under the close supervision of Dr. Venkatesan. Dr. Khan reviewed the model and provided feedback. The candidate also undertook the design and testing of the samples and also conducted experiments. Candidate has also prepared manuscripts based on the work presented in this thesis as first authors and supervisors (Drs. Venkatesan and Khan) as co-authors. The candidate has prepared the original draft of the thesis, which is reviewed and agreed upon by supervisors.

2 Literature review

2.1 Background

This section presents a comprehensive review of research articles published in the areas of early kick detection by monitoring either downhole parameters or surface parameters. Irrespective of the location of sensors, kick detection models have been developed using a variety of model-based and data-driven methods. A summary of published works can be found in Table 2-1. Surface parameter monitoring have been widely explored in most of these works [1], [2], [5], [10]–[13], [10], [14]–[19], [13], [3], [20], [21], [22] however fewer works have considered downhole parameter monitoring for early kick detection such as those reported in [7], [8], [9]. Selected works related to both surface and downhole parameter monitoring for kick detection will be discussed together with possible areas for improvement in the following subsections. General remarks will be provided at the end of this section together with a motivation that leads to the current work.

Table 2-1: Selected kick detection articles, type of monitoring and modelling employed.

Author	**Type of monitoring**	**Parameters**	**Modelling technique**
Jiang et al. [21]	Surface	Flowrate and pressure	Numerical modelling: Single phase transient temperature and pressure coupling model to an Unscented Kalman Filter (UKF) algorithm
Tang et al. [10]	Surface	ROP, WOB, rotary speed and bit size, flow-out rate, flow-in rate, Stand-Pipe Pressure (SPP) and reference Pressure	Physics-based dimensionality reduction, along with time series data mining
Adedigba et al. [16]	Surface	Bottom-hole pressure, pore pressure and fracture pressure	Bayesian Tree Augmented Naïve Bayes algorithm, Fault tree analysis, event tree analysis

Author	Type of monitoring	Parameters	Modelling technique
Sun et al. [2]	Surface	Gas and liquid flow parameters such as pressure, phase distributions and velocities; wellbore pressure distribution, reservoir properties; stand-pipe pressure, flow-in rate, flow-out rate, and pit gain	Dynamic wellbore flow by solving the momentum conservation and continuity equations, the drift model; a transient reservoir model and a weighted combined parameter pattern recognition model using piecewise approximation and similarity measure algorithms
Hargreaves et al. [15]	Surface	Flow rate and tank volume	Model-based Bayesian probabilistic approach
Sabah et al. [23]	Surface	Northing, easting, depth, weight on bit, hole size, pump pressure, pump rate, shear stress, viscosity, drilling meterage, drilling time, gel strength, solid percent from retort test, formation type, bit rotational speed, drilling mud pressure, pore pressure and formation fracture pressure	Decision Tree (DT), Artificial Neural Networks (ANNs), Adaptive Neuro-Fuzzy Inference System (ANFIS) and Genetic Algorithm – Multi Layer Perceptron (GA-MLP)
Tamim et al. [14]	Surface	Pit gain, flow differential, rate of change in penetration, changes in pump pressure	Decision support algorithms, probabilistic barrier failure model, Bayesian network model
Ribeiro et al. [24]	Surface	Annulus pressure, choke pressure, water, and mud pump frequencies, choke opening index, flow rate and time	Artificial Neural Network
Deregeh et al. [25]	Surface	Depth, d-exponent	Artificial Neural Network and Adaptive Neuro-Fuzzy Inference System, ANFIS
Chhantyal et al. [20]	Surface	Upstream pressure	Dynamic artificial neural networks with real time recurrent learning algorithm, static artificial neural network, and support vector regression

Author	Type of monitoring	Parameters	Modelling technique
Unrau et al. [26]	Surface	Mud volumes and flow rates	Machine learning (specific algorithm not stated)
Fu et al. [3]	Surface	Annular flow velocity	Doppler principle
Karimi et al. [27]	Surface	flow in/out readings and downhole pressure variations	Transient two-phase model
Zheng et al. [11]	Surface	Wellbore temperature	Discretized wellbore and formation heat transfer model using Finite Volume (FV) method.
Yang et al. [28]	Surface	Multipoint pressure measurements	Pressure fluctuation model considering the water hammer effect
Nayeem et al. [7]	Downhole	Downhole pressure, drilling fluid density, conductivity, mass flow rate	
Islam et al. [8]	Downhole	Downhole pressure, drilling fluid density, conductivity, mass flow rate	Computational Fluid Dynamics (CFD), Risk assessment modelling
Sule et al. [9]	Downhole	Downhole pressure, drilling fluid density, conductivity, mass flow rate, Weight on Bit (WOB), rotary speed, drilling bit vibrations, Torque on Bit (TOB), Rate of Penetration (ROP), choke pressure	Frequency analysis
Nhat et al. [29]	Downhole	Downhole pressure, drilling fluid density, conductivity, mass flow rate	Dynamic Bayesian Network

2.2 Surface parameter monitoring for kick detection

Previous efforts have focused on developing model-based mathematical techniques as seen in [30],[10]–[13]. Probabilistic methods have been developed in [10], [14]–[19]. Acoustic tools have been employed for kick monitoring in [13] to predict the response to gas influx in real time. Ultrasonic tools have also been employed in [3], [20]. Signal processing have been used in kick detection in [21]. It has also been used in [22] to reconstruct downhole pressure measurements in the event of a faulty permanent downhole gauge.

The probability of the occurrence of a kick event was calculated using physics-based dimensionality reduction, along with time series data mining approach in [10]. The authors used this to propose an algorithm for analysis of real time drilling data to detect influx events. The method was tested on data from offshore drilling wells. They presented two kick indicators that integrated several drilling and circulation parameters. Parameters influencing d-exponent which alerts of abnormal formation pressure zones were lumped to create a Drilling Parameter Group (DPG). Parameters influencing flow and pressure were also lumped to create a Flow Parameter Group (FPG). Parameters affecting the d-exponent include ROP, WOB, rotary speed and bit size, while those affecting flow and pressure include flow-out rate, flow-in rate, Stand Pipe Pressure (SPP) and reference Pressure (P_{ref}). The proposed algorithm in [10] works as follows:

1. First check if the input real-time drilling data conforms to drilling or non-drilling processes.
2. If it conforms to a drilling process, it checks if it conforms to a transient operational activity.
3. Non-conformance to a transient operational activity triggers the extraction of kick indicators and local trend features. This enables proper initialization for probability

analysis. Trend features include a Divergence of Moving Average (DMA) and Divergence of Moving Slope Average (DMSA).

4. Probability analysis is done if the DMA shows an increasing trend or the DMSA shows a decreasing trend. The Kick Risk Index (KRI), which is a weighted sum of the DPG and FPG, is the output of probability analysis.

This approach requires setting appropriate weights when calculating the KRI. There also exists the challenge of threshold setting to obtain a reasonable tradeoff between missed alarms and false alarms. It was reported that from the testing of the method on offshore field data, drilling parameters are better indicators of kick in terms of detection speed and robustness because these parameters are measured near the drilling bits and flow parameters responded very slowly. Despite this, they suffer a setback as they cannot detect kicks that occur during circulation or tripping. They are limited to only active drilling periods. Flow and pressure parameters were recognized to be relevant kick indicators for both drilling and non-drilling periods. More so, since only surface flow parameters were considered, we can say that if flow and pressure parameters are measured downhole, they have the potential to be more robust, faster and reliable for kick detection than drilling parameters although both can be combined to improve the fidelity on the resulting detection system.

Overall, downhole flow and pressure monitoring together with proposing a standard method for choosing the appropriate window length, weighting factor and alarm threshold are areas for further investigation based on the proposed methodology in [10].

A data-driven dynamic risk analysis methodology was proposed in [16] to predict time dependent probability of kick occurrence. The Bayesian Tree Augmented Naïve Bayes algorithm was used to model the probabilistic relationship among primary drilling parameters; the

developed structure is updated based on the current state of the key drilling parameters; then tested using real drilling data. The key parameters in the structure were BHP, pore pressure and fracture pressure while the probability of kick occurrence computed from the time variant behavior of the key parameters is used to estimate the failure probability of the six safety barriers from probability assessment using fault tree analysis and the probability of end state events from the consequence assessment obtained from event tree analysis. The result of the probability and consequence assessment are then combined to predict the risk of the different category of end state events in a time dependent fashion.

A gas kick diagnosis model was proposed in [2] for deep-water operations which comprises a dynamic wellbore flow model to extract modes of kick events through multiphase flow simulation and a weighted combined parameter pattern recognition model using piecewise approximation and similarity measure algorithms to generate a synthetic kick probability. The dynamic wellbore flow model incorporated gas and liquid flow parameters such as pressure, phase distributions and velocities. This was achieved by solving the momentum conservation and continuity equations, relationship between gas and liquid phase velocities using the drift model, a transient reservoir model to estimate the gas influx rate based on wellbore pressure distribution and reservoir properties, and the relationship between stand-pipe pressure, flow-in rate, flow-out rate and pit gain during a gas kick. The pattern recognition model first performs dimensionality reduction by applying piecewise approximation to extract features from time series drilling data for different parameters then similarity measurement against a set of kick and non-kick events by calculating the Morphological distance (geometric mean of Euclidean distance and an improved slope distance). The individual similarity result of a feature for all events was normalized by the total sum of all similarity results. The inverse of this value yielded the relative probability for each event to be represented by the feature. Finally, to achieve reliable multi-parameter based

detection, the relative probabilities of kick events for different parameters were assigned confidence degrees (weights) then summed using the Analytic Hierarchy Process method described in [31]. The condensed relative probabilities are eventually displayed in a probability log. One limitation of this work is the static assignment of confidence degrees using AHP to detect dynamic kick. Drilling is a dynamic operation and the confidence degree (weights) should be dynamically adjusted based on drilling activity. Another limitation lies in the subsequent interpretation of the probability log. The overall kick probability reached 50% only after a kick event was detected in pit gain data. Even if the alarm sounded when pit gain was 11.1% of traditional threshold value, it does not reflect the benefit of combined parameter-based weighting as the developed model in [2] followed the most sluggish parameter in the parameter set.

A kick detection system was proposed in [15] for Deepwater applications which uses model-based Bayesian probabilistic approach and presented results from the field. The traditional threshold approach was not followed, the system comprised of two components; a model set which contains different length of time series information of flow rate and tank volume regimes during normal (connections, tripping etc.) and abnormal drilling event (different rates of kick) and a model matching Bayesian framework which probabilistically matches the incoming data in the data buffer to all models in the model set. A match with high probability of resembling a kick event in the model set will be flagged. The data buffer is a sliding window with length up to that of the longest model in the model set. The tank volume system was used as a back up to the flow rate system to track small rates of influxes that would not be captured in the kick flow rate model set.

The data is streamed into a buffer in a sliding window fashion, probabilistic matching using Bayes rule between the window and each model based on their length is carried out. As

described earlier, the model set contains different families of drilling events. The probabilities calculated were normalized then grouped by families. For kick detection, normalized kick probabilities for different kick rates were summed up and displayed on a probability log. An alarm goes off when the kick probability is up to 0.9. This is useful as it maintains time-based profile of kick conditions during drilling operations and can inform the operators of events that have occurred. Normalizing the kick probabilities to 1 in each window is not straightforward as all models in the model set were said not to have same length. Very short models may be compared more than once in a single window which raises the question on which comparison is to be considered when normalizing, although it was stated that the difference in model length will reduce the effect of varying levels of noise on the sensitivity of the system. The procedure for standardizing the models in [15] to capture different operating conditions is unclear when considering differences in magnitude and ramp rates of the models.

Assessment of drilling operations to predict kicks and prevent blowout using a leading indicator-based approach was proposed in [14]. Decision support algorithms were employed to understand kick progression scenario while probabilistic barrier failure model was employed to assess the performance of the primary well control barrier. The decision support algorithms and probabilistic barrier failure model were combined to build a Bayesian network model to obtain the probability distribution of real-time parameters as kick progresses. This serves as a means of detecting kicks as they propagate and appropriate actions to regain well control. The framework for categorizing the relevant leading indicators was developed in [32].

An early gas kick detection method that combines a transient temperature and pressure coupling model to an Unscented Kalman Filter (UKF) algorithm which is suitable for water based muds have been proposed in [21]. This method requires:

1. Developing a gas kick detection model from the single-phase transient temperature and pressure coupling model under normal drilling conditions. Factors will be applied to flowrate and pressure state values to model the effect of a gas kick. These factors will be the parameters to be estimated and not the actual states.
2. Synthetic pressure and liquid flow rate data to estimate the four kick detection factors which includes outlet flow rate factor and three pressure factors in the annulus, drill string and bit nozzle respectively from the gas kick detection estimator using the UKF algorithm
3. Performing a generalized likelihood ratio test on a vector containing the estimated factors. The test result is compared to an adaptive detection threshold to detect changes in the mean of the pressure and flow rate factors that could indicate a gas kick.

The detection threshold was based on parameters estimated from normal drilling conditions. The method was compared with delta flow and pit gain monitoring method and reported to perform better with reduced detection time and high sensitivity to small gas kick rates [21].

Permanent Downhole Gauge (PDG) pressure reconstruction methodology based on digital signal processing on Christmas tree pressure measurement was proposed in [22] to demonstrate its superiority over neural network and transfer function estimation-based methodologies in oil and gas production using real well data. While this does not relate directly to drilling, it provides some insight for building new kick detection systems. This work proceeded under the presumption that information about the downstream/downhole pressure is contained in the well surface pressure measurement since the information flows from the bottom to the topside of the well with wave reflection and water hammer effect subdued by the large distance between well surface/sea bed and downhole measurements.

Available measurements for this study were permanent downhole gauge pressure near the reservoir, christmas tree pressure on the seabed, surface pressure readings, gas-lift flow, and choke opening. Slug mechanisms appear as high peaks in the frequency domain of the pressure measurements which occurs at the same frequency for all three measurements. The difference is the addition of information as different frequencies and amplitudes but with the same principal components. However, all three measurements look different in the time domain. Both neural network and transfer function estimation models used christmas tree pressure, gas lift flow and choke opening to reconstruct the PDG pressure while the digital signal processing method based on Fourier analysis and filtering used only the christmas tree pressure.

The proposed methodology requires spectral analysis of the christmas tree pressure to obtain the cutoff frequency of the low pass filter and design of low pass filter using the obtained cutoff frequency. The filter was applied to the christmas tree pressure measurements to reconstruct the downhole pressure. This method requires no model and requires only one measurement reading.

The success reported in [22] raises the question of designing a digital signal processing-based kick detection system that extracts downstream pressure information and transients from top stream pressure measurements then uses it as a basis for detecting potential drilling problems such as kicks.

Kicks could be induced in a zone above the drilling bit as a result of lost circulation which dampens the equivalent circulating density of the circulating fluid. Prediction models such as Decision Tree (DT), Artificial Neural Networks (ANNs), Adaptive Neuro-Fuzzy Inference System (ANFIS) and Genetic Algorithm – Multi Layer Perceptron (GA-MLP) were employed in [23] to predict the severity of a lost circulation using field data from Marun oil field in Iran. It was concluded that due to the values of regression coefficient for all models, they could be

accurate for predicting amount of lost circulation fluid. A closer look reveals that DT was more accurate relative to other models since a large amount of variables including northing, easting, depth, weight on bit, hole size, pump pressure, pump rate, shear stress, viscosity, drilling meterage, drilling time, gel strength, solid percent from retort test, formation type, bit rotational speed, drilling mud pressure, pore pressure and formation fracture pressure were used as input into the models. It was also stated in [23] that ANN followed by ANFIS produced better results if a small number of variables is considered.

Neural network controllers capable of regulating the annular bottom hole pressure (BHP) in real-time under kick, lost circulation and pipe connection procedures have been developed and tested in [24] using data from an experimental drilling unit and validated with real data from an offshore oil well. This was achieved by predicting the BHP, then using the predicted value to manipulate the choke valve opening index in order to regulate equivalent circulating density (ECD). This found application in a managed pressure drilling (MPD) scenario but could also be applied to a conventional overbalanced drilling scenario by predicting the pump pressure which becomes the manipulated variable. The controller was compared to a classic PI controller and reported to be a suitable adaptive control scheme for real time closed loop implementation [24].

A model for estimating the BHP in vertical wells with multiphase flow using hybridized Artificial Neural Network with backpropagation training and Optimized neural networks using each of Grey Wolves Optimization (GWO), Particle Swarm Optimization (PSO) and Genetic Algorithm (GA) respectively was proposed in [33] and tested using field data from oil fields in Algeria. The input parameters were gas flow rate, oil flow rate, water flow rate, gas gravity, oil gravity, inside pipe diameter, well head pressure, well head temperature, gas/oil ratio, and depth. All three hybrid models were reported to outperform mechanistic models while comparison of

the hybrid ANN models showed that the hybrid model with Grey Wolves Optimization for optimizing the weights and threshold of the neural network showed superiority based on accuracy ranking.

Artificial Neural Network predictive model for multiphase wellbore flow was developed in [34] using data from a numerical simulator to predict the BHP in the wellbore. The transient multiphase wellbore simulator captured the dynamics of different phase volume fraction distribution in the wellbore, slip (velocity difference between phases), phase compressibility, friction and release of gas in the wellbore as the pressure drops below bubble point while the input parameters were surface flow rates, wellhead pressure and wellbore geometry. Downhole pressure data in production wells that provides insights from reservoirs to improve oil and gas recovery has been investigated in [17] using Fisher's Discriminant Function (FDF) and Mean Deviant Function (MDF) to calibrate pressure changes in the downhole pressure gauge, Spatiotemporal Graphical Modelling (STGM), Synthetic Minority Oversampling Technique (SMOTE) and multilayer Artificial Neural Network (ANN) to classify risk and Long Short Term Memory (LSTM) and Fisher's Discriminant Function/Spatiotemporal based multilayer Artificial Neural Network (FS-MLP) to predict future risk characteristics . The noise associated with data acquisition and fluctuation of pressure as a result of changes of reservoir pressure was identified as critical problems in applying downhole pressure and temperature data making failure prognosis difficult especially when the data is collected over a long period of time. Real well data was acquired from an onshore well in Australia. While the application domain is enhanced oil and gas recovery in reservoirs and production wells, the technique can be studied in relation to early kick detection. Historical time series of downhole pressure was modelled to classify operational risk levels of the downhole pressure gauges to prevent the failure of the gauge that

occurs when the pressure exceeds a critical threshold after establishing normal and abnormal operating condition of the gauge [34].

Artificial Neural Network and Adaptive Neuro-Fuzzy Inference System, ANFIS were combined in [25] for early kick assessment. The system accepts input dataset, perform Gaussian normalization then uses subtractive clustering to extract a set of rules that generates a fuzzy inference system. The generated inference system is fed as input into an ANN to obtain d-exponent which captures the interaction between ROP, RPM, WOB and Hole (bit) diameter (excluding mud-weight). During testing, depth is fed as the only input and d exponent is the output. Given that depth is always fixed between the surface and the desired drilled depth, it is unclear how depth will reliably generate the d-exponent as the zone profile changes. The d-exponent is a better indicator of an abnormal pressure zone which may be prone to kick rather than detecting the actual occurrence of kicks. Kicks that occur due to depleted layers may be difficult to capture by this technique [25].

Dynamic artificial neural networks with real time recurrent learning algorithm was used in [20] and shown to perform better than static artificial neural network and support vector regression models when used to estimate the flowrate in an open channel venturi-rig of non-Newtonian drilling fluids measured from ultrasonic level measurements. The upstream pressure relative to the venturi flume in the control section was used to estimate flow rate. Different learning algorithms were compared, and it was found out that despite backpropagation through time and extended Kalman filters methods fast convergence, real time recurrent learning algorithm was more accurate and computationally less expensive. They also showed that an alternative to using expensive flow devices such as Coriolis mass flow meters for flow measurement is an open venturi channel [20]. This is a single parameter approach to the task of early kick detection.

Reliability of detection system can be improved when multiple parameters and their relative interaction are combined.

A system that keeps track of normal values of mud volumes and flow rates during different phases of drilling (making connections, putting and pulling pipes, transferring mud, changes in pump rate, increasing depth) was presented in [26]. The values are used as a basis to set adaptive alarm threshold with the aim of reducing false alarms. The system was tested on 12 hours of real-time drilling data and was reported to produce no false alarm. The machine learning adaptive threshold algorithm which was used was not explained. It was presented as a black box model creating ambiguity and knowledge gap on the part of the reader. Reasons for not explaining the algorithm was also not stated. The authors rightly pointed that connections and pulling/putting pipes may cause considerable variations in certain drilling parameters which can trigger false alarms in traditional alarm systems but did not discuss kicks that could potentially occur in such scenarios. The tight alarm threshold setting increases the risk of a missed alarm.

The authors in [3] reported developing an early kick detection prototype in the laboratory for deep-water drilling operations. The prototype monitors annular flow velocity with an ultrasonic sensor under the mudline using the Doppler principle and studied the effect of changes in drilling fluid density and gas injection rate on the measured return velocity. They used the return velocity as the main indicator of kick. They were also able to show that the sensors will operate well at bearing pressure up to 15MPA. The ultrasonic device non-intrusively measures and records the Doppler frequency shift from which the annular flow velocity can be determined. A 508mm diameter riser and 139.7 diameter drill pipe system was simulated with a 244.5mm diameter casing as riser and 73mm diameter tube as drill pipe, the ultrasonic sensor was placed at the lower part of the casing to simulate positioning near the mudline with the ultrasonic flowmeter

connected. Water based mud whose viscosity was reduced, and density increased was used as drilling fluid. Return velocity was calculated and measured at different flow rate and drilling fluid density for scenarios with and without gas injection. It was shown that Doppler principle can detect gas influxes from return velocity and ultrasonic attenuation varies directly with drilling fluid density and gas injection rate. It was also observed that changes in the ultrasonic wave propagation velocity in the drilling fluid impacted the measurement accuracy. Increase in drilling fluid density and gas injection rate resulted to decrease in measurement accuracy This points out the limitation of this study since inaccurate measurements gives room for delayed detection. The paper did not show the measurement error for one channel measurement when gas was injected [3].

A transient two-phase model that automatically selects the best MPD-CBHP response in the event of an influx based on the size of an influx was reported in [27]. To determine the size of the influx and detect it early, they combined flow readings and downhole pressure variations.

The impact of a well kick on wellbore temperature distribution that could be seen as changes in the flowing state and various properties of the drilling fluid motivated the work described in [11]. They developed discretized wellbore and formation heat transfer model for normal circulation and kick conditions in open hole formation for single phase incompressible fluids using Finite Volume (FV) method. This was solved with under-relation iterative method with data from the analytic model. The occurrence of well kick was seen to have significant influence on the formation radial temperature distribution and temperature difference profile.

It was pointed out in [28] that kick diagnosis can be error prone when detection is inferred from pressure fluctuation in a single measured point. This was shown from a wellbore fluctuation model and a laboratory experiment with BHP measured at two points. A pressure fluctuation

model considering the water hammer effect at the initial occurrence of a gas kick was developed to capture transient annular pressure variation during the kick. Then, based on the differences and consistencies between two measurement points, a dual measurement point approach was proposed. They found out that annular pressure measurements at the set points were affected by the bottom hole differential pressure, well depth, borehole diameter and formation permeability; kick capture time reduced with decrease in well depth and borehole diameter; kick capture time also reduces with increase in formation permeability and negative bottom hole differential pressure; and that distance between the measured points is mainly determined by the borehole diameter [28].

The need to automate well-control response to a kick occurrence led [1] to develop an integrated system capable of early reliable detection of kicks that could occur during drilling or circulation, connections and tripping in/out using two independent sets of sensors with different sensor technology for each parameter and distinct audio alarm systems.

2.3 Downhole parameter monitoring for kick detection

Identifying and recovering commercial quantity of hydrocarbons are crucial goals of any drilling campaign. These hydrocarbon fluids are usually trapped beneath several layers of rock formation; thus, they may exhibit varying properties due to compression by the overlaying rock formation. As drilling through hydrocarbon-bearing rocks progresses, one may encounter porous and/or rock formation layers containing formation fluids that may be higher or lower than the bottom hole pressure in the wellbore. Surface monitoring alone has been seen to have limited capabilities in monitoring the risks due to mechanical problems, gas solubility in drilling fluid, abnormal formation fluid properties, wellbore breathing and ballooning etc. [6]. Drilling fluid

can be lost in zones with low pore pressure. This loss of circulation fluid increases the potential of a kick once a high pore pressure zone is reached. It is therefore reasonable to monitor drilling fluid and formation fluid parameters downhole while drilling.

Highlighting that downhole monitoring is beneficial in a lost circulation induced kick scenario to enhance blowout prevention, a laboratory scale drilling rig model with a kick injection setup was reported in [8]. The study investigated relative changes in mass flow rate, drilling fluid density, electrical conductivity, and pressure in downhole when kick occurs. Drilling fluid was circulated through the experimental setup without actual drilling of a rock sample. The response of the circulation fluid parameters to an influx was used to identify the parameters that are most sensitive. Water was used as a drilling fluid and air was used as the formation fluid. A methodology to detect kicks without false alarms based on the experimental setup was also developed. The methodology detects the occurrence of a kick when

1. A minimum of two out of the four observed parameters exhibit variations beyond a predefined threshold.
2. This variation is sustained for longer than 10 s.

The thresholds were +15 psi for downhole pressure and +-5% for mass flow rate, density, and conductivity. This experiment was conducted maintaining two sets of pump flow rate (12 USGPM and 16 USGPM) for two sets of constant pressure margin (20 psi and 30 psi) between different downhole pressure and the air inject pressure. It was observed that all parameters gave indication of an influx, but downhole pressure and mass flow rate gave a quicker indication. The delay in response of density and conductivity parameters was attributed to sensor placement. The pressure response downhole was seen to follow the formation pressure (air inject pressure).

The limitation of the adoption of the methodology in [8] is the unavailability of miniaturized flow meters and density meters that can be deployed downhole. Areas identified for improvement includes experimentally comparing surface and downhole parameter monitoring, monitoring drilling fluid temperature, using water and oil-based drilling fluids, using water (liquid kick) as influx fluid and development of numerical models for simulating wide range of kick scenarios.

Experimental testing and validation of kick detection capability of a bowtie blowout risk assessment model based on changes in downhole parameters such as conductivity, density, pressure and mass flow rate were reported in [7]. A laboratory scale downhole sensor assembly and kick injection setup similar to that used in [8] was employed to generate data. Multiple downhole parameters were combined in different logical combinations to assess kick occurrence and the associated risk of a blowout. The bowtie approach combines fault tree analysis for kick detection and event tree analysis for safety barriers. It was concluded that a combination of flow rate and any one of the other parameters namely downhole pressure, electrical conductivity, and density of the resulting multiphase mixture due to an influx provides very reliable basis for detecting kicks and estimating the likelihood of blowout. Areas identified for improvement includes exploring blowout prediction models based on real time observation such as Dynamic Bayesian Network (DBN) models [7].

Downhole drilling parameters were explored for kick indication in [9] using a laboratory scale drilling rig. The significant finding reported was the dampening effect of drilling vibrations due to a kick. This was validated with field reports and confirmed by performing frequency analysis on the axial bit-rock displacement. The rock sample drilled was a synthetic rock of medium compressive strength. It was reported that a combination of bit-rock vibrations with dynamic

drilling models enables prediction of the response of a drilling system surface parameter such as choke pressure or standpipe pressure to a kick. Downhole parameters such as Weight On Bit (WOB), downhole pressure, rotary speed, drilling bit vibrations, Torque On Bit (TOB), Rate Of Penetration (ROP), and surface parameters such as choke pressure, return fluid mass flow rate, volume flow rate and density were measured. The effect of a kick on these parameters were observed and discussed. The significant decrease in the amplitude of the axial bit-rock displacement could be visualized in the time domain and showed up as higher order damped signals in the frequency domain. This was proposed to be a potential new kick indicator upon further field investigations [9].

Data-driven Bayesian Network has been applied in complex systems to solve problems that do not require a model-based method if accurate solution is to be found. It was applied in [29] to model downhole parameters for early kick detection.

2.4 General Remarks

Flow data is a widely acknowledged indicator of a kick; however, it suffers from noisy measurements as a result of flow sensors used to collect the data. Flow in rate is measured with pump stroke while flow out rate is measured with flow paddle [15] as Coriolis flow meters can be costly. Threshold detection has been the main technique applied to monitored parameters from previous kick detection systems [10]. It could either be sounding an alarm when the parameter exceeds a predetermined level or when a step change is observed, this could be as a result of a kick or a lost circulation. Kick indicators such as flow out rate and mud volume varies during rig activities such as pipe connections, tripping, increasing pump rate, mud transfer and increasing depth and could trigger traditional threshold alarms [26]. Kicks usually occur as

ramps thus sacrificing the performance of such system to how well the step sizes are tuned to imitate a ramp [15]. Most simple kick detection systems do not have the sensitivity required for applications in deep water environment, especially in the presence of heaves and as kick tolerance drops. Predictive models were built to model fluid circulation patterns on the rig. Such models considered connections and tripping but still used windowed thresholds for detection. It is also important to note that flow models are unique for different rigs and can be complex. There have been claims to improving the noise handling capacity of newer sensors but we are yet to see systems that can adapt to changes in noise levels [15], [35]. Also, when building predictive models, it is important to train with historical data collected in similar operating conditions. Deepwater wells are not as numerous as onshore wells, and hence the insufficiency of kick events data for *a priori* evidence, threshold determination, and network training, whichever method is used [2].

Pore pressure prediction gives early warning of abnormal pressure zones wherein a kick is likely to occur. Traditional methods such as d-exponent and sigma log do not account directly for the petrophysical properties of the formation but indirect pressure indications and may be less reliable when compared against resistivity data from the MWD tool. As a result, kick detection methods that rely chiefly on d-exponent may be less reliable [4]. As offshore drilling goes deeper into the oceans, the safe shut-in volume for kick fluid into the well bore decreases [15], the pressure margin between the fracture gradient and the pore pressure of the underlying formation drops exposing rig men to higher chances of kicks and losses [9], [27]. It takes more time for a kick to be detected on the derrick floor in offshore drilling when compared to onshore drilling as delta flow and pit gain are measured on the surface [10].

It was pointed out in [36] that kick modelling is dominated by deterministic numerical models which are approximations of a process highlighting the underlying dominant effects, capturing disturbances and uncertainties in such processes are intractable and further magnified by distortions in sensor data. The choice of data-driven modelling captures uncertainties and disturbances inherent in the monitored process.

Considering the above remarks and observations from literature reviewed, gaps identified in early kick detection research include the following:

1. There are limited modelling efforts that apply machine learning to downhole measurements in the area of early kick detection.
2. There is limited availability of downhole drilling data from oil fields with downhole pressure and flow measurements. As a result, data will have to be collected from existing and new experiments that records downhole measurements.
3. Kick experimental setup described in previous publications simulates kick by manually opening an air influx system connected to the bottom of a drilling cell while circulating or drilling through a predrilled rock sample. There is limited laboratory effort in simulating kick conditions by drilling into a rock zone of high-pressure formation fluid.
4. There are designs for synthetic rock samples with similar geological properties but limited knowledge on geometric design of such synthetic rock samples to enable them to contain trapped high-pressure air within.

Consequently, we propose that these gaps may be addressed by a combination of data-driven modelling and downhole parameter monitoring as it presents a huge reward in achieving early kick detection in any drilling campaign. It is also important to design a new experiment in which

a rock sample is designed to trap high-pressure fluid and kick happens once the drill bit drills into the high-pressure zone.

3 Synthetic rock sample design, casting, and preparation

3.1 Introduction

Sedimentary rock samples bearing trapped oil and gas are not readily available onshore in Newfoundland, Canada. This motivated the design of highly consistent synthetic rock samples that will have similar rock properties to those encountered while drilling. These samples should also possess the geometrical capability to create a trapped high-pressure fluid zone where kicks are very likely to occur once hit unexpectedly for laboratory research. The synthetic rock samples need to be reproducible to allow for multiple tests under varying operating conditions.

3.2 Rock sample properties design

A standard procedure proposed in [37] for casting reproducible and consistent sample with quality assurance for improving confidence is adopted for this study.

Table 3-1: Physical properties of the synthetic rock design proposed in [36].

Rock property	**Value**	**Units**
Unconfined compressive strength	51	MPa
Mohr friction angle	40	
Tensile strength	5.4	MPa
Young modulus	29	GPa
Poisson ratio	0.15	

The drillability of the produced rock samples is characterized by the procedures laid out in [38] while noting that there exist differences that can affect characterization and variability. This can be seen in the time it takes for natural rock to form compared to synthetic concrete. The properties for characterization include density, porosity, p-wave & s-wave velocities, unconfined compressive strength (UCS), Mohr friction angle, grain size and mineralogy as shown in Table

3-1. Medium strength concrete samples resembling real rocks were designed, formulated and tested with UCS as the control parameter. This is because it is difficult to control other rock properties using quality assurance procedures to guarantee repeatability and reproducibility.

3.3 Rock sample geometry design

The synthetic rock sample is to be inserted in a pressured drilling cell and held in place by its top cap and bottom cap within a cylindrical space with dimensions of 12 inches in height and 6 inches in diameter. This becomes the outer dimension of the rock sample. The upper part of the rock sample contains a void cavity of 3 inches by 4 inches to capture measurements during drilling fluid circulation before bit-rock interaction sets in as shown in Figure 3-1.

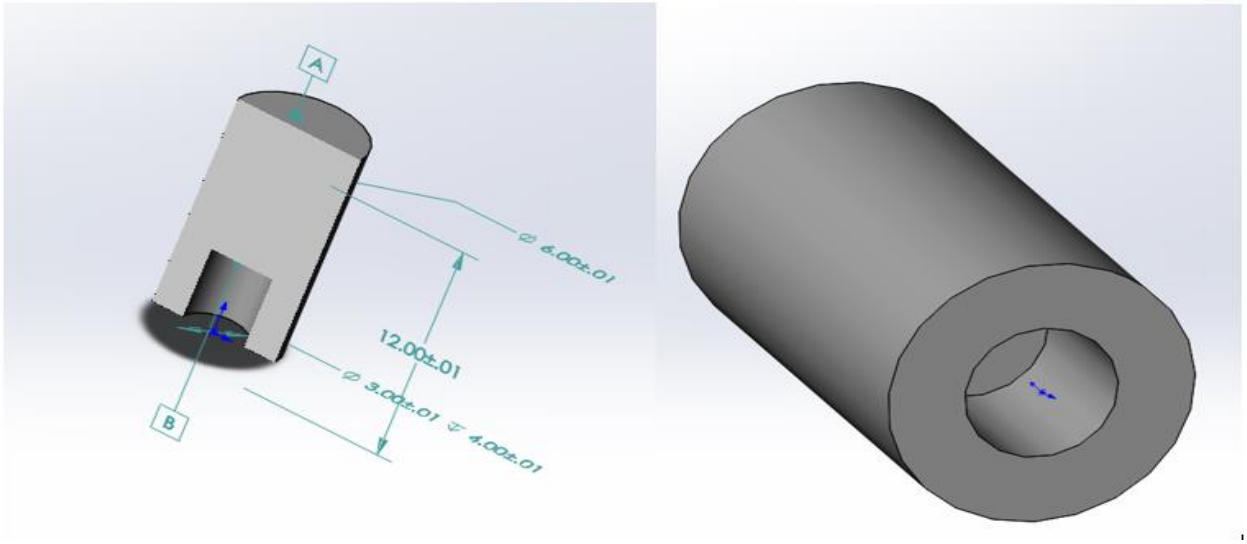

Figure 3-1: Rock sample geometry before predrilling.

Using a ½" masonry bit, the remaining 8 inches fully solid length is predrilled 3 inches from the top and 4 inches from the bottom. As a result, the zone that contains the high-pressure formation fluid wherein the kick will occur is at the bottom of the rock sample and has a cylindrical dimension of height of 4 inches and diameter of ½".

3.4 Rock sample materials design

Given the rock sample outer dimension and the void cavity at the top of the rock sample, the synthetic rock volume for a rock sample is calculated using Equation (3.4.1).

$$Vol = \frac{\pi(D^2H - d^2h)}{4} \quad (3.4.1)$$

In this equation, H is the height of the synthetic rock sample, D is the outer diameter of the rock sample, d is the diameter of the void cavity at the top of the rock sample while h is the height of the void cavity at the top of the rock sample.

$Volume\ of\ concrete\ sample = \frac{\pi(6^2*12 - 3^2*4)}{4} = \frac{\pi*396}{4} = 311in^3 = 0.0051m^3$ per sample.

Three ingredients/materials namely aggregate, cement and water are required for making concrete with water/cement ratio been the major determinant of compressive strength of concrete. The relative volumes of aggregate, cement and water is captured in the absolute volume method of concrete mix design shown in Equation (3.4.2).

$$V_{aggregate} + V_{cement} + V_{water} = 1m^3\ of\ concrete \quad (3.4.2)$$

Also, the volume of each material is related to its mass, specific gravity (SG) and the density (ρ) of water as shown in Equation (3.4.3).

$$V_{material} = \frac{m_{material}}{SG_{material} * \rho_{water}} \quad (3.4.3)$$

Further still, the mass of cement and water is related by the water/cement ratio as shown in Equation (3.4.4).

$$m_{water} = k * m_{cement} \quad (3.4.4)$$

In this equation, k is the water/cement ratio. Combining Equations (3.4.2), (3.4.3) and (3.4.4) yields Equation (3.4.5) which is a more descriptive form of the absolute volume method of concrete mix design stated in Equation (3.4.2).

$$\frac{m_{aggregate}}{SG_{aggregate} * \rho_{water}} + \frac{m_{cement}}{SG_{cement} * \rho_{water}} + \frac{k * m_{cement}}{SG_{water} * \rho_{water}} = 1\, m^3\ of\ concrete \quad (3.4.5)$$

From Equation (3.4.5) we can obtain the suitable aggregate/cement ratio and water/cement ratio. To improve the workability (degree of compactness of concrete), additives are added while casting. The quality of fine aggregates (sand) used is controlled by sieve analysis. Sieving is a standard procedure in the concrete industry used to assess particle size distribution and guarantees identification of fine aggregate in an aggregate sample for multiple batches and same sieve aperture diameter. This procedure should follow the ASTM standard C136 – Standard test method for sieve analysis of fine and coarse aggregates. Fine aggregates are usually stored in open area hence prone to varying moisture conditions which must be accounted for to adjust the water/cement ratio accordingly. The fine aggregate goes through a moisture removal process (heating in a dry pan and weighed continuously until the mass does not change with further heating). The Moisture Content (MC) is calculated as shown in Equation (3.4.6). After mixing, the concrete mix is internally vibrated on a vibration table to improve consistency.

$$MC = \frac{m_{wet\ aggregate} - m_{dry\ aggregate}}{m_{wet\ aggeregate}} * 100\% \quad (3.4.6)$$

In this equation, MC = Moisture Content.

Equipment and tools used in mixing the concrete to achieve the desired properties include 6 by 12 inches cylindrical plastic mold that meets ASTM standard C470/470M requirements for casting the samples vertically, 3 by 4 inches cylindrical solid for creating the void cavity at the top of the rock sample, 3⁄8 in. (10 mm) diameter and 12 in. (300 mm) long tamping rod to

eliminate air void while preparing the concrete, internal vibrator that meets ASTM standard C192/C192M-15 requirements, vibration table, hot plate to heat the wet aggregate to remove the moisture content, trowels, pails, head pan, scoop, rubber gloves, Workman II 350 rotating electronic mixer with capacity of 1 cubic foot, unified compressive strength tester to determine the compressive strength as the concrete mix sets and curing room to cure the cast samples. All apparatus was available in the Concrete laboratory of Memorial University.

The formulation and curing followed the ASTM Standard C192/C192M-15 standard practice for concrete test specimens in the laboratory. Special attention needs to be paid to the proportion of additives and vibration because the low water/cement ratio in medium strength concrete lowers the workability of the concrete upon mixing. The design formula for Aggregate:Cement:Water (A:C:W) adapted from [37] is 3:1:0.45, the quantities of the various components from this design is summarized in Table 3-2. Upon casting, curing will be done for 28 days in a controlled curing room. The recipe is shown in Table 3-2.

Table 3-2: Quantities of the various components for synthetic rock sample design

Sample component	**Designed Quantities**	**Adjusted Quantities**
Aggregate	30kg	31.654kg
Cement	10kg	10kg
Water	4.5kg(4500ml)	3.064kg(3064ml)
Superplasticizer	Duracem 19 (60ml)	Duracem 19 (60ml)

The moisture content in the aggregate needs to be calculated to adjust the quantity of sand and water to meet design requirements. Applying Equation 3.4.6, the moisture content is obtained.

$$Moisture\ Content = \frac{m_{wet\ aggregate} - m_{dry\ aggregate}}{m_{wet\ aggeregate}} = 4.568\%$$

The adjusted quantity of fine aggregate is calculated below using Equation (3.4.7).

$$m_{aggregate}^{adjusted} = \frac{m_{aggregate}^{designed}}{1-MC} \tag{3.4.7}$$

$$m_{aggregate}^{adjusted} = \frac{30kg}{1 - 0.004568} = 31.436kg$$

This adjusted value for the quantity of fine aggregate contains the designed quantity of aggregate and some water content which further requires adjusting the quantity of water to be introduced in the concrete mix to meet design requirements. This is shown in Equation (3.4.8). The volume of water is adjusted using Equation (3.4.9).

$$m_{aggregate}^{adjusted} = m_{aggregate}^{designed} + m_{water\ in\ aggregate} \tag{3.4.8}$$

$m_{water\ in\ aggregate} = 31.436kg - 30kg = 1.436kg$

$V_{water\ in\ aggregate} = \frac{m_{water\ in\ aggregate}}{\rho_{water}} = \frac{1.436kg}{1g/ml} = 1436ml$

$$V_{water}^{adjusted} = V_{water}^{designed} - V_{water\ in\ aggregate} \tag{3.4.9}$$

$V_{water}^{adjusted} = 4500ml - 1436ml = 3064ml$

3.5 Rock sample mixing

With all adjusted quantity values of concrete design materials ready, mixing is carried out in a Workman II 350 rotating electronic mixer with capacity of 1 cubic foot. The following procedure is followed in mixing the concrete:

1. Put 10kg of cement and 31.436kg of fine aggregate in the mixer before starting rotation.
2. Begin rotation of the mixer, wait for 60 s of rotating to ensure proper mixing before adding 3064ml of water.
3. Continue rotation of the mixer for 3 minutes with a rest period of 2 minutes during which the mixer must be covered to prevent evaporation.
4. Repeat the above step twice before adding a superplasticizer to improve the workability and slump value. Once the desired workability and slump value is attained, fill the concrete mix in the cylindrical plastic mold for setting and curing.

3.6 Rock sample casting and curing

The 3" by 4" cylindrical solid which creates the void cavity at the top is first centralized symmetrically on the bottom of the 6" by 12" cylinder before filling the space with scoops of concrete mix. Successive scoops are internally vibrated in between to enhance consolidation and improve workability. Each scoop of concrete is vibrated to remove air bubbles before applying the next layer of scoop. Also, care is taken to introduce a thin layer of covering on the inner cylindrical solid to allow for easy removal upon setting. Once a mold is filled with concrete mix and properly vibrated internally, it is allowed to set before removing the internal cylinder. Up on setting, the plastic mold with the set concrete mix contained is transferred into a curing room in line with ASTM Standard C192/C192M - 15 at a temperature of 23 ± 2C. The following day

remove the samples from the plastic mold and keep on water in the curing room to achieve the desired UCS. After 28 days, UCS value of 50MPa was reached.

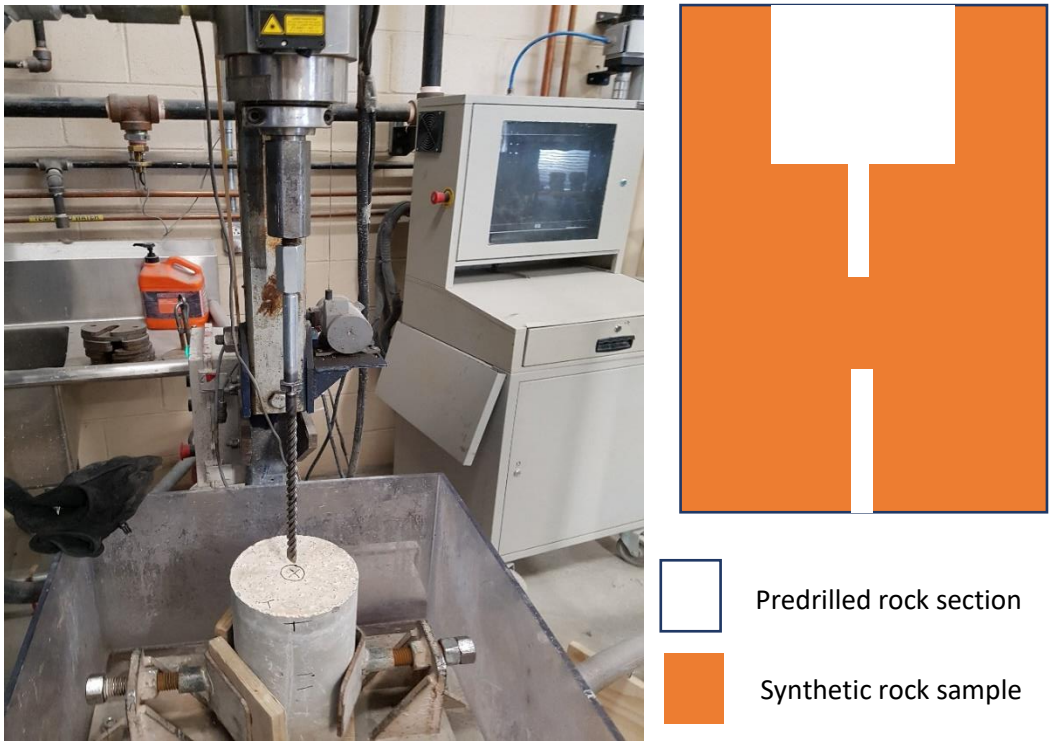

Figure 3-2: Left image showing the predrilling of a synthetic rock sample and right image showing cross section of synthetic rock sample with predrilled cavities

The cast synthetic rock sample is predrilled with a ½" masonry bit to achieve the cross-section shown in Figure 3-2. The resulting sample dimension is 6" by 12" for the outer cylindrical portion and 3" by 4" for the inner cylindrical portion at the top. Top predrilled hole is ½" by 3" and bottom predrilled hole is ½" by 4". The synthetic rock sample mass will bear a strength of 50 MPa.

4 Experimental System

4.1 Introduction

Due to the limited availability of downhole drilling data from oil fields with downhole pressure and flow measurements, data will be collected from experiments that record downhole measurements. This chapter presents a new kick experiment setup derived from the scale up of the kick experimental setup design proposed in [7] . It also presents an experimental methodology to collect downhole data in the laboratory using the scaled-up experimental setup and the synthetic rock samples. The scale up involved:

1. Replacing the Small Drilling Simulator (SDS) system used in [7], [8] and [9] with a Large Drilling Simulator (LDS) system.
2. The design and fabrication of a pressured drilling cell to hold the synthetic rock sample in place for drilling.
3. Integrating the LDS system, pressured drilling cell and kick injection system.
4. Instrumentation of the downhole sensor assembly (for downhole monitoring) and kick injection system for measurements.
5. Wiring of the sensors and transmitters to the Data Acquisition system to record process data.

The experiment involves the actual drilling of a synthetic rock sample with similar geological properties (unified compressive strength) to formation rocks encountered in the field. Kick occurs suddenly, only when the rotating drilling bit drills through the synthetic rock sample (6" by 12") held in place by a pressured drilling cell and hits a zone of trapped high-pressure air.

Before drilling, high-pressure air is trapped in a predrilled hole (½" by 4") at the bottom of the synthetic rock sample as shown in Figure 3-2.

The air is supplied by a pneumatic kick injection system connected to the bottom of the drilling cell. This high-pressure zone contains the fluid to initiate a kick. Parameters recorded include drill bit position, observed WOB, pneumatic applied WOB, hydraulic applied WOB, rotary speed, torque, downhole pressure, mass flow-out rate, electrical conductivity, and density. The LDS kick experiment system configuration is shown in Figure 4-1.

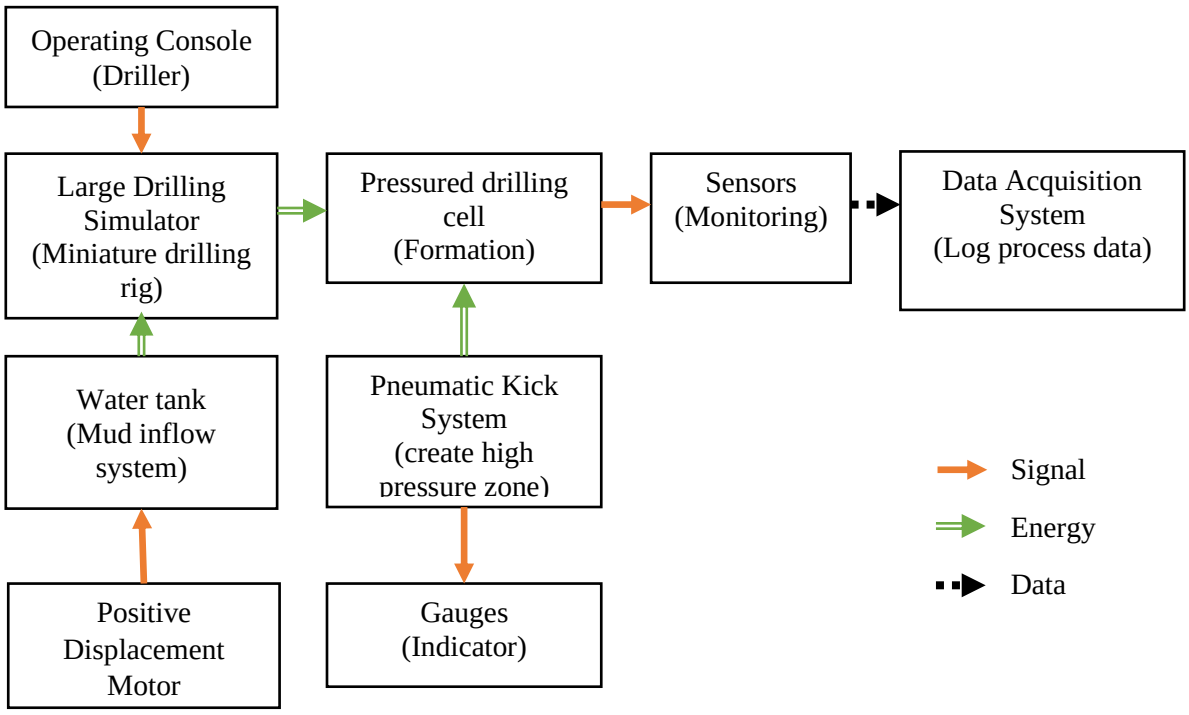

Figure 4-1: LDS System configuration showing flow of energy, signals and data.

4.2 Experimental Setup

The new experimental drilling setup and the setup designed in [7] are housed in the Drilling Technology Laboratory at Memorial University of Newfoundland, St John's, Canada.

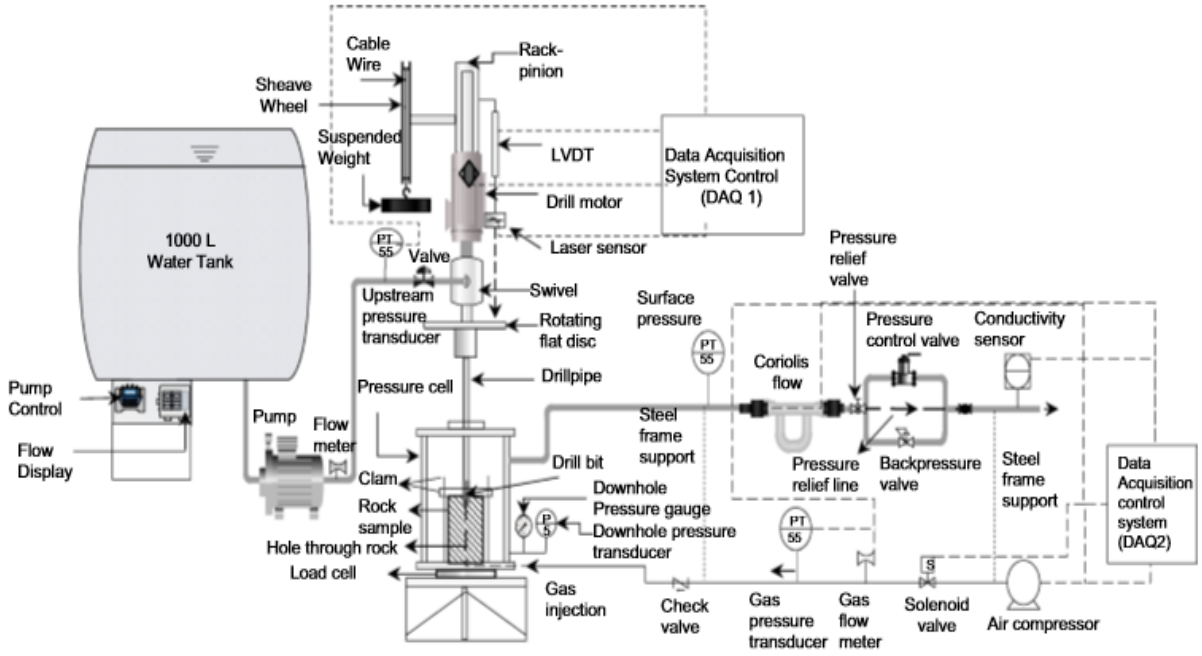

Figure 4-2: Process from diagram of experimental setup [9].

The process flow diagram is shown in Figure 4-2. The setup comprises:

1. Mud inflow system
2. Drilling system - Small Drilling Simulator (SDS)/Large Drilling Simulator (LDS)
3. Pressured drilling cell assembly
4. Downhole sensor assembly
5. Pneumatic kick injection system
6. Mud return flow system
7. Data acquisition system
8. Synthetic rock sample.

4.2.1 Mud inflow system

This system is in place to ensure adequate supply of drilling fluid to the drilling system. It comprises a mud tank that holds the drilling fluid circulated through the entire setup and a high-pressure triplex pump to move drilling fluid from the mud tank into the LDS system. The mud tank is a 1000 L capacity water tank that is fed at a rate of 3000 L/hr. The pump is driven by a positive displacement motor rated 7.5 hp. The pump sets the mud flow rate through its internal control system. The drilling fluid moves through a high-pressure hose rated 1000 psi. There is a normally closed needle valve along the hose that allows and disallows fluid flow into the drilling simulator. The mud flow rate is controlled by a variable frequency drive on the pump motor and the mud pressure is controlled by a valve which generates back pressure. A display panel on the pump serves to indicate the values of pressure and flow rate when in operation.

4.2.2 Large Drilling Simulator, LDS

The LDS is a fully automated drilling rig setup capable of atmospheric, pressurized and vibration assisted drilling. It has a drill motor rated 33 kW, 550 rpm for supplying torque and rotation to the drill string. Torque is measured by the torque transducer and rotary speed and position is measured by the SIN/COS resolver. The drill string assembly has an upper section, swivel, and the lower section. The upper drill string section is a stainless-steel pipe that appends the drill motor shaft and extends to the swivel. It transmits torque and rotation to the lower drill string section. The swivel continuously receives drilling fluid from the mud inflow system for onward transmission to the lower drill string section while it is rotating. The lower drill string section channels the fluid into the drill bit which is screwed firmly onto it. The fluid flows through the drill bit nozzle and flushes the cuttings as the drill bit grinds through the rock sample. The high-pressure hose from the mud inflow system delivers the drilling fluid into the swivel and is held in place by a reaction frame. The drill bit is a 35mm OD Polycrystalline Diamond Cutter (PDC) bit

with three teeth. It grinds through the synthetic rock sample held in place by the pressured drilling cell while the drilling fluid cleans away the cuttings during drilling operation. The LDS receives pressurized hydraulic fluid from the hydraulic pumping unit through a regulator and solenoid manifold on its top in a closed loop to produce vibrations in the system. Vibration is controlled from the operating console. Penetration depth is determined from the bit position measured by the displacement transformer sensor (variant of the linear variable displacement transformer). Vertical movement of the drill string is enabled through the pneumatic system and weight on bit is applied by the load cell with throttled pressure from the air compressor. The rotary head receives both dynamic weight on bit from the load cell and constant weight on bit from the drill motor and drill string assembly.

4.2.3 Pressured drilling cell assembly

The pressured drilling cell together with the predrilled pressurized rock sample is at the center of this experimental investigation. The pressured drilling cell used is different from that used in [8]. This is to enable it to fit a larger rock sample dimension and to suit the drilling simulator. It is an assembly of various components composed mainly of stainless-steel acting together to contain the pressurized rock sample and hold it in place for the drilling operation. It is built to withstand a pressure of 1000 psi and tested to a maximum of 1500 psi. It has a top cap and bottom cap with fitted groove, 6 in internal diameter to firmly secure the rock sample and an 8 in internal diameter cylinder to create a confined pressure area around the fitted rock sample. The rotating drill bit can rotate the sample if it is not secured rigidly. To cushion the torque action of the rotating drill bit, a top and bottom compression plate with four tension rods is employed to apply downwards pressure and prevent rotation once the bottom plate is clamped to the drill floor. A lift screw having its top and bottom plate that appends it to the top and bottom compression plates is in place to allow for clearance within the pressure cell.

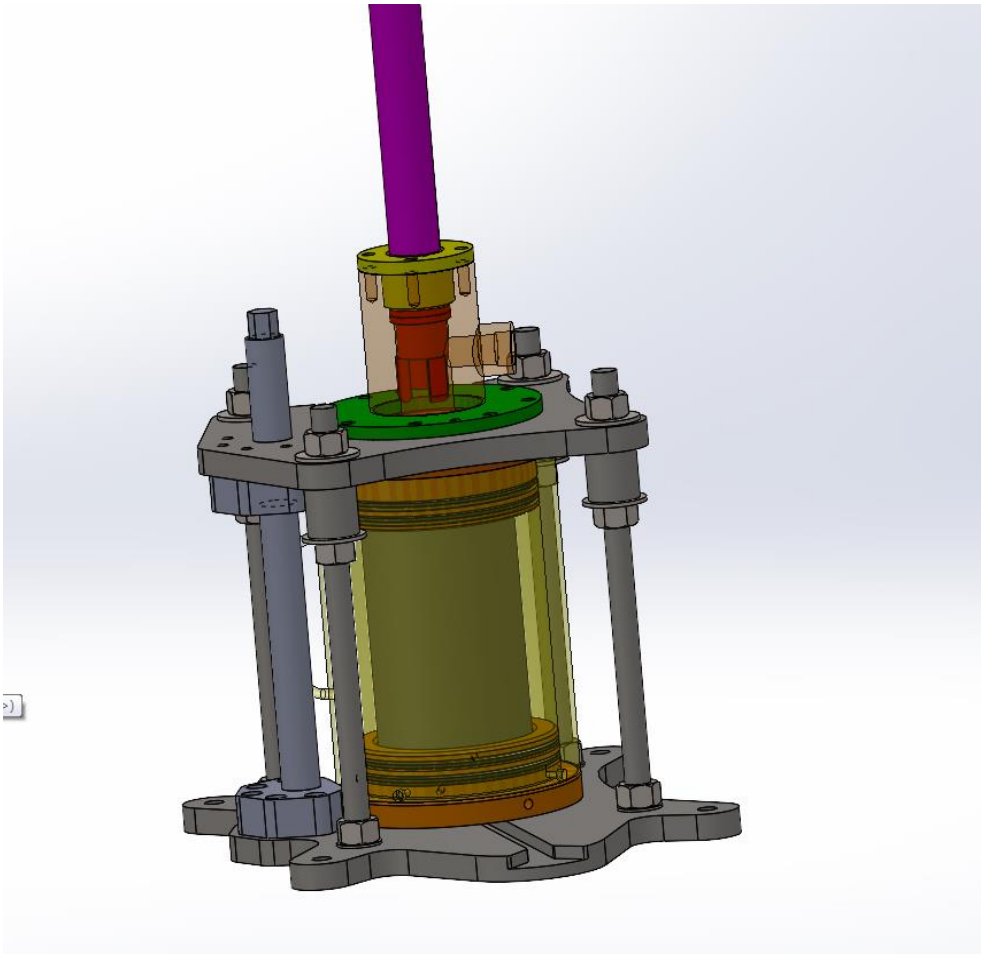

Figure 4-3: Pressured drilling cell with drill string and rock sample

The drill bit is held in place within the pressurized drilling cell assembly in a drill bit housing prior to drilling. This allows for symmetric placement of the drill sting within the pressure cell. At the side of the bit housing is a channel for interfacing with the mud return flow system as shown in Figure 4-3. The assembly procedure for the pressured drilling cell assembly is contained in appendix. There is also provision for connecting the kick injection system at the bottom cap to allow injection of air at a predetermined pressure to imitate an influx and hole at the top to allow for the drill bit to drill through the sample in place.

4.2.4 Mud return flow system

A high-pressure hose, rated to a maximum withholding pressure of 2400 psi, channels the drilling fluid circulated out of the pressured drilling cell together with sample rock cuttings and empties it through the drain hose. In this study, the circulation system is not designed to be a closed loop since there is no active level monitoring for the mud tank.

4.2.5 Downhole sensor assembly

The downhole sensors employed are the Coriolis flow meter for mass flow rate and density monitoring, conductivity meter for conductivity monitoring, general purpose output pressure sensor for downhole pressure monitoring. The output value of all sensors is in the 4 – 20 mA range. This output is wired through a patch panel to the data acquisition system.

4.2.6 Kick Injection System, KIS

To create a high formation pressure zone at the bottom of the predrilled rock sample, there needs to a means for maintaining formation fluid influx into the rock sample bottom at a predetermined pressure. The KIS serves this purpose. Formation fluid adopted for this study is air because of ease to get and associated safety concerns with using other gases/liquids in the laboratory. Air is supplied from an air compressor designed to deliver air at 175 psi for 23 ACFM and 100 psi for 25 ACFM flow rate through a pneumatic tubing rated at 145 psi (10 bar) working pressure. The air compressor is powered by an electric motor rated 7.5 hp. There are two pneumatic regulators between the air compressor and the KIS. The first regulator maintains a constant output air pressure from the compressor and feeds a distribution box from which the load cell in the drilling simulator and the KIS taps air supply. The second regulator maintains a constant input air pressure into the KIS. At the inlet of this regulator sits a pressure gauge to indicate the incoming air pressure from the distribution box. There is also a pressure gauge at the outlet of the

pneumatic regulator to indicate the value of formation pressure that is maintained downhole. This allows us to adjust the formation pressure to the desired value. The regulator used has the capacity to regulate an input pressure of 4000 psi max to 200 psi. In order to adjust the formation pressure in the bottom of the rock sample to a specified value, a needle valve is installed along the injection line at the outlet of the second regulator to disallow air flow into the drilling cell. This valve is normally closed, and it is opened only when the desired pore pressure has been set. Once the desired pore pressure is achieved from manipulating the pressure regulators, the needle valve is opened. Upon opening the needle valve, air flows through the injection line and is trapped beneath the rock sample to create a high formation pressure zone. A flow gauge on the injection line indicates the volumetric flow rate of trapped air when the kick process is initiated. Also, a volumetric flow rate transmitter and pressure transmitter is installed along the injection line to monitor and record the time-varying characteristics of the kick fluid. As a safety measure to disallow flow of drilling fluid and cuttings into the KIS, there is a filter at the outlet of the KIS that disallows drilling fluid/cuttings outflow from the bottom of the pressured drilling cell into the KIS and check valve that allows air outflow from the KIS into the bottom of the rock sample contained in the pressured drilling cell.

4.2.7 Data Acquisition System, DAS

This system performs the acquisition of real-time signals from sensors monitoring the drilling process and recording them in a computer using National Instruments (NI) Data Acquisition (DAQ) hardware and LabVIEW software. This system also generates analog and digital signals from the LabVIEW software in the computer for PC-based control and automation of the controller, drive, master control relay, hydraulic pump, pneumatic system pallet, pneumatic prop valve and load cell systems.

Data acquisition requires three essential components namely sensors, DAQ hardware and a computer. The sensor monitors the following physical quantities (pressure, flow rate, density, and conductivity) and delivers them as analog current outputs in the mA range. The DAQ hardware connects the sensors to the computer. It consists of the signal conditioning unit, analog-to-digital converter (ADC) and computer bus. The hardware unit possess counter, analog and digital channels for receiving input signals and delivering output signals as count, analog or digital signals, respectively.

Incoming current signal into the DAQ hardware from the sensor first passes through a signal conditioning unit which amplifies the mA current then coverts them to dc voltage via resistors. The ADC converts the analog dc voltage to a digital dc voltage value. The external bus (ethernet) serves as communication bridge to the computer using the UDP protocol. The computer with driver software such as DAQmx drivers and programmable application software (LabVIEW) monitors and controls the operation of the DAQ hardware. With this we are able to process, visualize and store data. The digital voltage obtained is transmitted via the bus to the LabVIEW software for calibration. This is done using a two-point calibration method to convert the digital voltage into the corresponding physical quantity monitored by the sensor.

This value is displayed on the operating console real-time and logged in an excel file by the Data Recorder program on the LabVIEW software. Recorded data includes drill bit position, observed WOB, pneumatic applied WOB, hydraulic applied WOB, rotary speed, torque, downhole pressure, mass flow-out rate, electrical conductivity, and density. These drilling parameters are recorded at a sampling rate of 10 Hz.

4.2.8 Operating console

The operating console is a standalone computer unit with LabVIEW software programs. The LabVIEW software serves to control the safe operation of the system and communicates with the DAQ and PLC units in the DAS. Relevant parts of the software program include the LDS state machine, dynamic function generator and data recorder. Calibration of the sensor output is also done here.

Figure 4-4: Graphical user interface of the operating console of the LDS system

The LDS state machine as shown in Figure 4-4 is a graphical user interface for providing control signals and setting system parameters. Drilling operation is conducted safely using this program. The dynamic function generator initiates and maintains communication with DAQ and PLC. The data recorder creates an excel file during system operation and records specified system data on the excel file. This data is extracted and subjected to further processing. When drilling, a Linear Variable Displacement Transformer (LVDT) measures the displacement of the drill bit inside the drilling cell. An LVDT stroke cylinder icon on the LDS user interface shows the penetration

depth (position of the drilling bit in the drilling cell) as shown in Figure 4-5. 52% indicates the bit is directly on top of the drilling sample while 92% indicates the bit is at the bottom of the drilling cell.

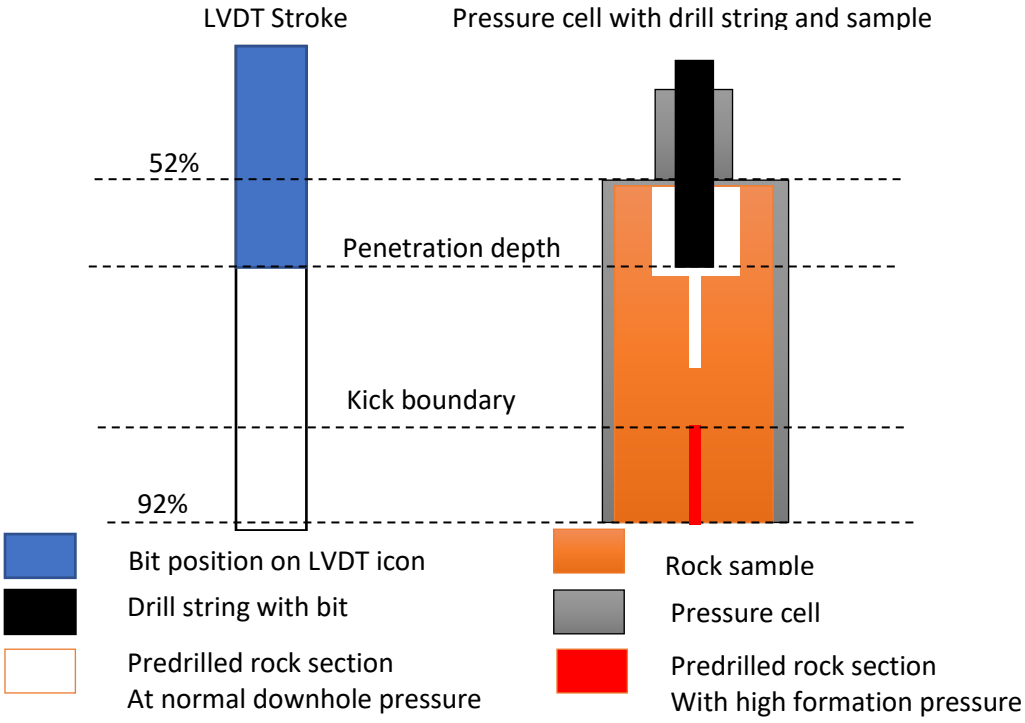

Figure 4-5: Cross-section of drilled sample in the drilling cell with drill bit in place showing the zone of trapped high-pressure air and penetration depth.

Kick is expected to occur at approximately 80% LVDT stroke. This is where the bit has drilled up to two-third of the sample as shown in Figure 4-5. The signs to monitor for a kick can be visualized on the user interface. They include increase in downhole pressure, sudden increase then decrease in mud flow-out rate, decrease in density, conductivity. When a kick occurs and is observed, drilling continues for up to 60 s to collect data provided LVDT stroke is below 92%. Only a single experimental run was carried out for purpose of testing the model built from the SDS kick system.

The complete experimental system is shown in Figure 4-6.

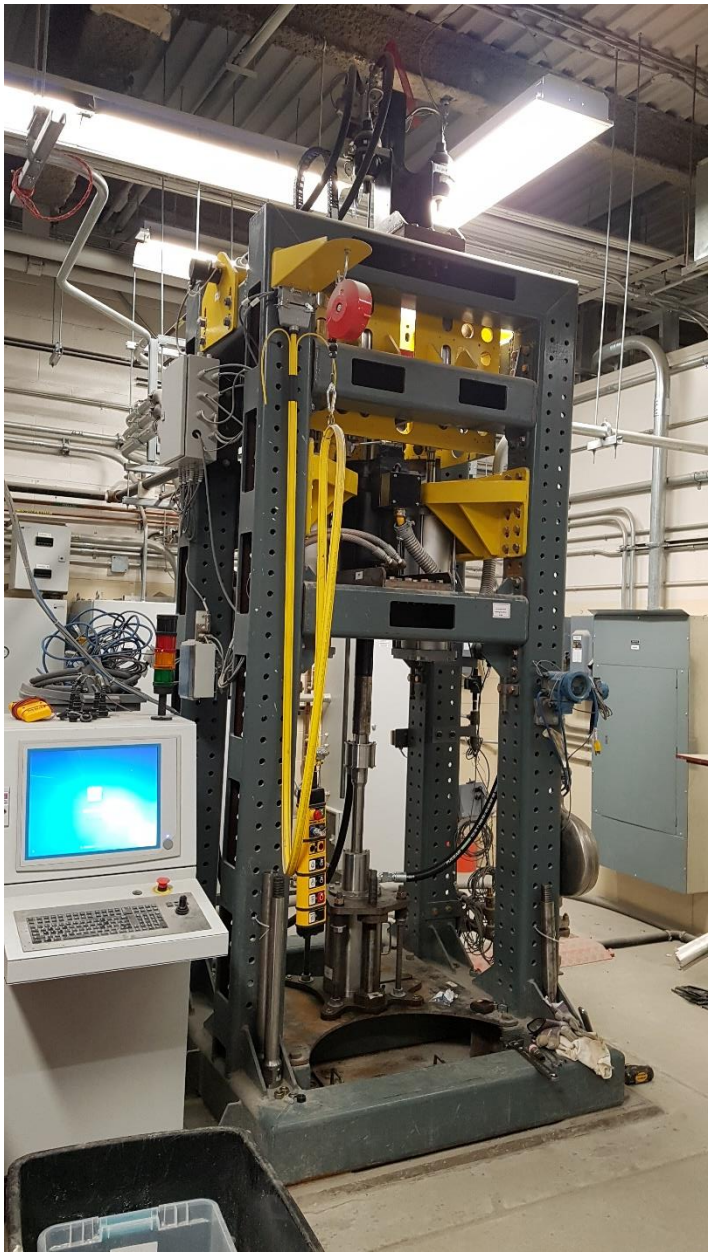

Figure 4-6: LDS kick experimental setup

4.3 Experiment Methodology

Kick event was investigated during drilling. The experiments capture the transient period between single phase and multiphase fluid flow downhole in the wellbore when a kick occurs. The system input parameters are shown in Table 4-1: System input parameters and their corresponding values in the LDS kick experiment.

Table 4-1: System input parameters and their corresponding values in the LDS kick experiment.

Parameters	**Values**	**Units**
Applied weight on bit	2	kN
Mud pump flow rate	5000	lb/h
Initial downhole pressure	10	psi
Air influx pressure	90	psi
Air influx flow rate	0	SCFM
Drilling motor rotary speed	60	rpm
Water based mud density	62.4	lb/ft^3

The system parameters include mud flow-in rate, air influx pressure (to initiate a kick), drilling motor rotary speed, drilling fluid density and applied weight on bit. The air influx pressure was chosen to create a differential with respect to the steady state downhole pressure as shown in Equation (4.3.1). The differential will ensure the influx pressure into the wellbore (drilling cell) always exceeds the steady state downhole pressure. This requirement is necessary and sufficient to initiate a kick.

$$\text{Pressure differential} = \text{Air influx pressure} - \text{Downhole pressure} \quad (4.3.1)$$

There will a single experimental run. Prior to any activity in the laboratory, conduct safety briefing for all personnel in the laboratory at the time of the experimental activity and ensure safety rules and regulations are strictly adhered to. There is a conspicuous system status light that indicates safety level. It is located on the operating console of the LDS system. Red light indicates unsafe and potentially dangerous operating conditions while green light indicates safe operating conditions. To successfully conduct the experiment, the following methodology is followed.

1. Set up the experiment as shown in Figure 4-2.
2. Fit the predrilled drilling sample into the drilling cell firmly and assemble without the drill bit housing as shown in Figure 4-7.
3. Position the drill string with drill bit in the drilling cell as shown in Figure 4-7.
    a. Insert the lower drill string into the drill bit housing section then tightly screw the drill bit to the lower drill string. Make sure the drill bit sits firmly within the drill bit housing.
    b. Adjust the drill string so the bit housing with the drill string sits on the top compression plate of the drilling cell then firmly secure the bit housing to its top.
    c. Care needs to be taken to prevent the drill bit from hitting the top and bottom of the drilling cell. This is controlled from the LabVIEW software in the operating console.
4. Turn on the air compressor and run for about 15 minutes to get it charged to 175 psi then turn it off.
5. Turn on the main controller/PLC/DAQ unit.
6. Power the variable frequency drive then run.

Figure 4-7: Rock sample in drilling cell and drill bit positioned in the drill bit housing.

7. Open the mud inflow line valve downstream of the pump. Turn on the mud pump and set drilling fluid flow-in rate to the desired value (3580 lb/h, 4652 lb/h, 5597 lb/h). Once circulation is started, the time varying values of all drilling parameters (drill bit position, observed WOB, pneumatic applied WOB, hydraulic applied WOB, rotary speed, torque, downhole pressure, mass flow-out rate, electrical conductivity and density) can be visualized on the LDS state machine once it is run. Take note of the downhole pressure.
8. Turn on the operating console, open the LabVIEW software.
    a. Start the LDS state machine program
    b. Start the Dynamic function generator program and run.
    c. Wait for a data response then run the LDS state machine program.
    d. System status light goes red. Set drilling mode to drill by pushing the blue key on the remote.

e. Activate Standby control signal and Master Control Relay (MCR) signal on the LDS state machine.

f. Get the system ready for safe operation. Hit reset button on the remote for 3 s, release and hit again for 3 s. The system status light goes green.

g. Set prop regulator valve slider on the LDS state machine to maximum value then open the air compressor output pressure regulator and adjust to 10 Bar (143 psi).

h. Start the Data Recorder program and set the storage location and name of the file to log the data.

9. Before drilling, trap high-pressure air at the bottom of the drilling cell. This high-pressure zone contains the fluid to initiate a kick.

    a. Ensure the air compressor is charged to desired pressure and balance the WOB from the load cell

    b. Circulate drilling fluid through the system to achieve steady state parameter values.

    c. Activate Air Pallet signal on the LDS state machine. Air is injected through the kick injection system connected to the bottom of the drilling cell.

    d. Regulate the kick system pressure regulator output to the value of the air inlet pressure (90 psi).

    e. Open the kick line valve to allow air flow into the drilling cell. The air will be trapped at the inner cylindrical portion at the bottom of the drilling sample. This is a zone of high formation pressure. Kick occurs when the bit drills into this zone.

10. Start drilling.

    a. Turn on the drill motor to start rotation of the drill string assembly by activating Quick Stop signal and Drive Enable signal on the LDS state machine.

b. Set input rotary speed parameter to 60 rpm, rotation of the drill string assembly coupled to the drill motor begins immediately and is observed.

c. Just before drilling, always monitor the LVDT stroke cylinder icon on the LDS state machine once the input static WOB is set to a non-zero value. Make sure it is at 52%. The LVDT stroke shows the position of the drilling bit in the drilling cell.

d. To commence drilling, set the input static WOB to 2. Immediately the drill string starts moving vertically down the drilling cell as it rotates to provide the grinding action on the drilling sample with help of the drill bit.

11. While drilling.

a. Ensure that the LVDT stroke shown below does not go below 52% and above 92%.

b. Normally kick should occur at approximately 80% LVDT stroke. This is where the bit has drilled up to two-third of the sample. It is possible that the sample fractures and kick occurs earlier. This is not out of place. Due to this possibility, do not always rely on the LVDT stroke. Also motor the signs for kick indication.

c. The signs to monitor for a kick can be visualized on the operating console. They include increase in downhole pressure, sudden increase then decrease in mud flow-out rate, decrease in density, conductivity.

d. When a kick occurs and is observed, allow drilling to continue for 60 s to collect data provided LVDT stroke is below 92%.

e. Stop drilling if any of the above two conditions are achieved.

12. Stop drilling whenever the objective of the experiment is achieved or during an emergency.
    a. If not an emergency, quickly set the input static WOB to zero to halt downward motion of the drill string assembly. This does not alter rotation of the drill string. To stop rotation, deactivate the Quick Stop and Drive Enable signal on the operating console.
    b. If it is an emergency, hit the Emergency stop on the remote. Anytime you hit the emergency stop, always deactivate the Quick Stop and Drive Enable signal on the operating console. To proceed with system operations, you have to reactivate these signals then set input static WOB to a non-zero value (typically 2 kN).
    c. To return the drill bit to the top position, make sure the input static WOB is set to zero then hit and hold the reverse button besides it. Immediately the drill string downwards motion ceases and it starts to move in the upward direction. Once the LVDT stroke reaches 52%, release the reverse button to stop further upward motion.
13. End of drilling.
    a. At the end of the drilling operation, follow the step 12 (a) and (c) above.
    b. Stop the Data Recorder program and close. This saves the file with the logged data automatically to the specified storage location. Set rotary speed to zero and make sure input static WOB is also zero.
    c. Turn off the mud pump, close the mud inflow line valve and the kick line valve.
    d. Allow the multiphase fluid in the pressure cell to drain.
    e. Vent the drilling cell by activating the pneumatic vent signal on the LDS State machine. Deactivate the signal once the drilling cell pressure reads zero.

Figure 4-8: Sliding the drilling cell out of the setup to fit or replace the synthetic rock sample.

14. More experiment runs.
    a. If more experimental runs need to be done, with the drill bit in the bit housing, unscrew the drill bit housing from the drilling cell.
    b. Slide the drilling cell out to fit a new drilling sample. Remove the drilled sample and fit a new one as shown in Figure 4-8. The drilled rock sample is shown in Figure 4-9.
    c. Go back to step 7 and repeat appropriately.

Figure 4-9: Rock sample after drilling.

15. Shut down drilling system.
    a. Shut off prop regulator by setting the prop regulator valve slider on the operating console to zero.
    b. Adjust the air compressor output pressure regulator to zero then close the valve.
    c. Make sure both load cell reads zero to confirm there is no residual weight on bit in the system.
    d. Deactivate all control signals in the following order (Pneumatic Vent, Quick Stop, Drive Enable, Prop Regulator Valve, Standby, Master Control Relay).
    e. Hit the STOP ALL button on the LDS state machine.
    f. Check to make sure the Dynamic function generator program is not running and there is no data response.
    g. Close the Dynamic function generator program, LDS State machine program, the LabVIEW software and turn off the operating console.

During the pilot experiment on the new LDS kick experiment setup, the drill pipe got stuck in the bit housing after kick occurred. This may be attributed to the selection of the internal diameter of the drill bit housing subsystem in the design of LDS. There was not enough clearance between the outer walls of the drill string and the inner walls of the bit housing. This clearance served as part of the annulus and rock cuttings were transported through it by the drilling fluid. However, some larger diameter cuttings were stuck in the bit housing area. This caused the drill string to deflect while rotating which culminated in making the drill string to wear in the region of the bit housing. This eventually caused the drill string to get stuck. It was observed on the operating console as a sudden and rapid rise in Torque. This prompted the operators to shut down the system using the emergency switch. It was also observed that some cutter in the drill bit was also worn out.

5 Data-driven Model Development Methodology

5.1 Introduction

Early detection of kicks is facilitated with the availability of downhole measurements, efficient communication of data to the processing devices and accurate processing of the data to identify anomalies. The authors have put forward the proof of concept for a simple computational data-driven solution that can be applied to early kick detection. This effort will motivate research for simpler computational solutions as kick monitoring technologies transition to miniaturized sensors, wireless communication, and machine learning. The development and adaptation of downhole monitoring and data-driven approaches are being seriously considered for field application. One such effort is led by a major oil and gas company, Total S.A., to address the three crucial areas that facilitate early detection. The first part is to develop miniaturized sensors that are easier to integrate to the bit/bottom-hole assembly and the drill-string to measure bottom-hole and annular flow. The second part is the development of wireless technology to efficiently transmit large amounts of data to the surface. The third part is to leverage on analytics and artificial intelligence to process the large amount of data and get the correct information out of them. More details can be found in [6]. Given the limited availability of downhole data from the field, a methodology that relies on experimental data in a laboratory is developed for data-driven modelling. The choice of machine learning algorithm to solve a real-world problem depends on how the problem statement is defined, source of data, aspects of the data that will guide decision making and the application domain. Machine learning could be carried out in a supervised, unsupervised, or semi-supervised manner. A supervised learning approach was adopted for building the kick detection model. This is because:

a. We want to quickly detect when an abnormal situation (kick event) occurs in a monitored process (drilling) from logged process data (data-driven inference).
b. The process data was obtained from a controlled experiment (supervised).
c. The collected data contains parameters (features) that are sensitive to a kick event.

The methodology in this research includes:

1. Data collection from two existing and a new kick detection experiment.
2. Data processing using neural network-based supervised machine learning technique.

The overall methodology is summarized in Figure 5-1. The author was further motivated to look for simple ANN models that would be sufficient for the kick detection problem because numerous papers report the use of complex neural networks to solve the problem without justifying the need for such complex solutions [23], [33], [39]–[41]. In many cases, the researchers arbitrarily select a complex neural network architecture, e.g. a neural network consisting of several neurons, then demonstrate that successful kick detection is achieved. However, in most cases, they do not provide a rationale for choosing such a complex network. One of the main motivations of the research reported in this paper is to explore whether simple ANNs would be capable of accomplishing this task. The author, however, acknowledge that the simple model has been tested only on a limited dataset, and so, for large field datasets, more complex networks might be warranted to achieve early kick detection. The authors believe that it would be prudent to try and identify the simplest possible solution in every case, and also contend that complex neural network architectures might not be necessary even if large datasets from oil fields are available. This is because a binary classification (kick or no-kick) is inherently a simple task, especially when combined with judicious selection and appropriate preprocessing of the input signals prior to applying them to the neural network.

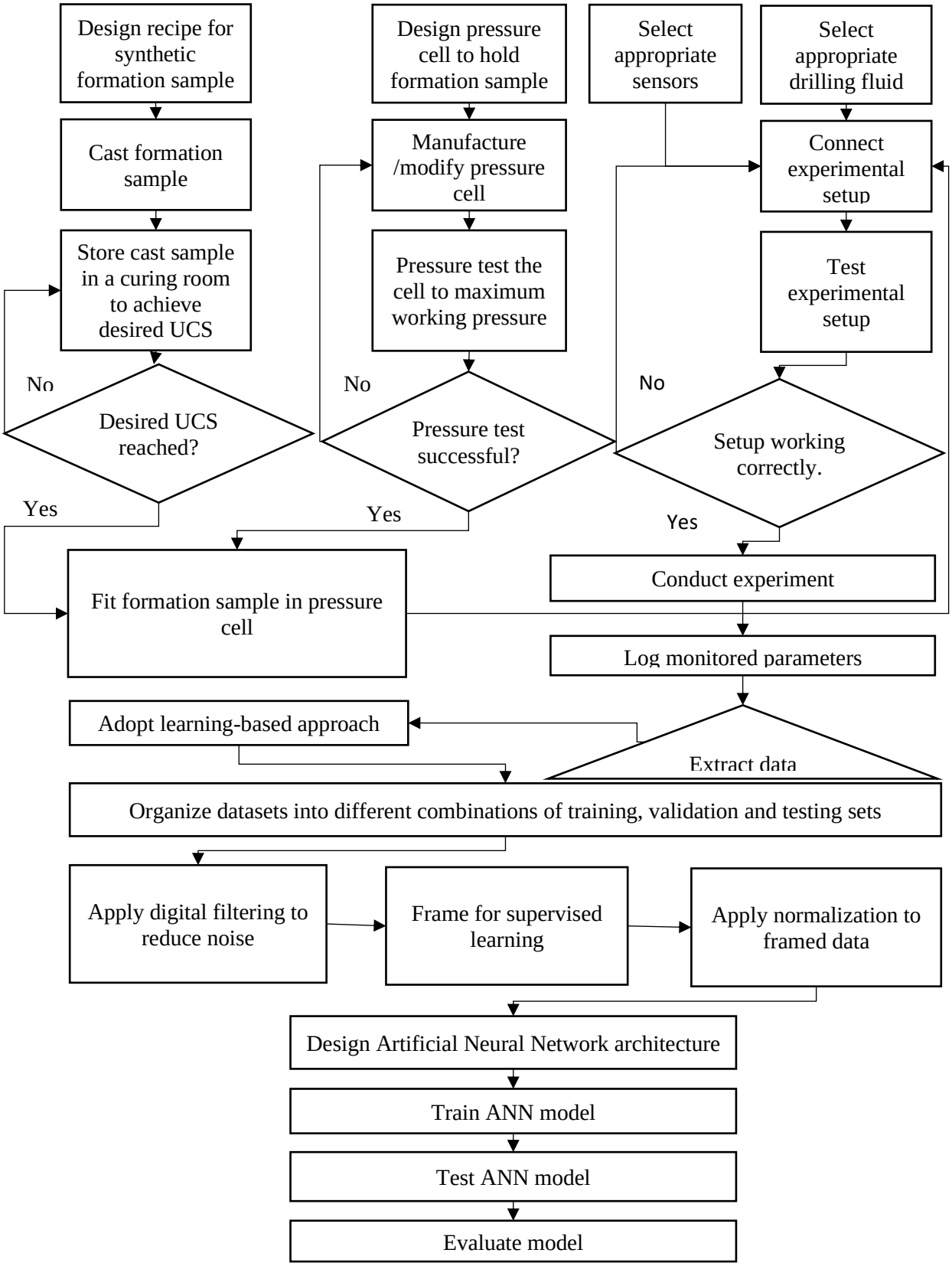

Figure 5-1: Flow diagram summarizing the methodology

5.2 Data Collection

Existing experimental data was collected from two kick detection experiments reported in [8] and [9]. This experiment was carried out on a Small Drilling Simulator (SDS) system with a kick injection system attached. New experimental data was collected from pilot kick detection experiment using a Large-scale Drilling Simulator (LDS) system with kick injection system attached. Both drilling systems are similar in processes but differ in three ways namely:

1. Size of drill motor.
2. Mode of operation.
3. Manner of kick initiation.

The SDS is powered by a 20kW drill motor and manually operated while the LDS is powered by a 33kW drill motor and fully automated with graphical user interface for control. Kick is initiated in the SDS system by manually opening the outlet valve of the kick injection system during drilling fluid circulation to allow air influx into the wellbore. In the LDS system, kick is initiated by drilling through a synthetic rock sample into a zone of trapped high-pressure air. The rock sample is designed to contain a cavity at the bottom where air can be trapped. Indeed, the small-scale kicks are different from large-scale field kicks. The present study provides a proof of concept.

5.2.1 Data from SDS kick experiments in [8].

This is an existing data source. In this experiment, kick happens during drilling fluid circulation. Details of the SDS system are provided in [9]. Time duration for each run in the experiment was at least 150 s, with influx manually initiated around the 70 s mark to last for 50 s before being terminated. The system input parameters are shown in Table 5-1. Six experiments were conducted with three scenarios (each repeated once) representing unique combinations of pump

mass flow-in rates (to circulate drilling fluid) and air influx volumetric flow rates (to inject kick fluid into the wellbore). Downhole pressure, mud flow-out rate, density and electrical conductivity values were monitored and recorded. The system input parameters and steady state values of monitored parameters when there was no influx, are shown in Table 5-1. Values recorded for air influx flow rate are representative of air leak into the pressure cell.

Table 5-1: System input parameters and corresponding values in the SDS kick experiment in [8].

Parameters	**Values**			**Units**
	Scenario 1	**Scenario 2**	**Scenario 3**	
Number of runs	2	2	2	
Mud pump flow rate	3580.00	4652.00	5597.00	lb/h
Initial downhole pressure	10.85	25.13	40.07	psi g
Air influx flow rate due to leak	0.80	0.67	0.65	SCFM
Maximum air influx flow rate during kick	7.00	4.00	2.700	SCFM
Electrical conductivity	106.00	108.00	108.00	uS/cm
Water based mud density	60.75	61.86	62.13	lb/ft3

5.2.2 Data from SDS Kick experiment in [9]

This is the second existing data source. In this experiment, kick is manually initiated after drilling through one-third of a completely predrilled synthetic rock sample. Influx continues until two-third of the rock sample is drilled and then stopped before proceeding to completely drill through the rock sample. In this experiment, air is not trapped within the rock sample. The system input parameters are shown in Table 5-2. It was reported in [7] that conductivity was not monitored because the conductivity sensor was incompatible with the drill cuttings. However, the SDS dataset obtained from the author in [7] contained conductivity data which exhibited anomalous behavior in every experimental run. This study attempts to investigate the impact of such anomalous behavior when contained in the test dataset. This provides insight on the detection capability of the ANN model when one of the four input parameters is faulty. In this

experiment, the conductivity data was abnormal because of a faulty conductivity sensor. This will enable us to demonstrate how our model will handle missing/faulty sensor data for a single parameter. The dataset contains six experimental scenarios.

Table 5-2: System input parameters and corresponding values in the SDS kick experiment in [9].

Parameters	**Values**	**Units**
Applied weight on bit	54.3	kg
Mud pump flow rate	6256	lb/h
Initial downhole pressure	30-35	psi
Air influx pressure	170-180	psi
Air influx flow rate	8-9	SCFM
Drilling motor rotary speed	292-300	rpm
Water based mud density	1000	kg/m3

5.2.3 Data from LDS kick experiment

This is new data, obtained from the experiment that was designed and conducted for the purpose of this research. In this experiment, kick is induced during actual drilling. Drilling fluid is circulated when the drill bit grinds through the synthetic rock sample (6" by 12") held in place by a pressured drilling cell and hits a zone of trapped high-pressure air.

Table 5-3: System input parameters and corresponding values in the LDS kick experiment conducted as part of this work.

Parameters	**Values**	**Units**
Applied weight on bit	2	kN
Mud pump flow rate	5000	lb/h
Initial downhole pressure	10	psi
Air influx pressure	90	psi
Air influx flow rate	0	SCFM
Drilling motor rotary speed	60	rpm
Water based mud density	62.4	lb/ft3

Before drilling, high-pressure air is trapped in a predrilled hole (½" by 4") at the bottom of the synthetic rock sample as shown in Figure 3-2. The air is supplied by a pneumatic kick injection system connected to the bottom of the drilling cell. This high-pressure zone contains the fluid to initiate a kick. The system input parameters are shown in

Table 5-3. Parameters recorded include drill bit position, observed WOB, pneumatic applied WOB, hydraulic applied WOB, rotary speed, torque, downhole pressure, mass flow-out rate, electrical conductivity, and density.

Supervised learning-based anomaly detection thrives on correctly labelled data that contains both input features and output labels during normal and abnormal conditions. Output labels are not always available in every dataset. The process of designating output labels is referred to as output labelling. This entails selecting some features on the dataset as the output of a supervised learning model or creating new labels in cases where no feature in the dataset corresponds to the desired output. There is no parameter in the collected data that reflects the desired model output. Typically, there are several anomalous drilling conditions such as pipe sticking, hole deviation, mud contamination etc. It is possible for a machine learning model to capture a wide range of drilling problems however this research focuses on kick events. A categorical attribute that indicates kick occurrence (‘Kick’ and ‘No kick’) will be added to every dataset. Therefore, for each instance of parameters in our dataset, a label that indicates ‘Kick’ or ‘No kick’ is assigned.

There are several machine learning algorithms such as logistic regression, decision tree [23] that could suffice for kick detection. However, they may not be easily tuned to capture complexities as the process dynamics evolves rapidly. Neural networks can be easily tuned to capture these complexities. Data-driven process models are derived from using historical process data (training data) to train a network (neural network). The training process maps functional relationships

between input and output features in the training data using an optimization algorithm that iteratively adjusts the network weights values. The weight values are adjusted to minimize the loss function between the model's predicted value and the supervised label of the training data. Optimization helps to fine tune the model based on the loss function calculated while training. Care needs to be taken to make sure the model performs well for new data from the same underlying process. To ensure this, validation data from the same process is used to monitor the model's ability to generalize. Weight regularization using the L2 norm was employed during training to avoid overfitting. It adds a fraction of the sum of squares of the model weights at the current training episode to the loss function during optimization, hence penalizing large weights. The trained and validated model is subsequently tested using new data from the same process (test data). The performance of the model in detecting kicks will be evaluated by calculating the classification accuracy between the model output when applied to the test data with the actual output from the drilling process.

5.3 Data Processing

5.3.1 Technology stack for data processing

Anaconda Distribution data science platform was chosen for data processing because it is an open source platform/industry standard for developing, training, testing data science and machine learning models on a single machine. Details such as scientific computing and machine learning libraries used are shown in Table 5-4.

Table 5-4: Details of technology stack used for data processing.

	Item	**Description**
Platform	Anaconda	Data science platform
Operating system	Windows	
Language	Python	
Dependency Manager	Conda	Manage packages needed for research analysis
Packages (Libraries)	Pandas	High level data structure handling from excel
	NumPy	Low level data handling and manipulation via multidimensional arrays
	Matplotlib	Data visualization
	Statsmodels	Filter design
	SciPy	Preprocessing algorithms
	Keras	Neural network modelling
	TensorFlow	Keras backend engine
	Scikit-learn	Model evaluation metrics
Virtual Environment used		Yes, above packages were installed in the virtual environment

5.3.2 Machine learning problem formulation

The machine learning system proposed in [42] is adopted to properly define our problem for suitability with supervised machine learning. The method requires identifying the Experience to be learnt from so that a Task can be performed with improving Performance. In this study, Experience, Task and Performance are defined as outlined:

Experience: Historical drilling data preprocessed into a multidimensional array of selected features which includes downhole pressure, mud flow-out rate, density, and electrical conductivity with corresponding label of 'kick' or 'no-kick' at each time step.

Task: Infer the kick label at the current time step by binary classification of the output of an ANN model. The model is developed to learn the interactions among downhole pressure, mud flow-out rate, density, and conductivity at the same time step. Kick occurs when there is an increase in downhole pressure and mass flow rate and decrease in conductivity and density. The functional relationship mapping is mathematically shown in Equation (5.3.1).

$$K_t = f\left(P_t^{downhole}, \dot{m}_t, \rho_t, \sigma_t\right) \tag{5.3.1}$$

In this equation, f is the classified ANN function that transforms time instances of the preprocessed experimental data to an output value, K is the kick label, P is the downhole pressure, $\dot{m}$ is the mass flow out rate, ρ is the density, σ is the electrical conductivity of the drilling fluid and n is the number of time steps considered.

Performance: Confusion matrix, classification accuracy, missed detection rate, false detection rate, and detection time.

5.3.3 Selecting training and test datasets

Datasets were obtained from three experiments and combined for selecting training, validation, and test sets used in building and evaluating the neural network model. The datasets captured three periods of the kick experiment namely 'Before Kick', 'During Kick' and 'After Kick'. However, only two periods of the dataset capturing 'Before Kick' and 'During Kick' will be extracted for analysis. This is because the focus is on detecting when the kick event occurs. Each

dataset will be assigned a pseudo-name for easy referencing in this Thesis. The available datasets are shown in Table 5-5.

Table 5-5: Available dataset, source and pseudo name.

Pseudo name	**Scenario**	**Number of datapoints extracted**	**Data Source**	**Purpose**
SDS1-run1a	Scenario 1a	1100	Islam et al. [8]	Training
SDS1-run1b	Scenario 1b	1100	Islam et al. [8]	Validation
SDS1-run2a	Scenario 1b	1100	Islam et al. [8]	Training
SDS1-run2b	Scenario 1b	1100	Islam et al. [8]	Validation
SDS1-run3a	Scenario 1b	1100	Islam et al. [8]	Training
SDS1-run3b	Scenario 1b	1100	Islam et al. [8]	Validation
SDS2-run1	Scenario 1	520	Sule et al. [9]	
SDS2-run2	Scenario 2	684	Sule et al. [9]	
SDS2-run3	Scenario 3	1145	Sule et al. [9]	
SDS2-run4	Scenario 4	1238	Sule et al. [9]	Testing
SDS2-run5	Scenario 5	2457	Sule et al. [9]	Testing
SDS2-run6	Scenario 6	948	Sule et al. [9]	Testing
LDS-run1	Scenario 1	380	Current work	Testing
Any of the dataset can be used for validation during the training process except those used for training. Scenario refer to operating conditions. a, b refers to repeat experimental runs for the same scenario				

Each of the experimental datasets contains a single kick event. A major drawback of applying neural network solutions is the difficulty in maintaining accurate performance for new input data that was not encountered during training. This happens when there has been overfitting of the training data and is known as the generalization problem. Special attention was paid to the ability of the developed neural network model to generalize well when deployed. It is important to note that the dataset from [9] contains faulty conductivity data. As a result, it will not be used in training any model. Given that available dataset covers three circulation scenarios from [8], six drilling scenarios from [9] and a single drilling scenario from the current work, three neural

network models will be trained using each scenario in [8] respectively which represents data from the SDS system.

Table 5-6: Combination of available dataset to select training, validation and test dataset.

Instance	Model	Training set	Validation set	Test set	Drilling system
1.	1	SDS1-run1a	SDS1-run2b	SDS1-run3a	SDS
2.				SDS2-run4	
3.				LDS-run1	LDS
4.	2	SDS1-run2a	SDS1-run3b	SDS1-run1a	SDS
5.				SDS2-run5	
6.				LDS-run1	LDS
7.	3	SDS1-run3a	SDS1-run1b	SDS1-run2a	SDS
8.				SDS2-run6	
9.				LDS-run1	LDS

The trained model will be tested to demonstrate its ability to generalize and handle faulty sensor data in the following ways:

1. To show that the model trained from one scenario of the SDS kick experiment data in [8] has the potential for generalization with other scenarios of the same system, the trained model was tested with data from a different scenario of the SDS experiment in [8].
2. To evaluate the impact of a faulty sensor data on the detection capability of the trained model, the model was tested with data from SDS kick experiments in [9] which contains faulty conductivity data.

3. To show that the model trained with data from one drilling system (SDS) has the potential to generalize to LDS system (LDS), the trained model from the SDS kick experiment in [8] was tested with data from the LDS kick experiment in this research.

This approach was adopted because of the non-availability of large amount of data. Only three models were trained, each model using a particular scenario from [8] respectively. The selection approach described above affords the opportunity to test a trained model with data from same and LDS system as shown in Table 5-6. It also affords us the opportunity to demonstrate the capability of the model to handle faulty sensor data.

5.3.4 Preprocessing

The experimental data was preprocessed to make it a suitable input for the neural network. Four parameters from the pool of recorded parameters, namely, downhole pressure, mud flow-out rate, density and conductivity were filtered and normalized. These parameters are selected considering fluid flow and pressure parameters variation are quickly evident downhole during a kick. The higher pore pressure of the kick fluid would force the existing fluid up (increase in downhole pressure) and cause an influx (increase in mass flow rate), then mix with the existing fluid (alter density and conductivity). Other parameters recorded are weight on bit, rotary speed, pump pressure and torque which are surface parameters.

Process and measurement noise in the recorded data were filtered out using a lowpass digital Finite Impulse Response (FIR) filter. Transformation of the selected features from time domain signal to frequency domain spectrum revealed the contributing discrete frequencies and was achieved using the Fast Fourier Transform (FFT) algorithm of the Discrete Fourier Transform described in [43].

Spectral analysis is useful in determining the cutoff frequency of the appropriate digital filter. The cutoff frequency and a filter order of 4 were used to generate an impulse response, the convolution of noisy data and the impulse response yields our filtered response as shown in Figure 5-2 and Figure 5-3.

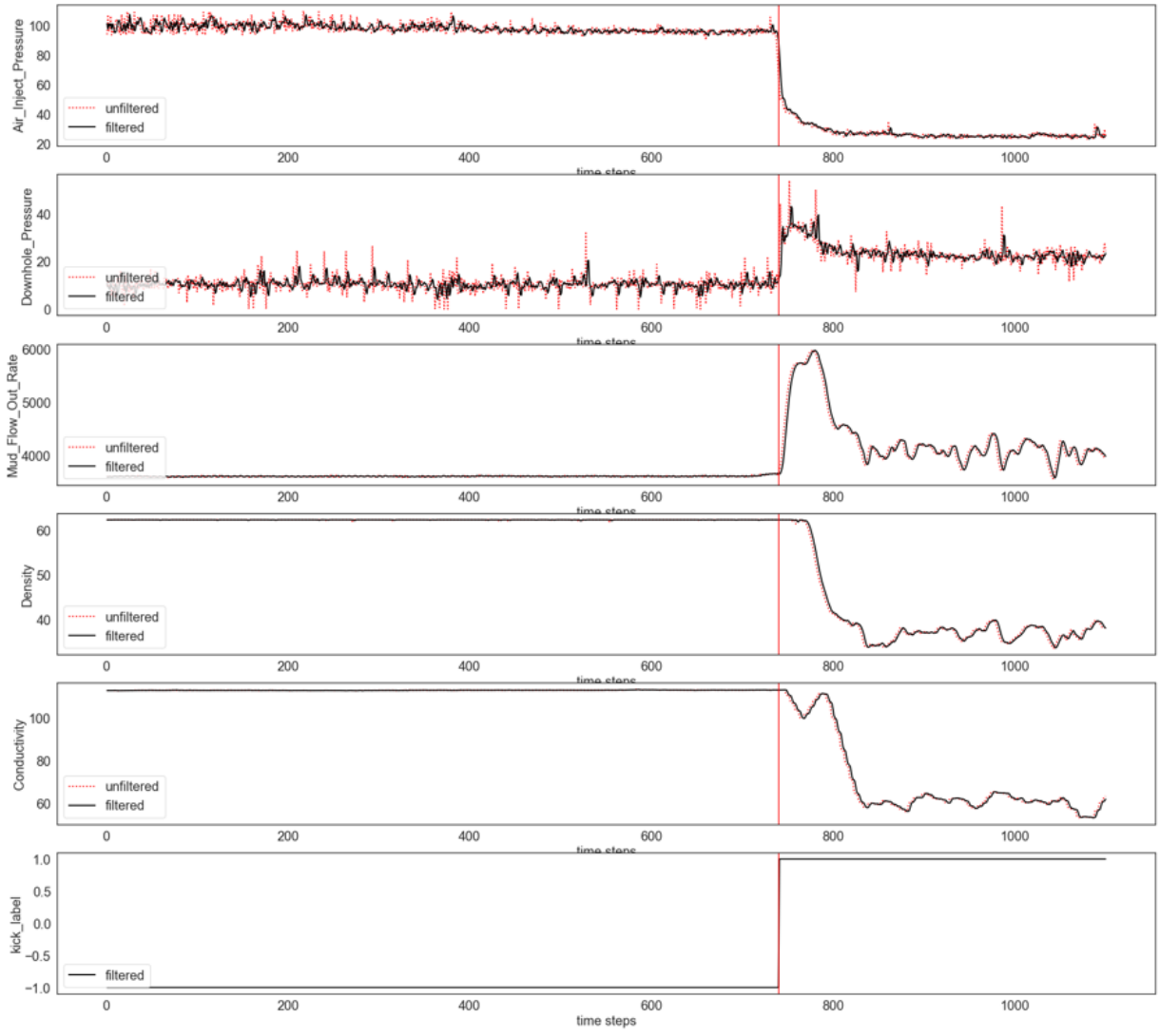

Figure 5-2: Plot of raw and filtered experimental data from scenario 1a of the SDS kick experiment. Pressure units in psi, flow rate in lb/h, density in lb/ft3 and conductivity in uS/cm.

Data values are normalized using Equation (5.3.2) to a feature range of -1.0 to +1.0 which corresponds to the encoded values of the system condition (-1 for no-kick and +1 for kick).

$$X_{norm} = \frac{X_i - X_{min}}{X_{max} - X_{min}} * (R_{max} - R_{min}) + R_{min} \quad (5.3.2)$$

In this equation, X is the unnormalized data, i, refers to a data point and R is the chosen feature range. The last plot in Figure 5-2 and Figure 5-3 titled “kick label” represents encoded values of the system condition namely no-kick (-1) and kick (+1). These will be the class labels for binary classification of the neural network model output.

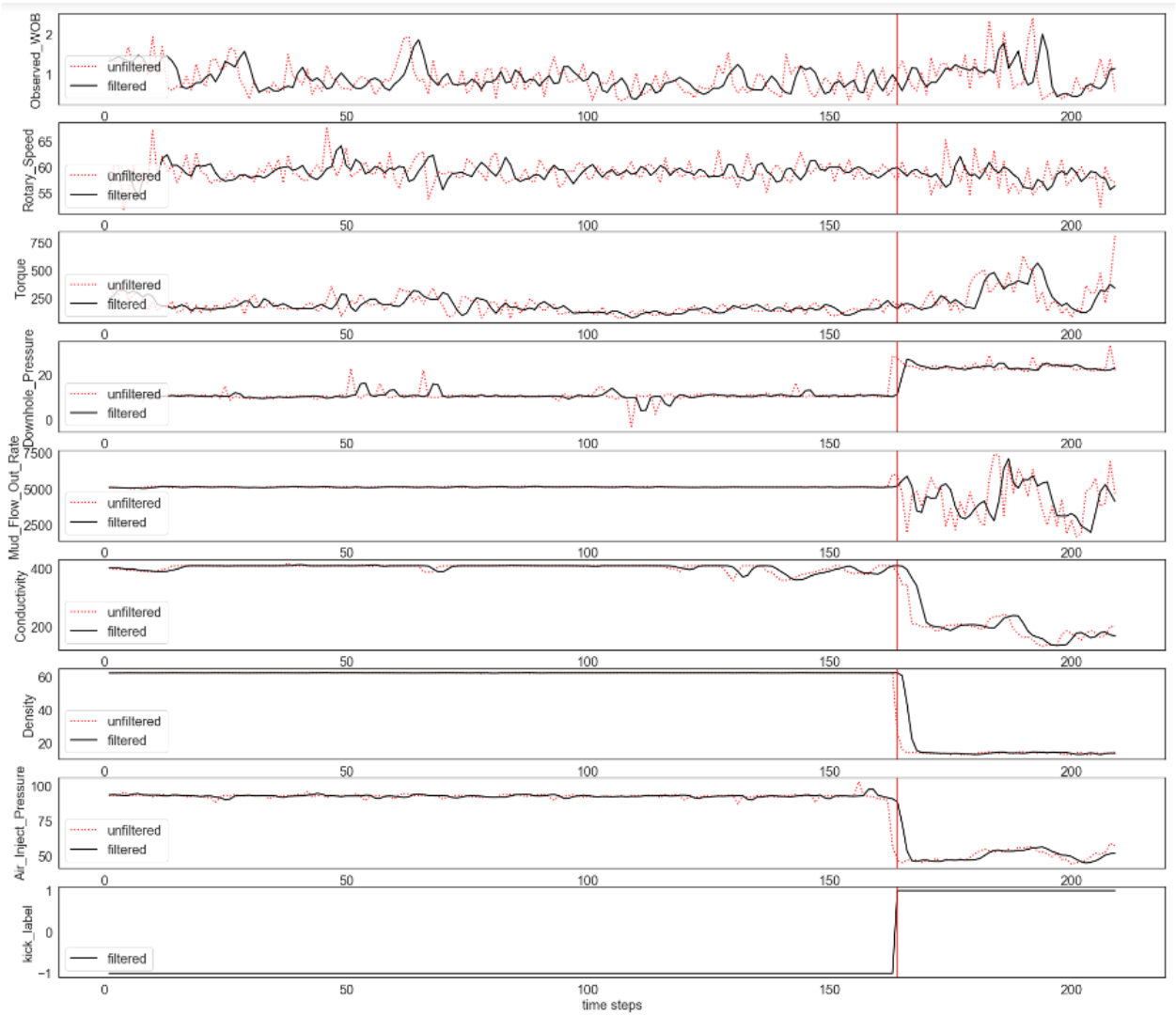

Figure 5-3: Plot of raw and filtered experimental data from LDS kick experiment. Pressure units in psi, flow rate in lb/h, density in lb/ft3, conductivity in uS/cm, WOB in kN, rotary speed in rpm and torque in lb-ft.

5.3.5 Comparing simple and complex neural network architectures

Several neural network architectures were investigated for training a supervised learning-based kick detection model using the available data. They include Artificial Neural Network (ANN), Recurrent Neural Networks (RNN) [44], [45], [46], Long Short Term Memory variant of RNN, (LSTM-RNN) [47], [48] and Gated Recurrent Unit variant of RNN, (GRU-RNN) [49], [50]. Other classical machine learning algorithms such as logistic regression, decision tree [23] could suffice for kick detection. However, they may not be easily tuned to capture complexities as the process dynamics evolves rapidly. Neural networks can be easily tuned to capture these complexities. The train-validation-testing data combination employed was instance 1 from Table 5-6. To begin, an arbitrary network structure for each architecture was built for this purpose. All network structure had four nodes in the input layer. The LSTM-RNN and GRU-RNN structure had two LSTM/GRU hidden layer with sixteen nodes and an output layer of a regular feedforward neural network with one node. The ANN and RNN structures had two hidden layers with eight and two nodes, respectively, and an output layer with one node. Kick was successfully detected for every structure tested with no false alarms or missed detections.

Furthermore, the simplest network structure for each architecture was then investigated. All network structure had four nodes in the input layer. The ANN and RNN structure had no hidden layers and an output layer with one neuron. The LSTM-RNN and GRU-RNN structure had one LSTM/GRU hidden layer with one neuron and an output layer of a regular feedforward neural network with one neuron. The learning curve showing training and validation loss for LSTM, GRU, RNN and ANN models are shown in Figure 5-4, Figure 5-5, Figure 5-6 and Figure 5-7 respectively.

Table 5-7: Simplest network structure of several neural network architecture compared for kick detection modelling.

Neural network architecture	Input layer	Hidden layer	Output layer
LSTM-RNN	4 nodes	1 LSTM unit	1 node
GRU-RNN	4 nodes	1 GRU unit	1 node
RNN	4 nodes	0	1 node
ANN	4 nodes	0	1 node

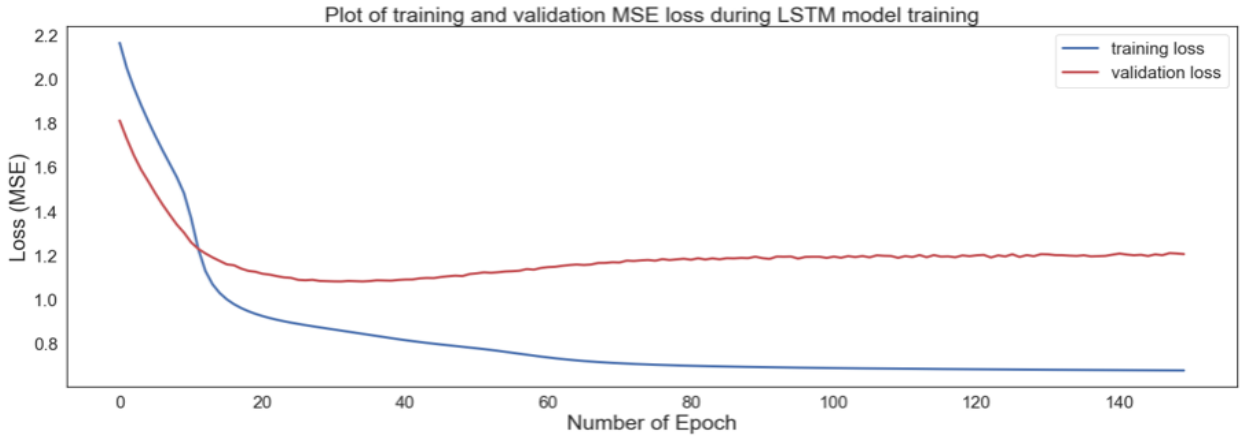

Figure 5-4: Learning curve showing training and validation loss for LSTM model training.

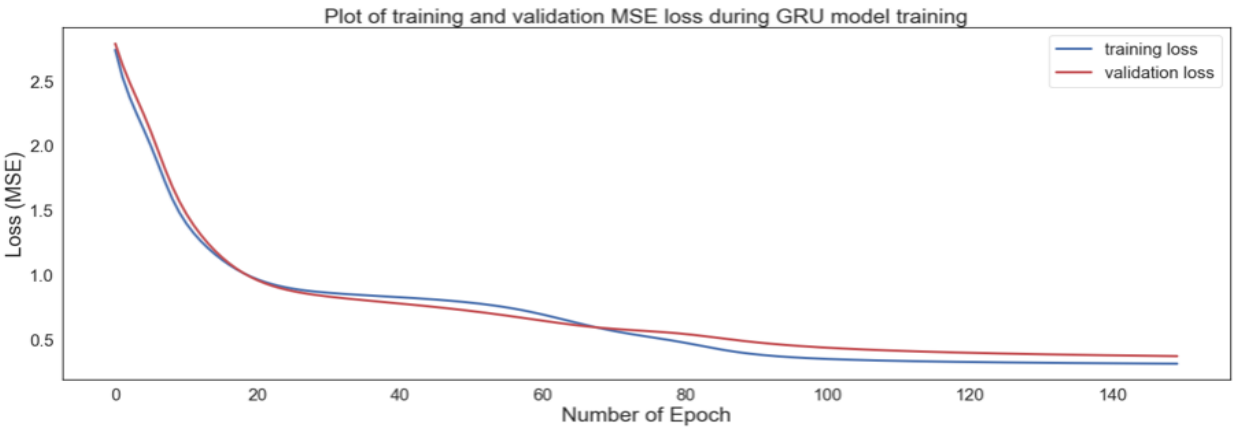

Figure 5-5: Learning curve showing training and validation loss for GRU model training.

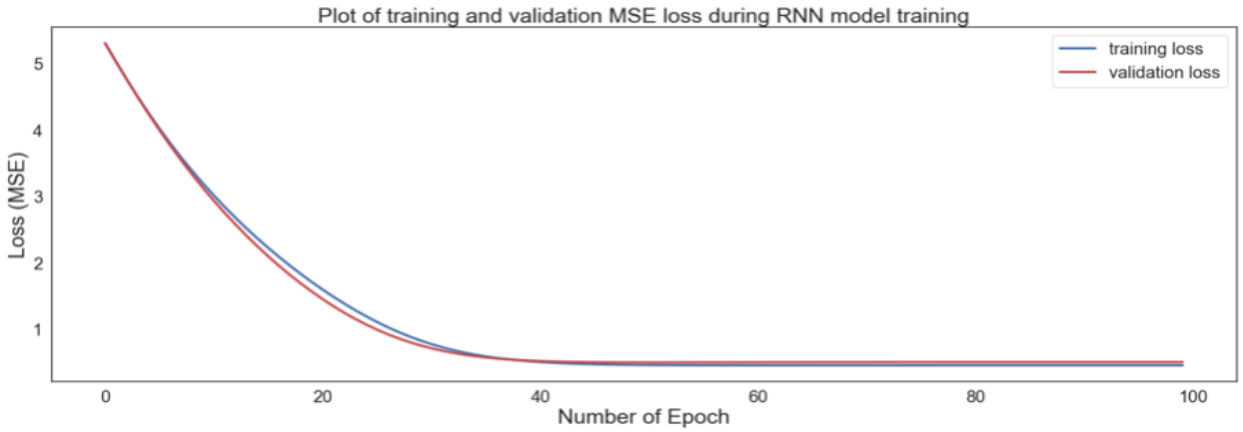

Figure 5-6: Learning curve showing training and validation loss for RNN model training.

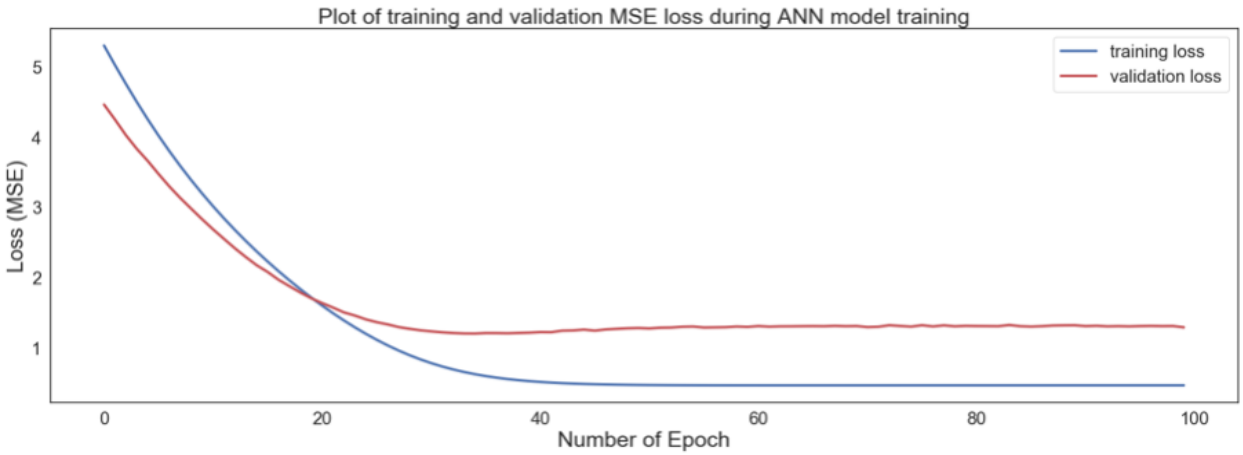

Figure 5-7: Learning curve showing training and validation loss for ANN model training.

The RNN structure and its variants were implemented as a standard fully connected network where the output is fed back to the input and not as an unfolded structure. Model performance such as classification accuracy, precision, recall, F1-score, false alarm rate and missed detection rate achieved was similar for the above architectures as shown in Table 5-8. The plot of the result from testing the LSTM, GRU, RNN and ANN kick detection model using scenario 3a of the SDS data in [8] is presented in Figure 5-8, Figure 5-9, Figure 5-10 and Figure 5-11 respectively.

Table 5-8: Performance evaluation of the LSTM, GRU, RNN and ANN model for kick detection.

		LSTM	**GRU**	**RNN**	**ANN**
Classification accuracy		0.96	0.95	0.95	0.95
Confusion Matrix	0,0	722	722	722	722
	0,1	0	0	0	0
	1,0	46	58	58	58
	1,1	332	320	320	320
Precision	No-Kick	0.94	0.93	0.93	0.93
	Kick	1.00	1.00	1.00	1.00
Recall	No-Kick	1.00	1.00	1.00	1.00
	Kick	0.88	0.85	0.85	0.85
F1-Score	No-Kick	0.97	0.96	0.96	0.96
	Kick	0.94	0.92	0.92	0.92
Support	No-Kick	722	722	722	722
	Kick	378	378	378	378
False Alarm		No	No	No	No
Missed Detection		No	No	No	No

The capability of a simple ANN architecture, as can be seen in Figure 5-11, to model the available experimental data and deliver on the task of kick detection makes it attractive. Most papers in the literature use much more complex structures [23], [33], [39]–[41]. We concluded not to proceed with a complex architecture for the current study after trying several complex and simple architecture. Simplicity improves reliability when implemented in hardware, requires fewer components (thus improving dependability), and reduces the carbon footprint of our solution.

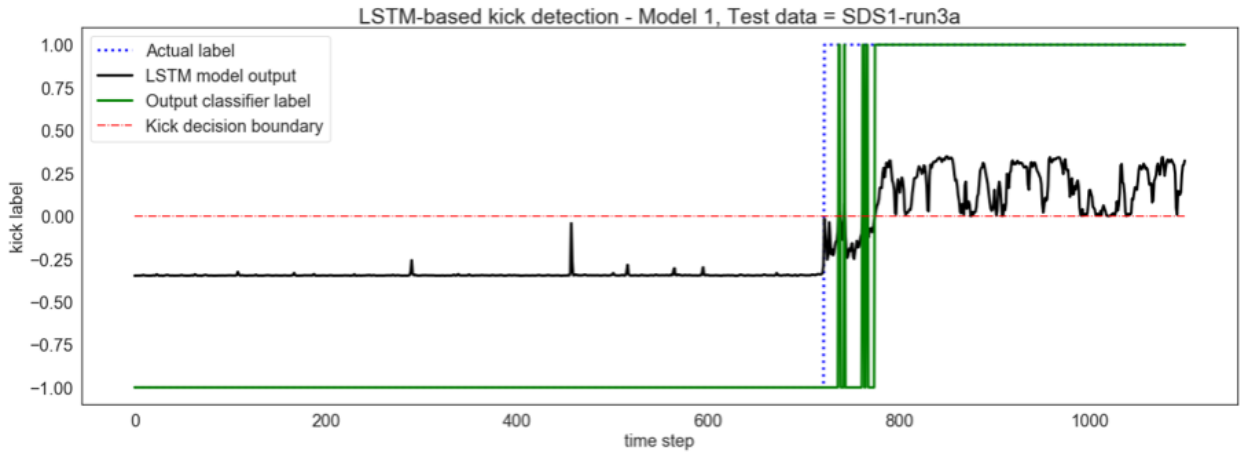

Figure 5-8: LSTM-based kick detection using downhole pressure, mud flow-out rate, density and conductivity – Model 1.

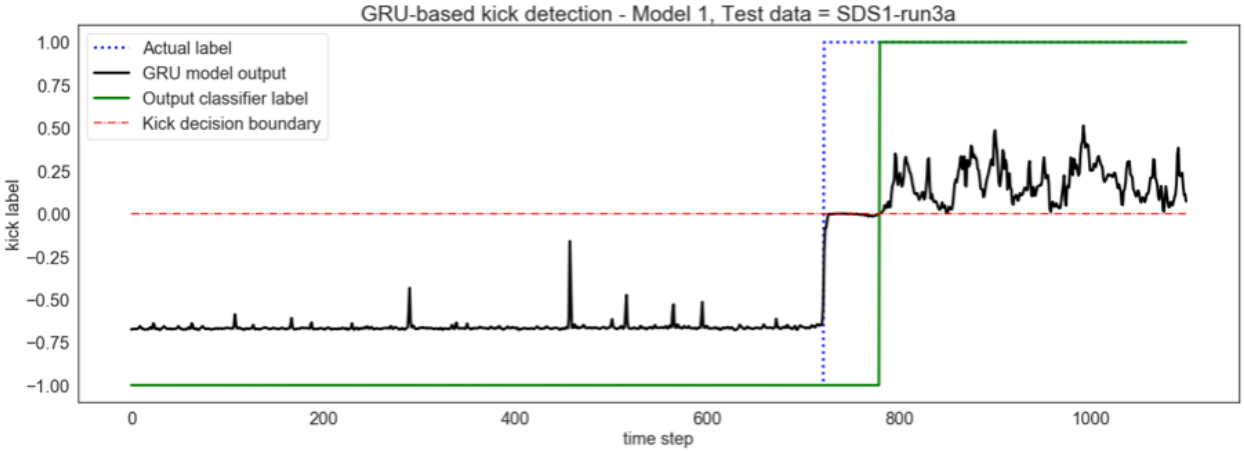

Figure 5-9: GRU-based kick detection using downhole pressure, mud flow-out rate, density and conductivity – Model 1.

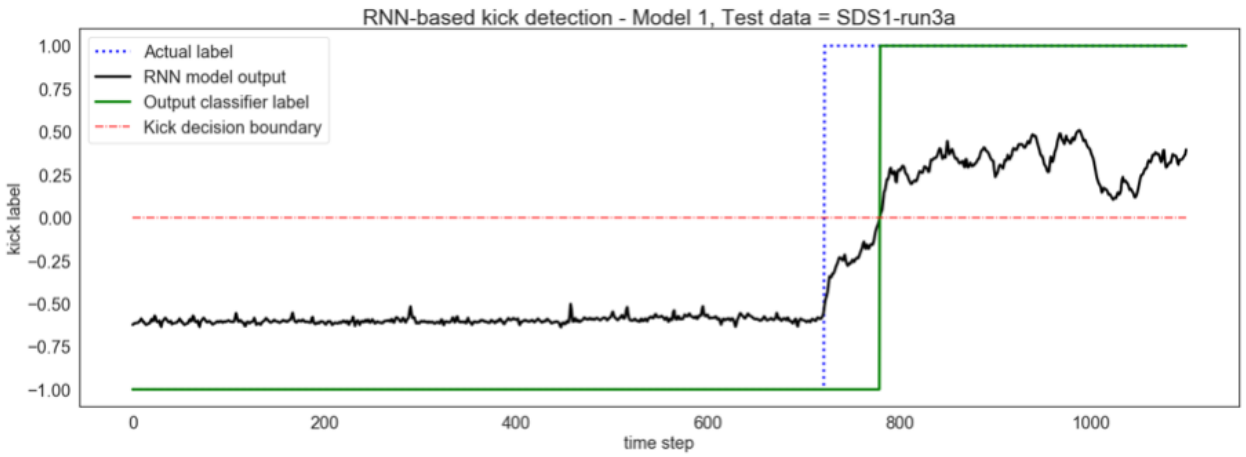

Figure 5-10: RNN-based kick detection using downhole pressure, mud flow-out rate, density and conductivity – Model 1.

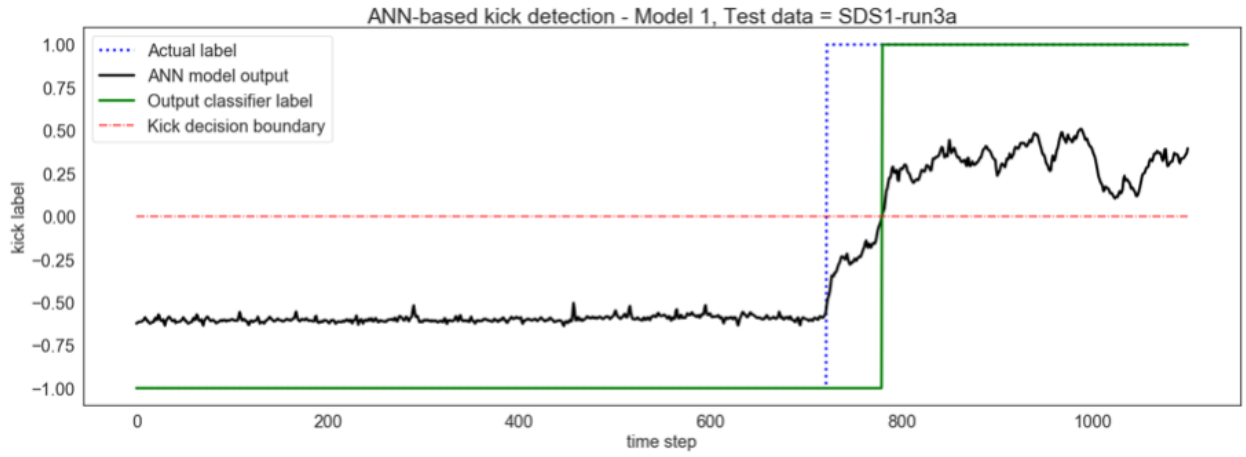

Figure 5-11: ANN-based kick detection using downhole pressure, mud flow-out rate, density and conductivity – Model 1.

The ANN architecture is adopted and further tested. There are other machine learning methods which are simpler, for example, logistic regression. Such methods were not employed because this work focuses on the use of neural network-based machine learning technique considering its learning ability and simple architecture.

5.3.6 ANN architecture design

The details of the ANN architecture used to model the experimental data are further discussed. A simple feedforward ANN with four, three or two nodes in the input layer, no hidden layer and one neuron in the output layer as shown in Figure 5-12 is capable of learning the relationship between the values of the four input parameters and the kick status at any given timestep. The one neuron model is a basic linear model if the activation function used is a linear activation function. Such a model is simply a linear transformation of input to output. In this study, a nonlinear activation function such as tanh is used. This introduces nonlinearity to the linear weighted sum of inputs during training. Also, to capture the corresponding increase and decrease in different parameters when a kick occurs, normalization was done in the range -1 to +1. This favored the use of tanh which has a range of -1 to + 1.

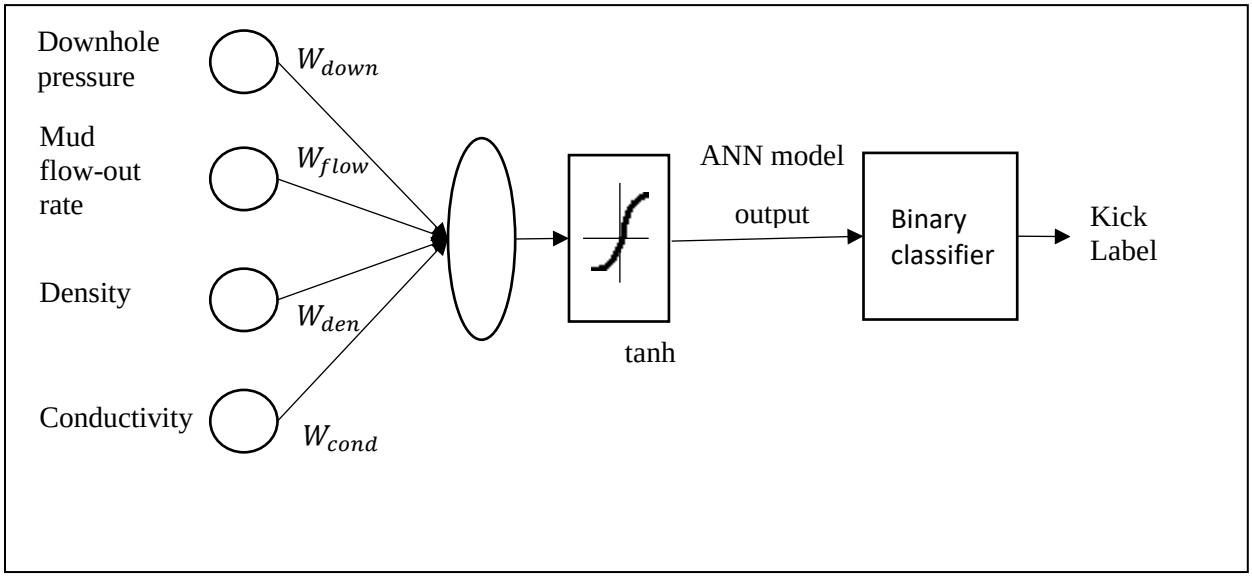

Figure 5-12: Hybrid ANN-Binary classifier architecture with four input parameters and no hidden layer used in modelling the experimental data.

The resulting hybrid architecture is represented by Equation (5.3.3).

$$f(x)_t = \begin{cases} -1, & \tanh(x_t.\mathrm{W}) < 0 \\ 1, & \tanh(x_t.\mathrm{W}) \geq 0 \end{cases} \quad (5.3.3)$$

In this equation, tanh is an activation function, $x_t$is the 4 by 1 input vector at time t with members shown below in Equation (5.3.4), W is the 1 by 4 input weight matrix, $f(x)_t$ is the kick label at time t.

$$x_t = [Downhole\ pressure, Mud\ flow_{out} rate, Density, Conductivity] \quad (5.3.4)$$

Thus, a hybrid supervised learning algorithm using a feedforward ANN with no hidden layer and one output neuron coupled to a binary classifier was adopted and tested in this work.

5.3.7 Parameter significance

This work dwells on the significance of drilling parameters in characterizing the early onset of anomalous drilling event such as a kick. It is proposed that this significance can be derived from proper interpretation of link weights in the ANN model as studied in [51], [52] and [53]. Weights represent the magnitude of influence an input value has on a neuron. Most discussions in literature on ANN assume that the neural network contains one or more hidden layers. In this general case, it would be difficult to come up with a direct relationship between link weights and parameter significance. In the degenerate case of ANN being used in this study, i.e. ANN without any hidden layers, basically, we have one neuron at the output layer that does a weighted sum of the input values and applies the activation (tanh) function to get a value between -1 and 1. The simplicity of this structure makes it straightforward to come up with a direct relationship between the significance of the input parameter and the weight of the corresponding link. Further still, the weights assigned to input parameters could be positive or negative. While positive-valued weights can be said to positively influence (excitatory) the output neuron, negative-

valued weights act in reverse (inhibitory). Therefore, parameters that consistently get assigned positive-valued weights in the ANN model would be more significant in achieving early detection.

5.3.8 Model training

The weight matrix in the input layer is initialized to a column vector containing all-ones. This assigns equal influence on all input parameters prior to training. The weights are updated iteratively during training by adaptive moment estimation (Adam) optimization algorithm given in [54]. Adam algorithm was employed with a default hyperparameter settings of learning rate of 0.001 and exponential decay rates of 0.900 and 0.999 for the first and second moment estimates, respectively. The mean squared error (MSE) is used as loss/objective function as can be seen from the learning curve in Figure 5-7. To maintain the output of the neuron in the output layer between -1 for normal operating condition (no-kick) and +1 for kick conditions, tanh activation function is applied at the output layer and then the result after activation goes into a binary classifier to determine how that data instant is to be classified. A four-input parameter model is trained, resulting in one trained model for each scenario. It was observed after training that the resulting model weights for any given scenario are the same, irrespective of the validation set considered. This happens because the models are fit on a training set. The validation set serves to monitor the loss when the trained model is tested with it as shown in Figure 5-13, Figure 5-14 and Figure 5-15. If undesirable, this loss guides us in tuning the hyperparameters of the architecture then retraining the model until we achieve the desired performance while the training set determines the weights of the model.

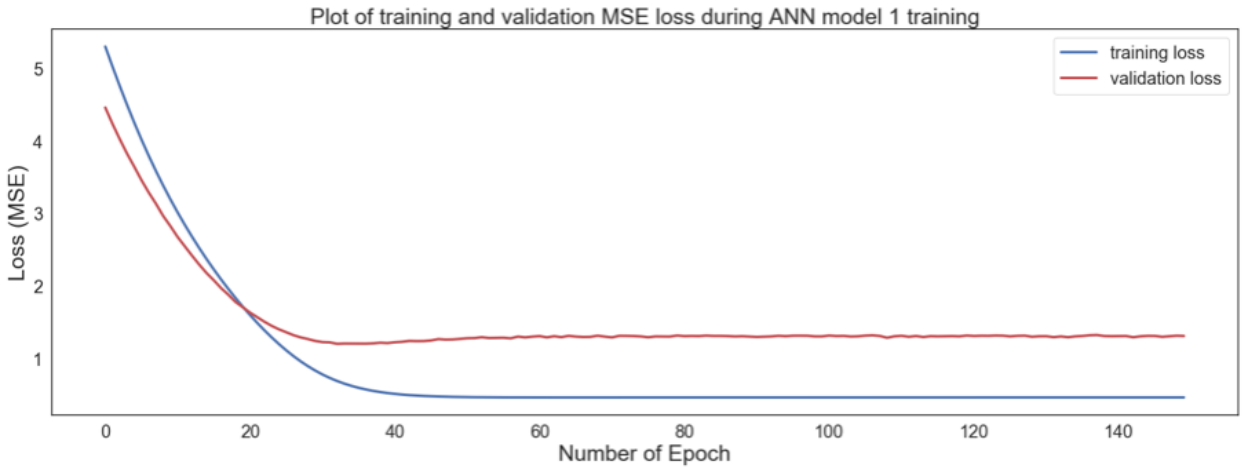

Figure 5-13: Learning curve showing training and validation loss for ANN model 1.

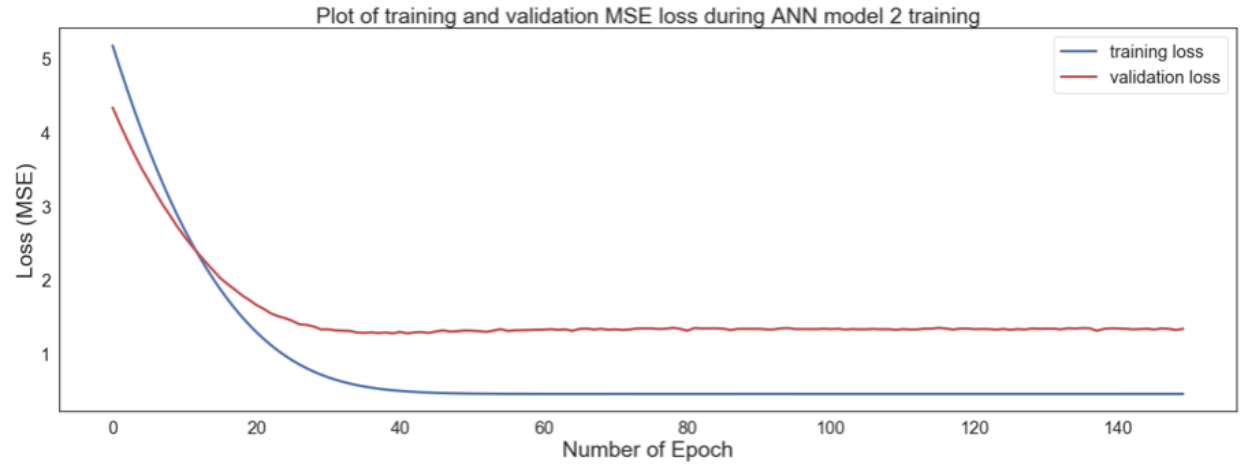

Figure 5-14: Learning curve showing training and validation loss for ANN model 2.

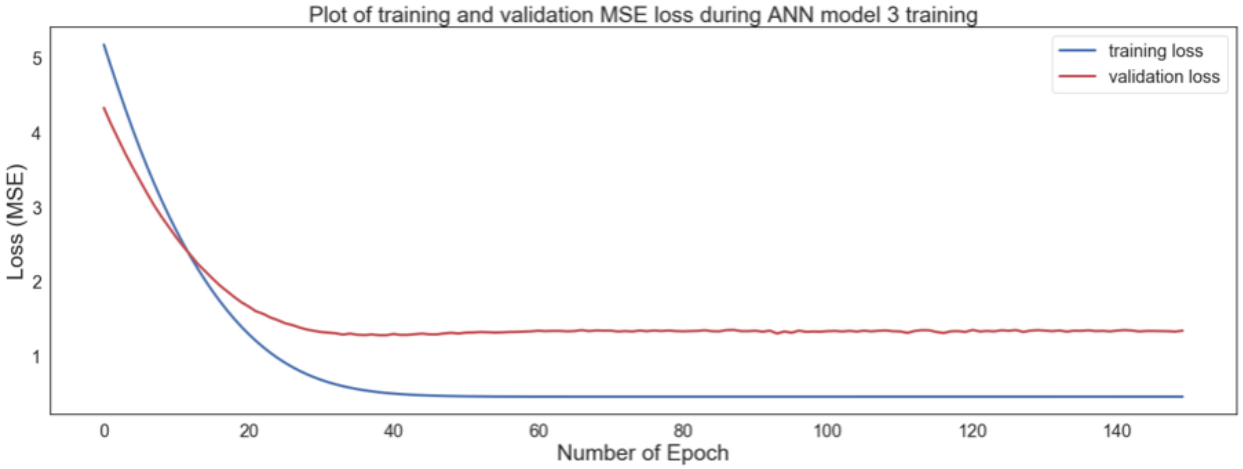

Figure 5-15: Learning curve showing training and validation loss for ANN model 3.

Different combinations of downhole parameters are also trained, tested, and evaluated as follows:

1. Two out of four parameters at a time are used to train an ANN model. This results in six possible combinations.
2. Three out of four parameters at a time are used to train an ANN model. This results in four possible combinations.

5.3.9 Model testing and evaluation

Test data from two LDS systems were applied to the trained model with view of quickly detecting the kick event as outlined in Table 5-6. The two, three and four input-parameters models were evaluated on basis of classification accuracy, precision, recall, F1-score, false alarm rate and missed detection rate.

Missed detection would imply the inability of the model to correctly identify all the data points representing a kick event in any of the test dataset. This could be potentially flagged by a low classification accuracy. False detection is said to occur if the model outputs a kick label in the period before a kick. This can be present even in presence of a high classification accuracy as shown in Table 6-7. Detection time accounts for how long it takes the model to capture the kick event upon occurrence. This is a very critical factor in any early warning system. The test results are presented in the following section and evaluated in Table 6-2, Table 6-4 and Table 6-6.

A confusion matrix provides the ability to visualize the performance of a machine learning classification model. It allows more insight on performance compared to classification accuracy. It provides information such as false positives, false negatives, true positives, and true negatives in a table with two rows and columns. This information can be used to calculate the recall

(probability of detection), probability of false alarm, precision, accuracy, F1-score etc. as shown in the Equations (5.3.5), (5.3.6), (5.3.7), (5.3.8), (5.3.9), (5.3.10), (5.3.11) and (5.3.12).

Table 5-9: Confusion matrix for "No kick" and "Kick" class labels.

Confusion matrix		**Actual class label**	
	Total datapoint	No kick	Kick
Predicted class label	No Kick	True Positive (TP)	False Positive (FP) Type I error
	Kick	False Negative (FN) Type II error	True Negative (TN)

True Positive Rate (TPR) or Recall or Sensitivity or the Probability of detection is obtained by

$$TPR = \frac{TP}{TP+FN} \tag{5.3.5}$$

False Positive Rate (FPR) or Probability of false alarm is obtained by

$$FPR = \frac{FP}{FP+TN} \tag{5.3.6}$$

False Negative Rate (FNR) or Miss rate is obtained by

$$FNR = \frac{FN}{FN+TP} \tag{5.3.7}$$

True Negative Rate (TNR) or Selectivity or Specificity is obtained by

$$TNR = \frac{TN}{TN+FP} \tag{5.3.8}$$

Positive Predictive Value (PPV) or Precision is obtained by

$$PPV = \frac{TP}{TP+FP} \tag{5.3.9}$$

Negative Predictive Value (NPV) is obtained by

$$NPV = \frac{TN}{TN+FN} \tag{5.3.10}$$

Accuracy is obtained by

$$Accuracy = \frac{TP+TN}{TP+TN+FP+FN} \tag{5.3.11}$$

F1 Score is obtained by

$$F1 = \frac{2TP}{2TP+FP+FN} \tag{5.3.12}$$

Recall that during training, all model inputs were initialized to have unit and equal weight on the output parameter (kick label). Varying values of this weight at the end of training are obtained from the gradient descent-based optimization algorithm used.

6 Results and Discussion

The results from testing the four-input, three-input, and two-input parameter ANN models have been presented here. The vector representing the four input parameters fed into the input layer of the network is shown in Equation (5.3.4). All selected input features into our model are known to be practically relevant in detecting kick events. However, as time to detect a kick is paramount to preventing a blowout and executing the appropriate well control strategy with minimal downtime, emphasis should be shifted to early detection parameters to enhance their monitoring capabilities and improve safety. ANN has been used to model surface parameters such as weight on bit, rpm, torque, pump pressure, rate of penetration. It works well for these surface parameters. The use of ANN for the downhole measurements provide an early kick detection tool and this approach is first time attempted in [55]. This study builds on previous studies and dynamic similarity between experiment and real scenario data have been demonstrated in previous studies [7], [9].

The authors understand and agree that one-neuron model testing may give impression of overly simplistic testing that is far away from the reality. While this impression has a reasonable basis, testing results may be true in most cases; one of such cases is the present study.

The authors acknowledge the limitation in accessing real world data and also that an experimental model is only a replica of real-life situation (often a simplified replica), which is true in the present case. The present study focused on few parameters (pressure and fluid-related) and discovered that these parameters behaved in a manner similar to in real life. However, other parameters which are better controllable were kept constant like ROP, WOB, and torque. Holding these parameters constant has simplified the experiment and observation. It is mentioned in the conclusion section that these parameters can be considered in future studies.

The model performance is analyzed using confusion matrix in order to provide a better perspective. The confusion matrix for the present study is based on the test results, and it provides understanding of classification efficiency. The training and testing data used to develop the confusion matrix comes from two periods during a drilling operation namely 'Before Kick' and 'During Kick'. The output label of the ANN model contains two classes namely 'No Kick' and 'Kick'. Given below are the details of the confusion matrix elements.

Before Kick:

- Predicted 'No kick' is equivalent to first row in confusion matrix TP [0,0] and FP [0,1].
- Actual 'No kick' is equivalent to first column in confusion matrix TP [0,0] and FN [1,0].

The model must label every data instance as 'No Kick' throughout this period (TP = number of data instances in 'Before Kick' period). Any data instance in this period labelled as 'Kick' implies a false alarm (FP = 0).

During Kick:

- Predicted 'Kick' equivalent to second row in confusion matrix FN [1,0] and TN [1,1].
- Actual 'Kick' equivalent to second column in confusion matrix FP [0,1] and TN [1,1].

The model needs to label a data instance in this period as 'Kick' (TN > 1). It must not label every data instance as 'Kick' throughout this period (FN >= 0). Subsequent data instance in the "During Kick" period may assume any class label.

The next subsection shows the results of the three four-input parameter ANN models which are trained from the three scenarios of the SDS kick experiment in [8]. The following subsection shows results of the three-input parameter ANN model. This model considered a combination of three out of four parameters from the first scenario of the SDS kick experiment in [8]. The third

subsection shows results of the two-input parameter ANN model. This model considered a combination of two out of four parameters from the first scenario of the SDS kick experiment in [8]. The last subsection in this section features further discussions related to three-input, two-input and single-input parameters, and a brief mention of ANN application in a managed pressure drilling system**.**

6.1 Four-input parameter ANN model

There are five sets of results for each four-input parameter ANN model. They include values of training features for each model and their corresponding label, plot from testing with data from SDS system, plot from testing with data from SDS system that includes faulty conductivity data, plot from testing with data from LDS system and model evaluation metrics for all three test cases. The results are presented for model 1, model 2 and model 3, respectively. For each model,

1. The first result in Table 6-1, Table 6-3 and Table 6-5 respectively shows the values of training features, corresponding label and four-input parameter ANN model output before and after kick event with data from different scenario of the SDS kick experiment in [8].
2. The second result in Figure 6-1, Figure 6-4 and Figure 6-7 respectively is a plot showing results of testing the model with the same data as above.
3. The third result in Figure 6-2, Figure 6-5 and Figure 6-8 respectively is a plot showing results of testing the model with data from SDS kick experiment in [9] that contains faulty conductivity data.
4. The fourth result in Figure 6-3, Figure 6-6 and Figure 6-9 respectively is a plot showing results of testing the model with data from LDS kick experiment.
5. The fifth result in Table 6-2, Table 6-4 and Table 6-6 respectively is a table that presents the confusion matrix and summarizes model performance metrics such as accuracy, recall, precision, F1-score, missed detection and false alarm rate for the three set of test data.

6.1.1 Model 1 testing

Values of training features, corresponding label, and four-input parameter ANN model output before and after kick event for instance 1 in Table 5-6.

Table 6-1: Corresponding training features and labels of four-input ANN (model 1), Test data – SDS1-run3a.

Time (sec)	Downhole Pressure (psi g)	Mud Flow-out rate (lb/h)	Density (lb/ft3)	Conductivity (uS/cm)	Actual Label (Encoded)	Actual Label	Classified Label (from model)	Model Output
71.00	12.18	561.22	62.37	301.07	-1	No-Kick	No-Kick	-0.59
71.10	12.35	564.85	62.39	301.03	-1	No-Kick	No-Kick	-0.59
71.90	13.31	604.31	62.09	299.92	-1	No-Kick	No-Kick	-0.58
72.00	14.77	625.92	62.09	299.41	-1	No-Kick	No-Kick	-0.57
72.10	18.87	663.38	62.36	299.10	-1	No-Kick	No-Kick	-0.55
72.20	25.75	748.32	62.39	298.68	1	Kick	No-Kick	-0.51
72.30	28.27	894.97	62.39	295.82	1	Kick	No-Kick	-0.48
72.40	26.36	1062.24	62.39	289.89	1	Kick	No-Kick	-0.46
72.50	26.71	1238.30	62.39	285.06	1	Kick	No-Kick	-0.43
77.00	23.48	1954.55	48.87	265.78	1	Kick	No-Kick	-0.16
77.10	23.41	1944.06	48.69	265.11	1	Kick	No-Kick	-0.15
77.20	22.89	1921.84	48.66	264.56	1	Kick	No-Kick	-0.16
77.30	22.92	1921.02	48.41	261.09	1	Kick	No-Kick	-0.15
77.40	22.89	1946.82	47.82	253.55	1	Kick	No-Kick	-0.11
77.50	22.31	1981.77	46.96	247.51	1	Kick	No-Kick	-0.08
77.60	22.35	2010.62	46.16	245.32	1	Kick	No-Kick	-0.06
77.70	22.43	2021.81	45.55	244.35	1	Kick	No-Kick	-0.05
77.80	22.11	2027.88	44.91	241.85	1	Kick	No-Kick	-0.04
77.90	21.95	2048.58	44.33	237.51	1	Kick	No-Kick	-0.01
78.00	22.91	2068.23	43.64	234.31	1	Kick	Kick	0.02
78.10	22.27	2082.16	42.57	233.05	1	Kick	Kick	0.03
78.20	21.47	2074.91	41.36	232.09	1	Kick	Kick	0.05
78.30	23.42	2069.22	40.04	226.39	1	Kick	Kick	0.10
78.40	23.39	2083.12	38.89	213.67	1	Kick	Kick	0.15
78.50	19.64	2078.73	38.12	202.99	1	Kick	Kick	0.16
78.60	21.48	2047.85	37.54	198.93	1	Kick	Kick	0.19
78.70	24.58	2011.73	36.92	197.45	1	Kick	Kick	0.22
78.80	22.55	1987.21	36.10	195.52	1	Kick	Kick	0.22
78.90	22.11	1990.38	35.31	192.42	1	Kick	Kick	0.24
79.00	25.51	1998.29	34.65	189.99	1	Kick	Kick	0.28

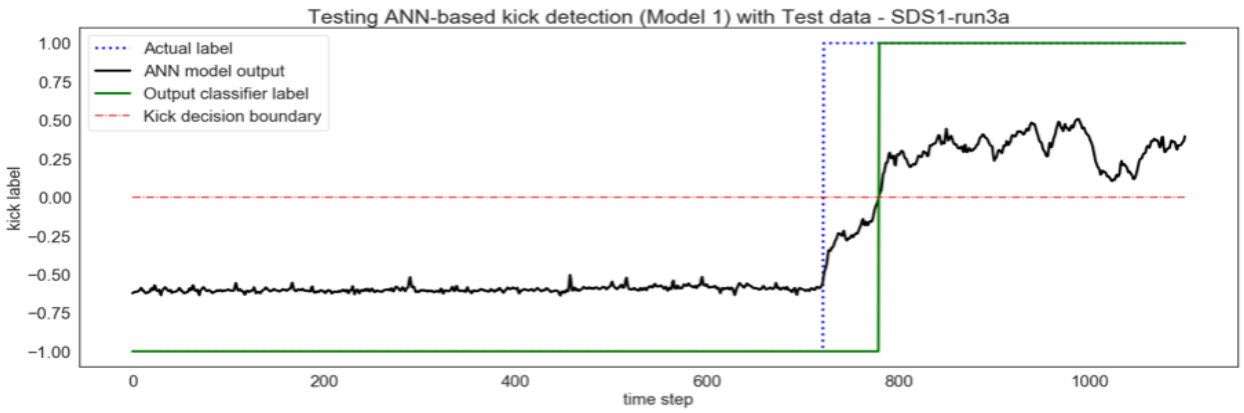

Figure 6-1: Plot from testing four-input ANN (model 1) with data from SDS system.

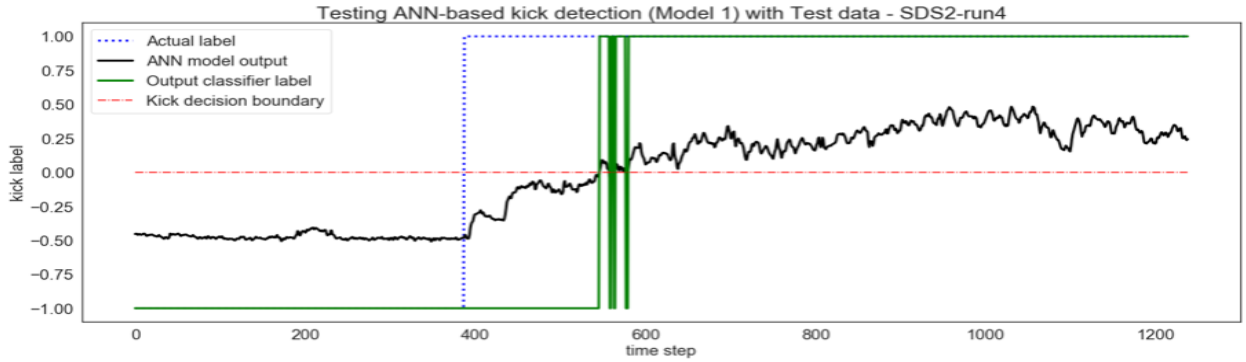

Figure 6-2: Plot from testing four-input ANN (model 1) with data from SDS system that contains faulty conductivity data.

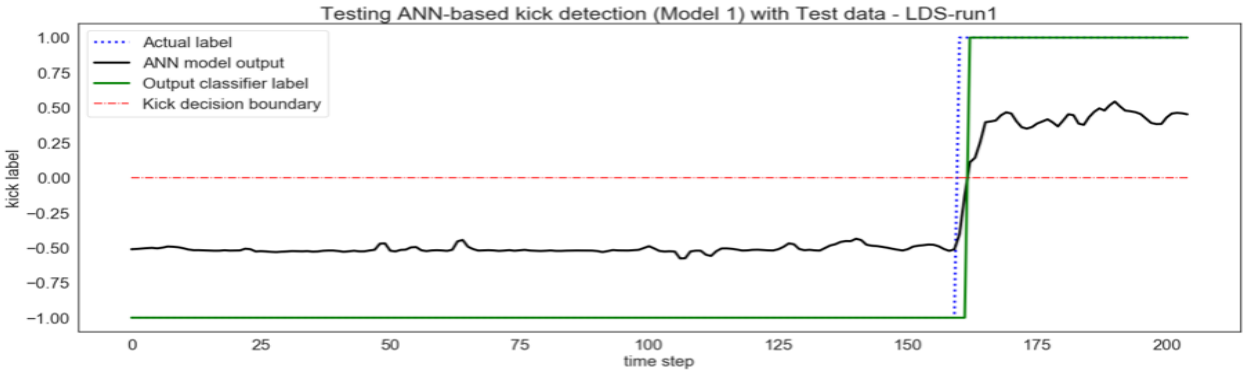

Figure 6-3: Plot from testing four-input ANN (model 1) with data from LDS system.

Table 6-2: Four-input ANN (model 1) performance metrics such as accuracy, recall, precision, F1-score, missed detection and false alarm rate for the three set of test data.

	Model 1			
Test data		SDS system SDS		LDS system LDS
		Different scenario	Faulty conductivity data	
Classification accuracy		0.95	0.87	0.99
Confusion Matrix	0,0	722	387	160
	0,1	0	0	0
	1,0	58	166	2
	1,1	320	685	43
Precision	No-Kick	0.93	0.70	0.99
	Kick	1.00	1.00	1.00
Recall	No-Kick	1.00	1.00	1.00
	Kick	0.85	0.80	0.96
F1-Score	No-Kick	0.96	0.82	0.99
	Kick	0.92	0.89	0.98
Support	No-Kick	722	387	160
	Kick	378	851	45
False Alarm		No	No	No
Missed Detection		No	No	No

6.1.2 Model 2 testing

Values of training features, corresponding label, and four-input parameter ANN model output before and after kick event for instance 4 in Table 5-6.

Table 6-3: Corresponding training features and labels of four-input ANN (model 2), Test data – SDS1-run1a.

Time (sec)	**Downhole Pressure (psi g)**	**Mud Flow-out rate (lb/h)**	**Density (lb/ft3)**	**Conductivity (uS/cm)**	**Actual Label (Encoded)**	**Actual Label**	**Classified Label (from model)**	**Model Output**
73.00	11.24	475.69	62.39	301.88	-1	No-Kick	No-Kick	-0.63
73.10	6.05	472.41	62.39	301.88	-1	No-Kick	No-Kick	-0.65
73.70	7.13	474.55	62.39	302.28	-1	No-Kick	No-Kick	-0.65
73.80	6.97	484.58	62.39	302.23	-1	No-Kick	No-Kick	-0.65
73.90	8.08	484.48	62.39	302.16	-1	No-Kick	No-Kick	-0.64
74.00	9.49	472.36	62.39	302.11	1	Kick	No-Kick	-0.64
74.10	10.01	479.27	62.39	302.17	1	Kick	No-Kick	-0.64
74.20	14.53	516.60	62.39	302.25	1	Kick	No-Kick	-0.61
77.80	31.36	2498.61	55.66	279.25	1	Kick	No-Kick	-0.02
77.90	27.67	2504.19	54.37	282.71	1	Kick	No-Kick	-0.03
78.00	24.70	2501.48	53.06	286.56	1	Kick	No-Kick	-0.04
78.10	24.96	2483.22	51.57	288.21	1	Kick	No-Kick	-0.03
78.20	32.90	2464.47	50.06	288.71	1	Kick	Kick	0.04
78.30	34.11	2427.82	48.64	289.50	1	Kick	Kick	0.05
78.40	24.22	2366.67	47.24	292.40	1	Kick	No-Kick	-0.01
78.50	22.14	2312.20	46.01	295.42	1	Kick	No-Kick	-0.03
78.60	23.56	2267.29	44.84	296.53	1	Kick	No-Kick	-0.01
80.20	19.85	1261.54	34.13	260.88	1	Kick	No-Kick	-0.03
80.30	18.33	1235.42	33.96	258.73	1	Kick	No-Kick	-0.04
80.40	19.12	1214.53	33.59	251.90	1	Kick	No-Kick	-0.02
80.50	20.22	1213.69	33.27	244.68	1	Kick	Kick	0.01
80.60	20.96	1229.98	33.12	241.82	1	Kick	Kick	0.03
80.70	22.14	1248.37	32.96	240.75	1	Kick	Kick	0.04
81.80	17.11	1220.00	31.24	191.50	1	Kick	Kick	0.14
81.90	19.29	1189.00	30.94	184.33	1	Kick	Kick	0.17
82.00	20.11	1158.96	30.69	176.40	1	Kick	Kick	0.19

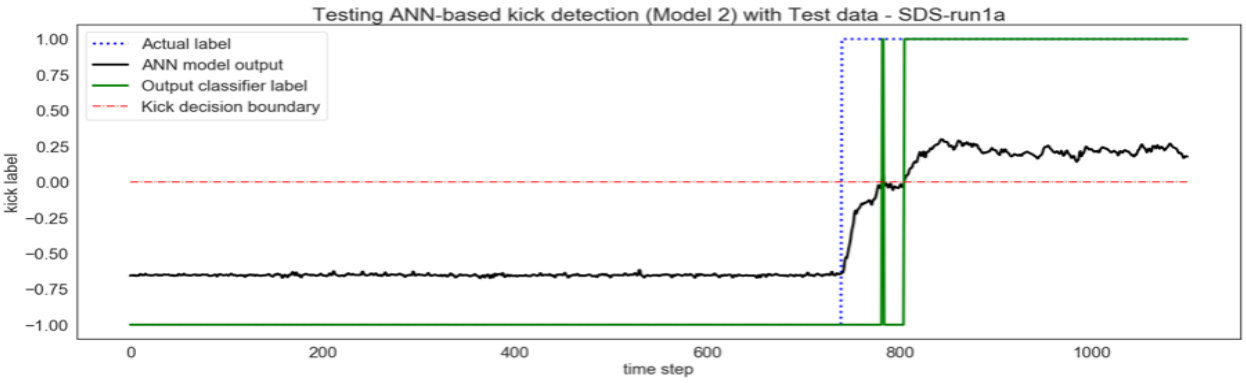

Figure 6-4: Plot from testing four-input ANN (model 2) with data from SDS system.

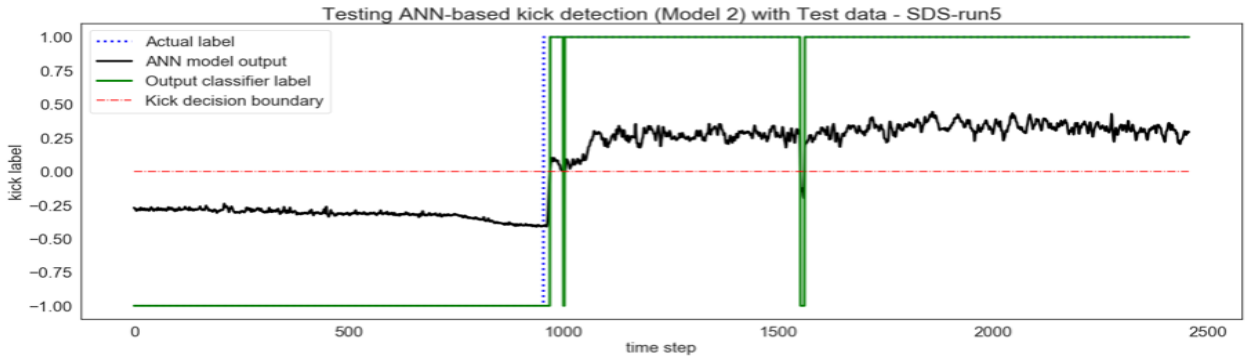

Figure 6-5: Plot from testing four-input ANN (model 2) with data from SDS system that contains faulty conductivity data.

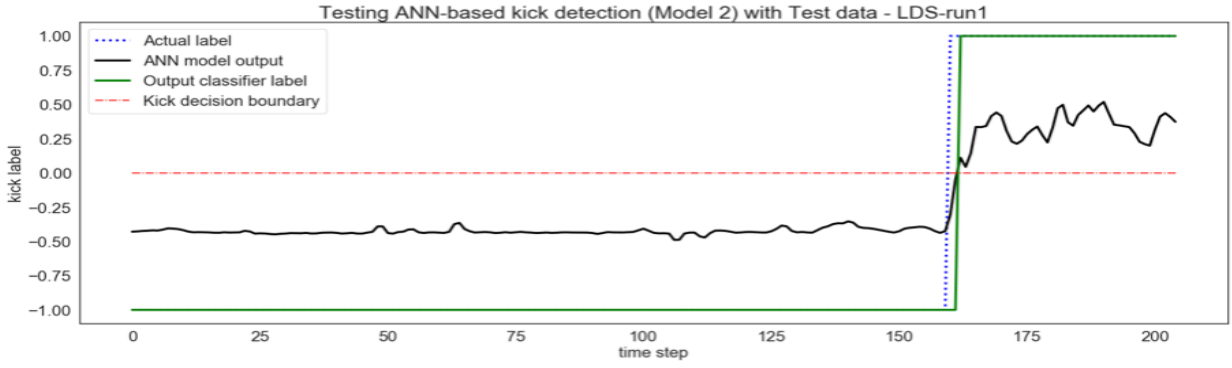

Figure 6-6: Plot from testing four-input ANN (model 2) with data from LDS system.

Table 6-4: Four-input ANN (model 2) performance metrics such as accuracy, recall, precision, F1-score, missed detection and false alarm rate for the three set of test data.

	Model 2			
Test data		SDS system SDS		LDS system LDS
		Different scenario	Faulty conductivity data	
Classification accuracy		0.94	0.99	0.99
Confusion Matrix	0,0	740	954	160
	0,1	0	0	0
	1,0	63	28	2
	1,1	297	1475	43
Precision	No-Kick	0.92	0.97	0.99
	Kick	1.00	1.00	1.00
Recall	No-Kick	1.00	1.00	1.00
	Kick	0.82	0.98	0.96
F1-Score	No-Kick	0.96	0.99	0.99
	Kick	0.90	0.99	0.98
Support	No-Kick	740	954	160
	Kick	360	1503	45
False Alarm		No	No	No
Missed Detection		No	No	No

6.1.3 Model 3 testing

Values of training features, corresponding label, and four-input parameter ANN model output before and after kick event for instance 7 in Table 5-6.

Table 6-5: Corresponding training features and labels of four-input ANN (model 3), Test data – SDS1-run2a.

Time (sec)	**Downhole Pressure (psi g)**	**Mud Flow-out rate (lb/h)**	**Density (lb/ft3)**	**Conductivity (uS/cm)**	**Actual Label (Encoded)**	**Actual Label**	**Classified Label (from model)**	**Model Output**
70.00	9.07	441.54	62.39	302.20	-1	No-Kick	No-Kick	-0.66
70.10	9.71	453.62	62.39	301.92	-1	No-Kick	No-Kick	-0.65
70.20	9.38	458.19	62.39	301.81	-1	No-Kick	No-Kick	-0.65
70.30	8.06	451.06	62.39	301.94	1	Kick	No-Kick	-0.66
70.40	6.91	444.22	62.39	302.11	1	Kick	No-Kick	-0.67
71.50	37.48	1899.68	62.39	289.89	1	Kick	No-Kick	-0.16
71.60	33.24	2034.88	62.39	281.55	1	Kick	No-Kick	-0.14
72.00	30.81	2363.93	62.20	270.11	1	Kick	No-Kick	-0.04
72.10	31.21	2420.82	62.37	264.56	1	Kick	No-Kick	-0.01
72.20	30.46	2452.84	62.39	261.46	1	Kick	Kick	0.00
72.30	30.52	2461.18	62.39	260.30	1	Kick	Kick	0.01
72.40	29.52	2469.70	62.38	259.65	1	Kick	Kick	0.00
72.50	29.11	2486.42	62.38	259.04	1	Kick	Kick	0.01
72.60	29.76	2504.19	62.39	258.22	1	Kick	Kick	0.02
72.70	29.94	2501.97	62.39	257.40	1	Kick	Kick	0.02
72.80	28.11	2471.11	62.39	257.20	1	Kick	No-Kick	0.00
72.90	26.45	2453.65	62.39	257.65	1	Kick	No-Kick	-0.02
73.00	25.94	2442.26	62.38	258.95	1	Kick	No-Kick	-0.03
73.10	26.41	2432.23	62.29	260.88	1	Kick	No-Kick	-0.03
74.90	20.98	2255.52	52.68	291.15	1	Kick	No-Kick	-0.09
75.00	19.32	2270.12	51.90	291.08	1	Kick	No-Kick	-0.09
75.10	18.80	2322.91	51.08	290.90	1	Kick	No-Kick	-0.07
75.20	21.23	2370.64	49.89	290.72	1	Kick	No-Kick	-0.03
75.30	21.89	2399.07	48.52	290.67	1	Kick	Kick	0.00
75.40	21.65	2426.45	47.25	290.55	1	Kick	Kick	0.02
75.90	17.18	2348.77	43.34	286.87	1	Kick	Kick	0.02
76.00	17.34	2329.75	42.79	284.72	1	Kick	Kick	0.03

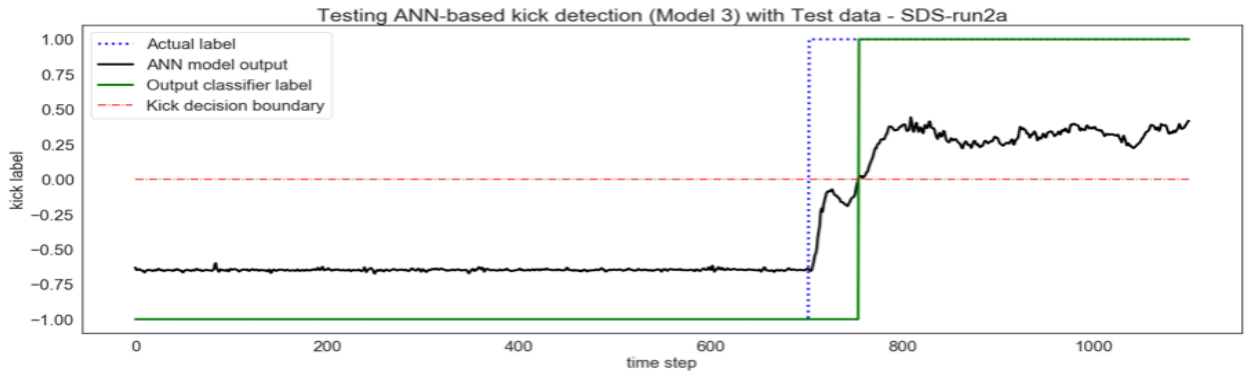

Figure 6-7: Plot from testing four-input ANN (model 3) with data from SDS system.

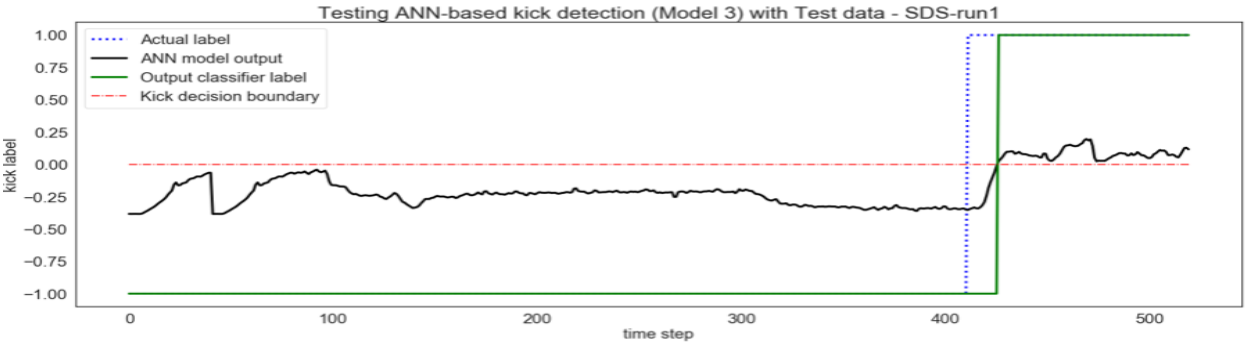

Figure 6-8: Plot from testing four-input ANN (model 3) with data from SDS system that contains faulty conductivity data.

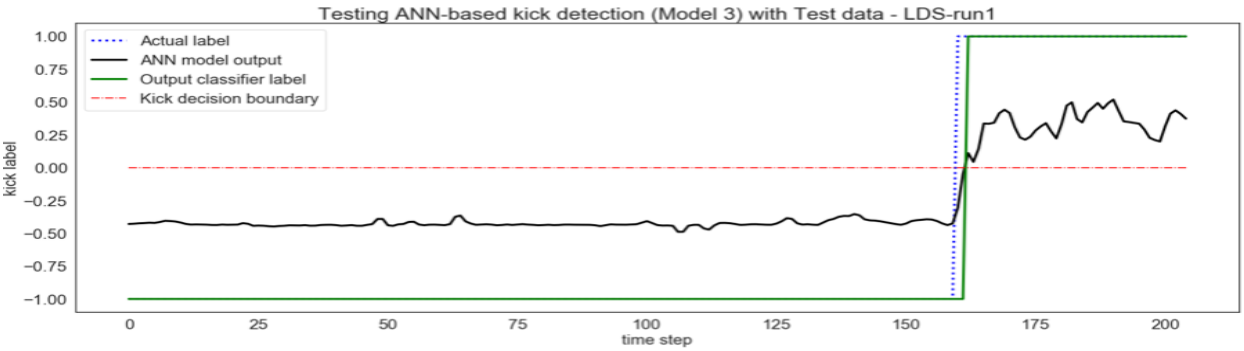

Figure 6-9: Plot from testing four-input ANN (model 3) with data from LDS system.

Table 6-6: Four-input ANN (model 3) performance metrics such as accuracy, recall, precision, F1-score, missed detection and false alarm rate for the three set of test data.

	Model 3			
Test data		SDS system SDS		LDS system LDS
		Different scenario	Faulty conductivity data	
Classification accuracy		0.95	0.97	0.99
Confusion Matrix	0,0	703	411	160
	0,1	0	0	0
	1,0	52	15	2
	1,1	345	94	43
Precision	No-Kick	0.93	0.96	0.99
	Kick	1.00	1.00	1.00
Recall	No-Kick	1.00	1.00	1.00
	Kick	0.87	0.86	0.96
F1-Score	No-Kick	0.96	0.98	0.99
	Kick	0.93	0.93	0.98
Support	No-Kick	703	411	160
	Kick	397	109	45
False Alarm		No	No	No
Missed Detection		No	No	No

6.1.4 Discussion of four-input parameter ANN results

As can be seen from Table 6-7, applying non-negativity constraints to the weights during training revealed the parameters that have more influence in an ANN kick detection model. With zero weight constraint on some input parameters, the model's inputs are observed to have just two effective parameters. Caution needs to be taken when applying constraints in training a model to avoid shutting off the effect of some parameters. It is important to understand how the constraint will impact the model. The sensitivity of the model to local fluctuations in any of the dominant parameters (downhole pressure and mud flow-out rate in this case) can lead to false alarm, as shown in Figure 6-10; thus, reducing the overall reliability of the system. This demonstrates how monitoring and modelling with multiple downhole parameters for early kick detection, as pointed out in [29], can reduce the susceptibility of the system to a false alarm.

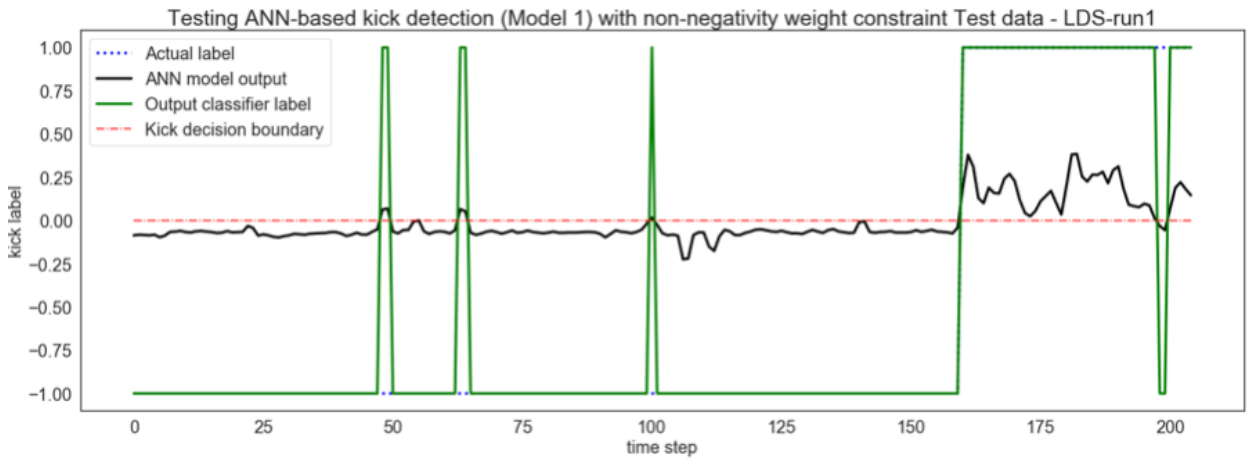

Figure 6-10: Plot showing false alarm when model is trained with weight constraint and tested on data from a LDS system.

Table 6-7: Model performance for 4-imput ANN (models 1, 2 and 3) and test result evaluation with/without model weight constraints.

	Model 1	Model 2	Model 3	Comments
Without constraints				No false alarm Downhole pressure and mud flow rate are positive valued in all 3 models. Density and Conductivity are negative valued in all 3 models
$W_{down\_pressure}$	0.13	0.11	0.14	
W_{flow}	0.10	0.23	0.27	
$W_{density}$	-0.29	-0.26	-0.21	
$W_{conductivity}$	-0.25	-0.21	-0.24	
SDS Test accuracy	95.00	94.00	96.00	
False positives	No	No	No	
LDS Test accuracy	99.00	99.00	99.00	
False alarm	No	No	No	
With Non-negativity constraints				Four-input ANN model becomes only 2 effective input parameter ANN model False alarm for test with LDS data on all 3 models. Downhole pressure and mud flow rate are more significant in building a kick detection model due to the positive-valued weights in all models. Density and Conductivity are negative valued in all 3 models
$W_{down\_pressure}$	0.28	0.21	0.21	
W_{flow}	0.23	0.38	0.43	
$W_{density}$	0	0	0	
$W_{conductivity}$	0	0	0	
SDS Test accuracy	99.00	72.00	93.00	
False alarm	No	No	No	
LDS Test accuracy	97.00	71.00	29.00	
False alarm	Yes	Yes	yes	

It is also important to note that high classification accuracy of model output does not always imply model will perform correctly without false alarm. This can be seen in Table 6-7. where LDS test data reported false alarms when the model was trained with the non-negativity weight constraint. This calls for tradeoff when complying with standard model metrics such as output classification accuracy of a model. Inclusion of domain attributes such as missed detection, detection time and false detection together with specifics of how it relates to the domain produces a reliable testing basis for a trained model. Results from testing SDS test data instances on each trained four-input ANN model show 100% success rate in detecting kick events, there was 0% false alarm rate, 0% missed detection rate and early detection within 5 s of the influx. It is noted that the training set determines the efficiency of our ANN model. Hence the need for proper supervised labelling of the target outputs in the training sets before building the model.

6.2 Three-input parameter ANN model

There are three sets of results for the three-input parameter ANN model. They include plot from testing with data from SDS system, plot from testing with data from LDS system and model evaluation metrics for all three test cases. The results will be presented for model 1 only.

1. The first result in Figure 6-11, Figure 6-13, Figure 6-15 and Figure 6-17 respectively is a plot showing results of testing the model with data from different scenario of the SDS kick experiment in [8].
2. The second result in Table 6-8, Table 6-9, Table 6-10 and Table 6-11 respectively is a table that presents the confusion matrix and summarizes the model performance metrics such as classification accuracy, recall, precision, F1-score, missed detection and false alarm rate for the test data.
3. The third result in Figure 6-12, Figure 6-14, Figure 6-16 and Figure 6-18 respectively is a plot showing results of testing the model with data from LDS kick experiment.

6.2.1 Downhole pressure, mud flow rate and density

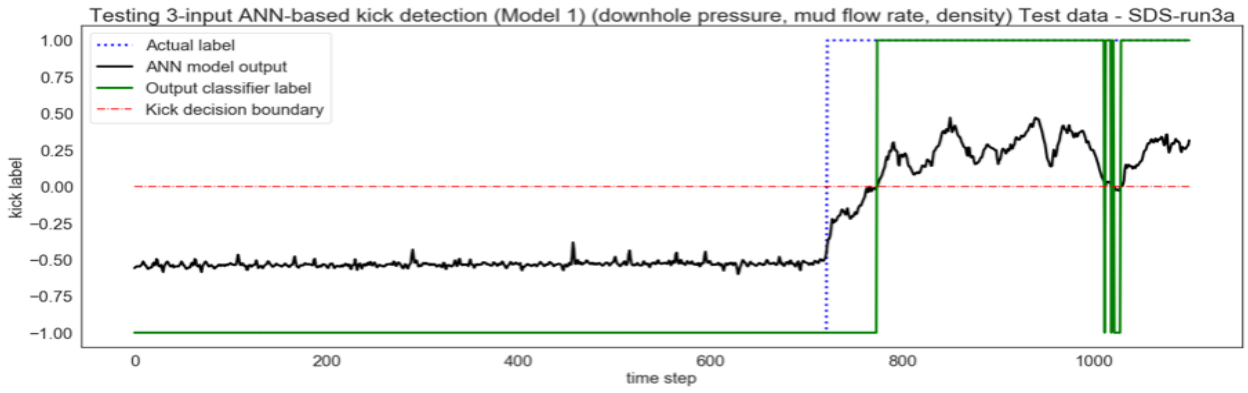

Figure 6-11: Plot from testing three-input ANN (model 1) with data from SDS system.

Table 6-8: Three-input ANN (model 1) performance metrics such as accuracy, recall, precision, F1-score, missed detection and false alarm rate for the three set of test data.

Model 1 (Three-input parameters)			
Input parameters	Downhole pressure, mud flow rate and density		
		Test data	
		SDS system SDS – different scenario	LDS system LDS Data
Classification accuracy		0.94	0.98
Confusion matrix	0,0	722	160
	0,1	0	0
	1,0	61	4
	1,1	317	41
Precision	No-Kick	0.92	0.98
	Kick	1.00	1.00
Recall	No-Kick	1.00	1.00
	Kick	0.84	0.91
F1-score	No-Kick	0.96	0.99
	Kick	0.91	0.95
Support	No-Kick	722	160
	Kick	378	45
False Alarm		No	No
Missed detection		No	No
Training data = SDS1-run1a Test data = SDS1-run3a			

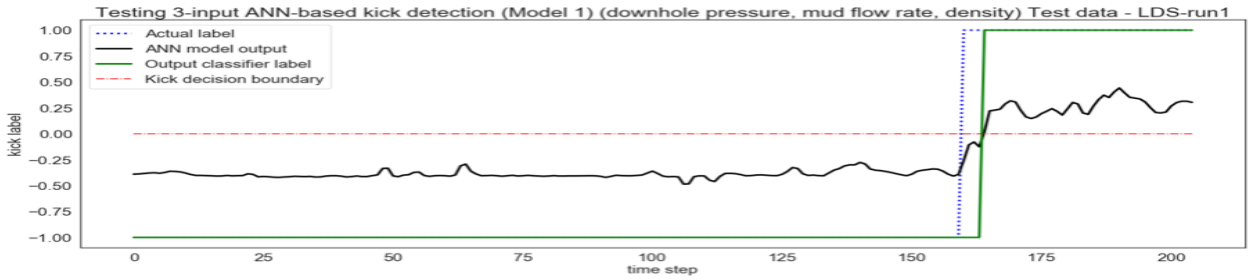

Figure 6-12: Plot from testing three-input ANN (model 1) with data from LDS system.

6.2.2 Downhole pressure, mud flow rate and conductivity

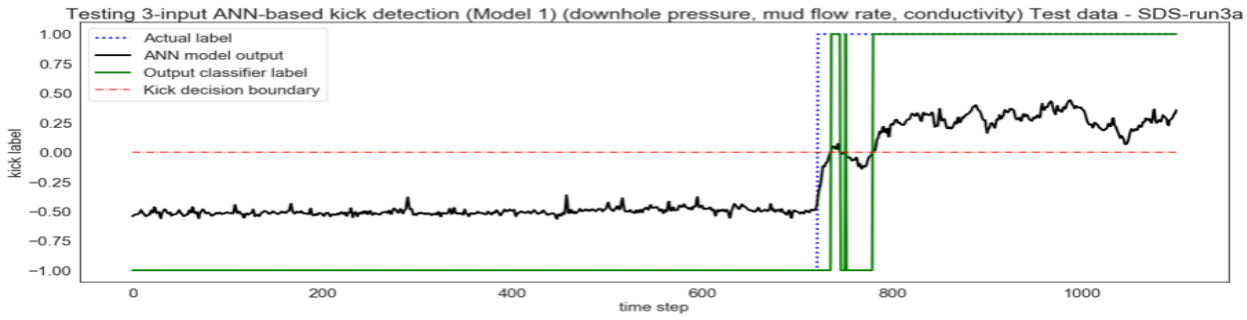

Figure 6-13: Plot from testing three-input ANN (model 1) with data from SDS system.

Table 6-9: Three-input ANN (model 1) performance metrics such as accuracy, recall, precision, F1-score, missed detection and false alarm rate for the three set of test data.

Model 1 (Three-input parameters)			
Input parameters	Downhole pressure, mud flow rate and conductivity		
		Test data	
		SDS system SDS – different scenario	LDS system LDS Data
Classification accuracy		0.96	0.96
Confusion matrix	0,0	722	160
	0,1	0	0
	1,0	47	1
	1,1	331	44
Precision	No-Kick	0.94	0.94
	Kick	1.00	1.00
Recall	No-Kick	1.00	1.00
	Kick	0.88	0.88
F1-score	No-Kick	0.97	0.97
	Kick	0.93	0.93
Support	No-Kick	722	722
	Kick	378	378
False Alarm		No	No
Missed detection		No	No
Training data = SDS1-run1a Test data = SDS1-run3a			

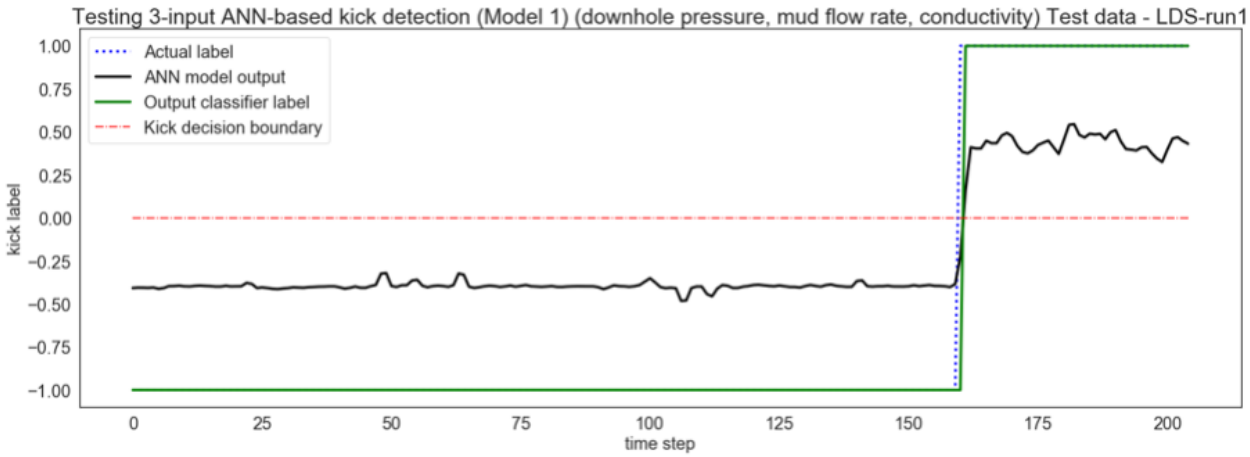

Figure 6-14: Plot from testing three-input ANN (model 1) with data from LDS system.

6.2.3 Downhole pressure, density, and conductivity

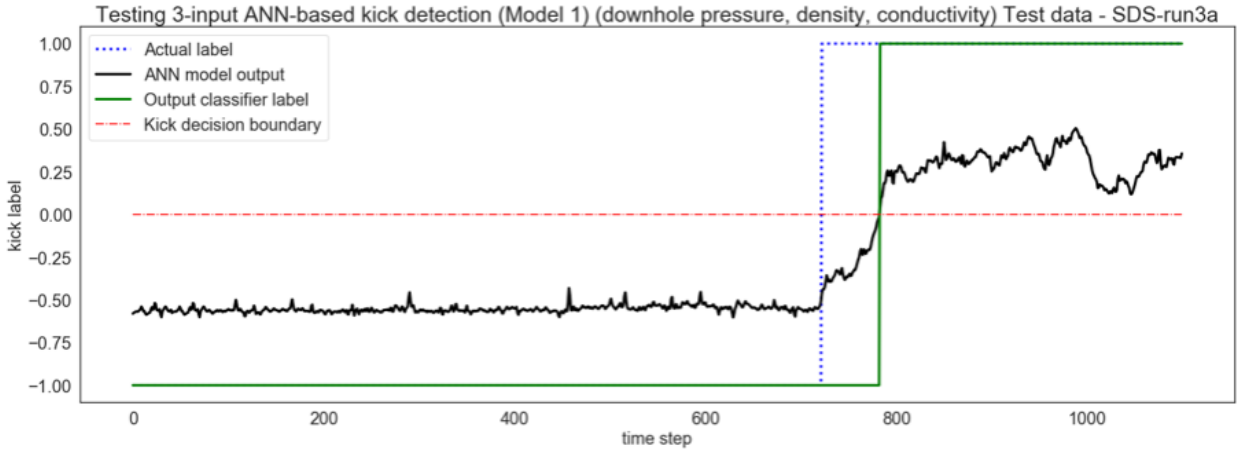

Figure 6-15: Plot from testing three-input ANN (model 1) with data from SDS system.

Table 6-10: Three-input ANN (model 1) performance metrics such as accuracy, recall, precision, F1-score, missed detection and false alarm rate for the three set of test data.

Model 1 (Three-input parameters)			
Input parameters	Downhole pressure, density, and conductivity		
		Test data	
		SDS system SDS – different scenario	LDS system LDS Data
Classification accuracy		0.94	0.99
Confusion matrix	0,0	722	160
	0,1	0	0
	1,0	61	2
	1,1	317	43
Precision	No-Kick	0.92	0.99
	Kick	1.00	1.00
Recall	No-Kick	1.00	1.00
	Kick	0.84	0.96
F1-score	No-Kick	0.96	0.99
	Kick	0.91	0.98
Support	No-Kick	722	160
	Kick	378	45
False Alarm		No	No
Missed detection		No	No
Training data = SDS1-run1a Test data = SDS1-run3a			

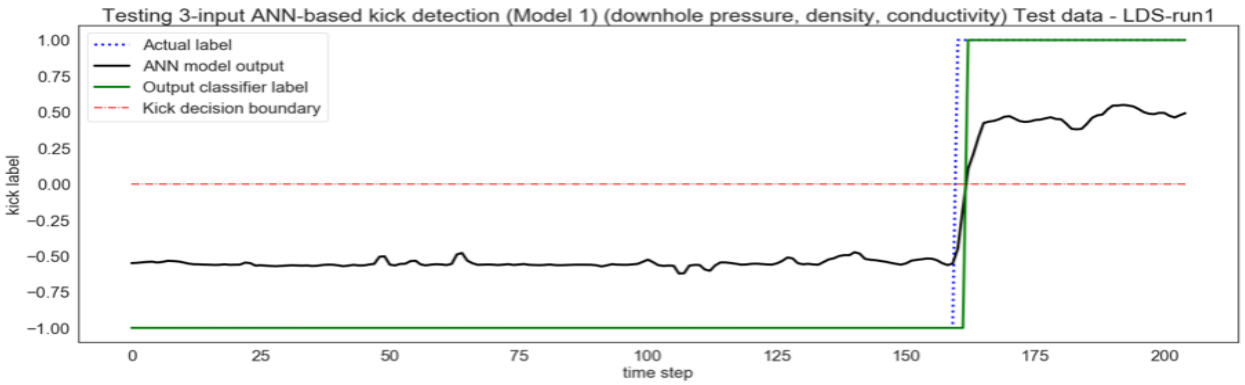

Figure 6-16: Plot from testing three-input ANN (model 1) with data from LDS system.

6.2.4 Mud flow rate, density, and conductivity

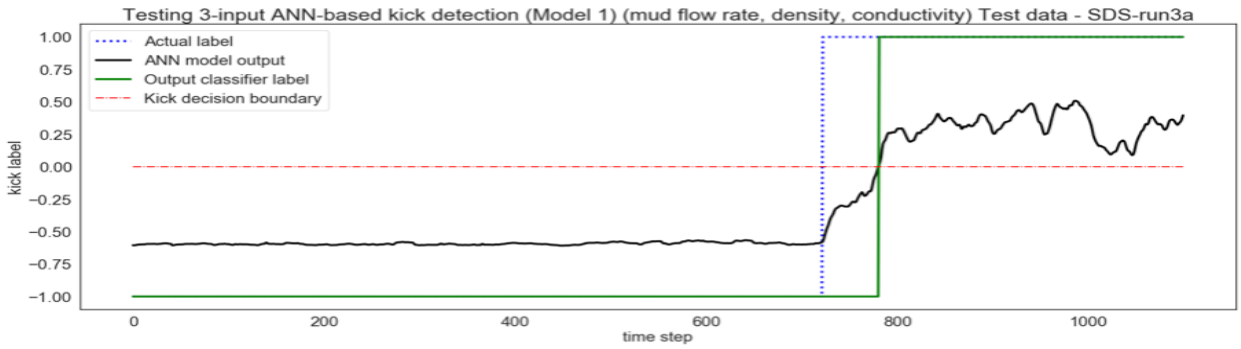

Figure 6-17: Plot from testing three-input ANN (model 1) with data from SDS system.

Table 6-11: Three-input ANN (model 1) performance metrics such as accuracy, recall, precision, F1-score, missed detection and false alarm rate for the three set of test data.

Model 1 (Three-input parameters)			
Input parameters	Mud flow rate, density, and conductivity		
		Test data	
		SDS system SDS – different scenario	LDS system LDS Data
Classification accuracy		0.95	0.99
Confusion matrix	0,0	722	160
	0,1	0	0
	1,0	59	3
	1,1	319	42
Precision	No-Kick	0.92	0.98
	Kick	1.00	1.00
Recall	No-Kick	1.00	1.00
	Kick	0.84	0.93
F1-score	No-Kick	0.96	0.99
	Kick	0.92	0.97
Support	No-Kick	722	160
	Kick	378	45
False Alarm		No	No
Missed detection		No	No
Training data = SDS1-run1a Test data = SDS1-run3a			

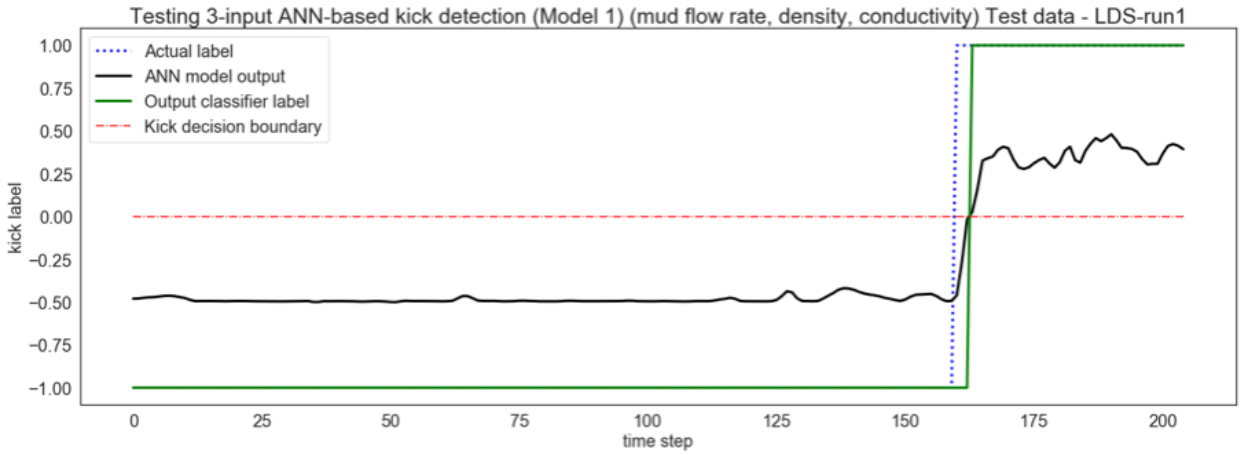

Figure 6-18: Plot from testing three-input ANN (model 1) with data from LDS system.

6.2.5 Discussion of three-input parameter ANN results

There were four possible combination of three parameters from the four parameters considered in this study. Model performance was similar as shown in *Table* 6-8, *Table* 6-9, *Table* 6-10 and *Table* 6-11. Each combination showed success in detecting the kick event without a false alarm (FP = 0) for all test instances. The results obtained are comparable to those obtained from testing the four-input parameter ANN models. This similarity in performance needs to be further tested with field to validate the finding.

6.3 Two-input parameter ANN model

This subsection presents three sets of results for the two-input parameter ANN model. They include plot from testing with data from SDS system, plot from testing with data from LDS system and model evaluation metrics for all three test cases. The results will be presented for model 1 only.

1. The first result in Figure 6-19, Figure 6-21, Figure 6-23, Figure 6-25, Figure 6-27 and Figure 6-29 respectively is a plot showing results of testing the model with data from different scenario of the SDS kick experiment in [8].
2. The second result in Table 6-12, Table 6-13, Table 6-14, Table 6-15, Table 6-16 and Table 6-17 respectively is a table that presents the confusion matrix and summarizes the model performance metrics such as classification accuracy, recall, precision, F1-score, missed detection and false alarm rate for the two set of test data.
3. The third result in Figure 6-20, Figure 6-22, Figure 6-24, Figure 6-26, Figure 6-28 and Figure 6-29 respectively is a plot showing results of testing the model with data from LDS kick experiment.

6.3.1 Downhole pressure and mud flow rate

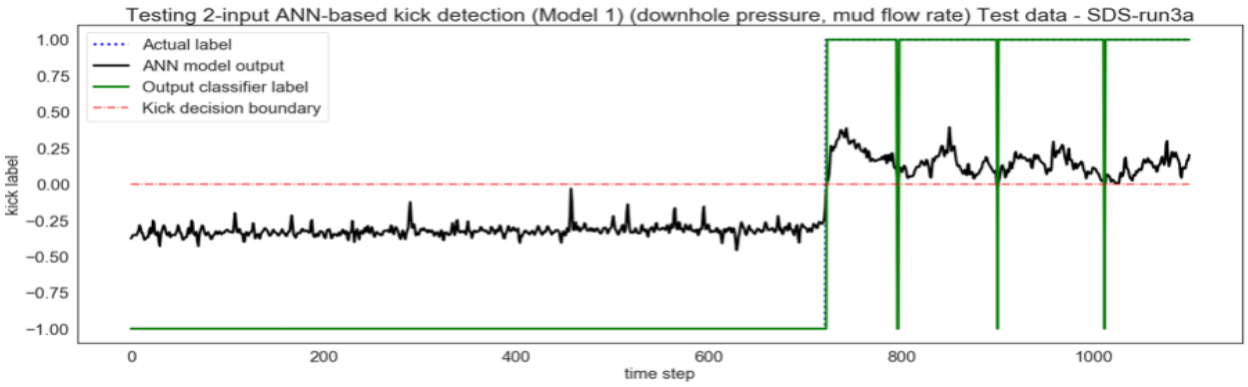

Figure 6-19: Plot from testing two-input ANN (model 1) with data from SDS system.

Table 6-12: Two-input ANN (model 1) performance metrics such as accuracy, recall, precision, F1-score, missed detection and false alarm rate for the three set of test data.

Model 1 (Two-input parameters)			
Input parameters	Downhole pressure and mud flow rate		
		Test data	
		SDS system SDS – different scenario	LDS system LDS Data
Classification accuracy		0.99	0.97
Confusion matrix	0,0	722	155
	0,1	0	5
	1,0	5	2
	1,1	373	43
Precision	No-Kick	0.99	0.99
	Kick	1.00	0.90
Recall	No-Kick	1.00	0.97
	Kick	0.99	0.96
F1-score	No-Kick	1.00	0.98
	Kick	0.99	0.92
Support	No-Kick	722	160
	Kick	378	45
False Alarm		No	Yes
Missed detection		No	No
Training data = SDS1-run1a Test data = SDS1-run3a			

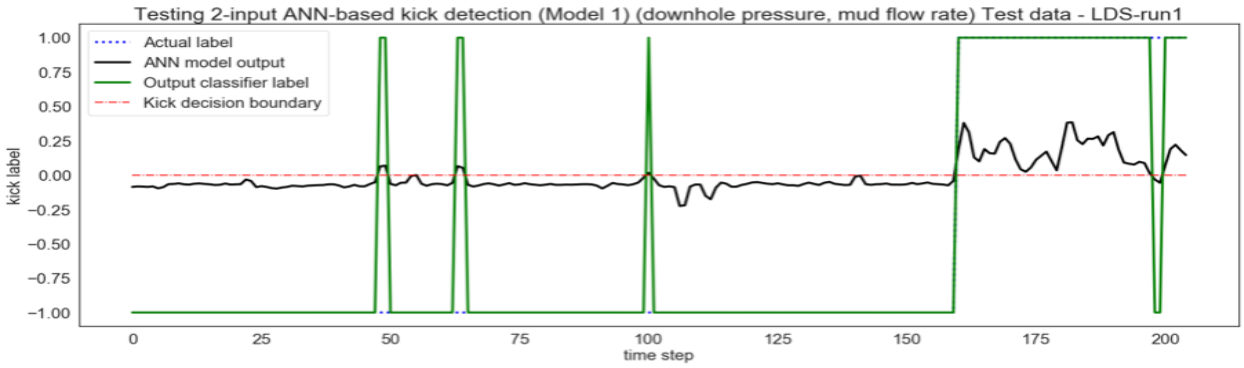

Figure 6-20: Plot from testing two-input ANN (model 1) with data from LDS system.

6.3.2 Downhole pressure and density

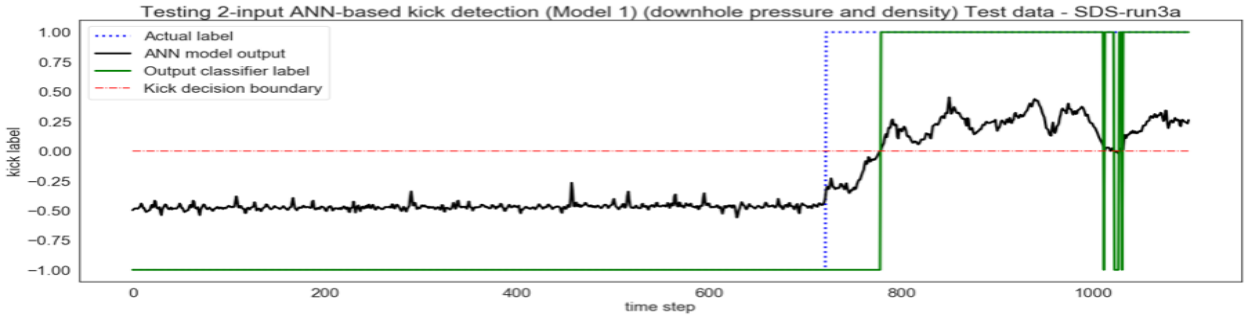

Figure 6-21: Plot from testing two-input ANN (model 1) with data from SDS system.

Table 6-13: Two-input ANN (model 1) performance metrics such as accuracy, recall, precision, F1-score, missed detection and false alarm rate for the three set of test data.

Model 1 (Two-input parameters)			
Input parameters	Downhole pressure and density		
		Test data	
		SDS system SDS – different scenario	LDS system LDS Data
Classification accuracy		0.94	0.98
Confusion matrix	0,0	722	160
	0,1	0	0
	1,0	64	4
	1,1	314	41
Precision	No-Kick	0.92	0.98
	Kick	1.00	1.00
Recall	No-Kick	1.00	1.00
	Kick	0.83	0.91
F1-score	No-Kick	0.96	0.99
	Kick	0.91	0.95
Support	No-Kick	722	160
	Kick	378	45
False Alarm		No	No
Missed detection		No	No
Training data = SDS1-run1a Test data = SDS1-run3a			

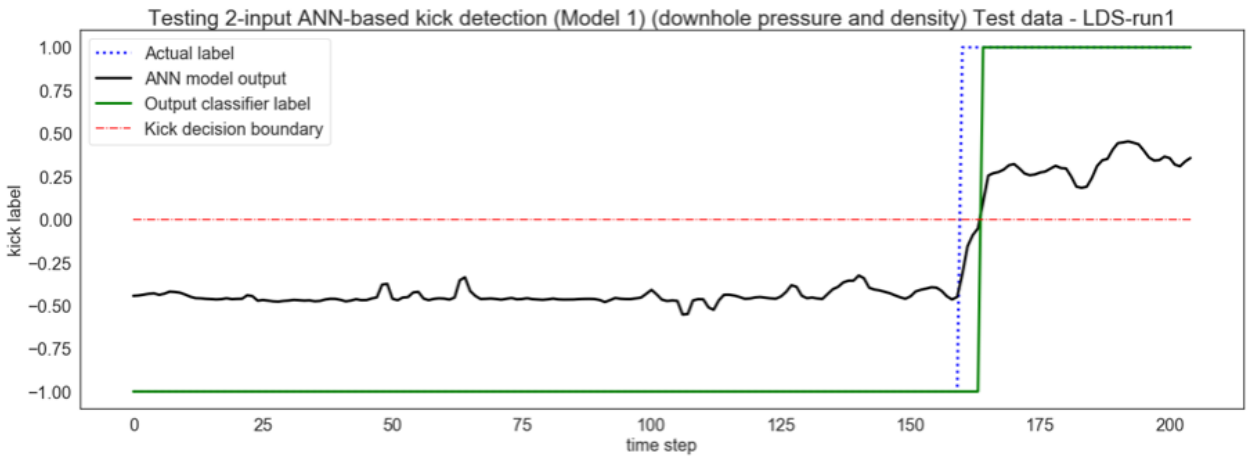

Figure 6-22: Plot from testing two-input ANN (model 1) with data from LDS system.

6.3.3 Downhole pressure and conductivity

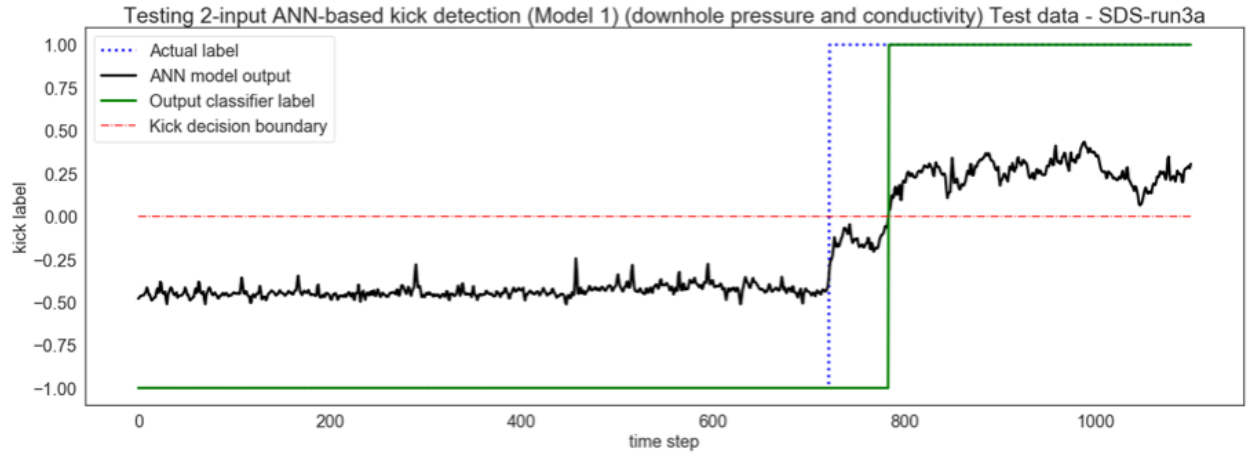

Figure 6-23: Plot from testing two-input ANN (model 1) with data from SDS system.

Table 6-14: Two-input ANN (model 1) performance metrics such as accuracy, recall, precision, F1-score, missed detection and false alarm rate for the three set of test data.

Model 1 (Two-input parameters)			
Input parameters	Downhole pressure and conductivity		
		Test data	
		SDS system SDS – different scenario	LDS system LDS Data
Classification accuracy		0.94	0.99
Confusion matrix	0,0	722	160
	0,1	0	0
	1,0	62	1
	1,1	316	44
Precision	No-Kick	0.92	0.99
	Kick	1.00	1.00
Recall	No-Kick	1.00	1.00
	Kick	0.84	0.98
F1-score	No-Kick	0.96	1.00
	Kick	0.91	0.99
Support	No-Kick	722	160
	Kick	378	45
False Alarm		No	No
Missed detection		No	No
Training data = SDS1-run1a Test data = SDS1-run3a			

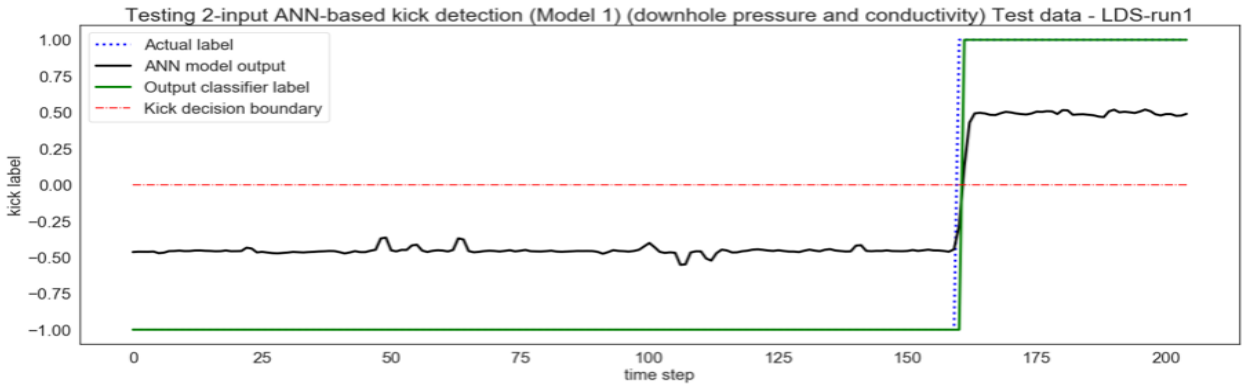

Figure 6-24: Plot from testing two-input ANN (model 1) with data from LDS system.

6.3.4 Mud flow rate and density

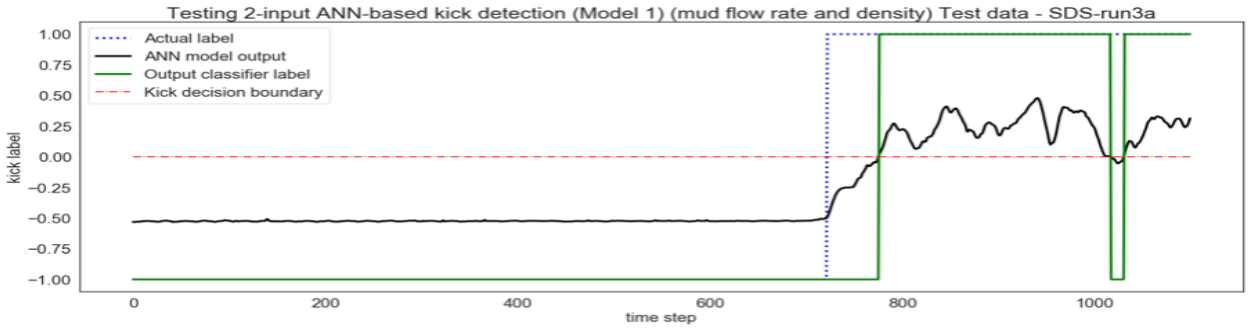

Figure 6-25: Plot from testing two-input ANN (model 1) with data from SDS system.

Table 6-15: Two-input ANN (model 1) performance metrics such as accuracy, recall, precision, F1-score, missed detection and false alarm rate for the three set of test data.

Model 1 (Two-input parameters)			
Input parameters	Mud flow rate and density		
		Test data	
		SDS system SDS – different scenario	LDS system LDS Data
Classification accuracy		0.94	0.98
Confusion matrix	0,0	722	160
	0,1	0	0
	1,0	68	5
	1,1	310	40
Precision	No-Kick	0.91	0.97
	Kick	1.00	1.00
Recall	No-Kick	1.00	1.00
	Kick	0.82	0.89
F1-score	No-Kick	0.96	0.98
	Kick	0.90	0.94
Support	No-Kick	722	160
	Kick	378	45
False Alarm		No	No
Missed detection		No	No
Training data = SDS1-run1a Test data = SDS1-run3a			

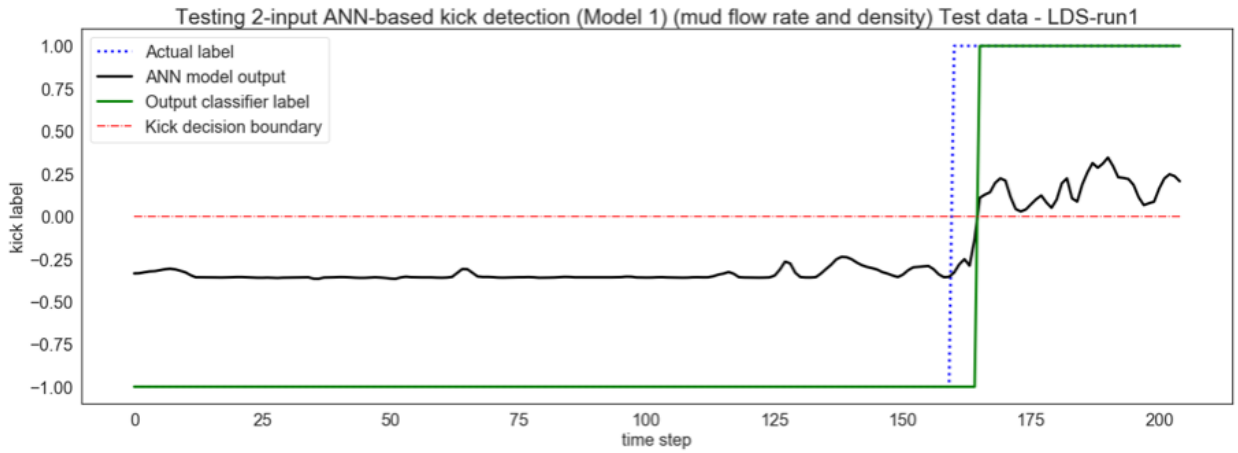

Figure 6-26: Plot from testing two-input ANN (model 1) with data from LDS system.

6.3.5 Mud flow rate and conductivity

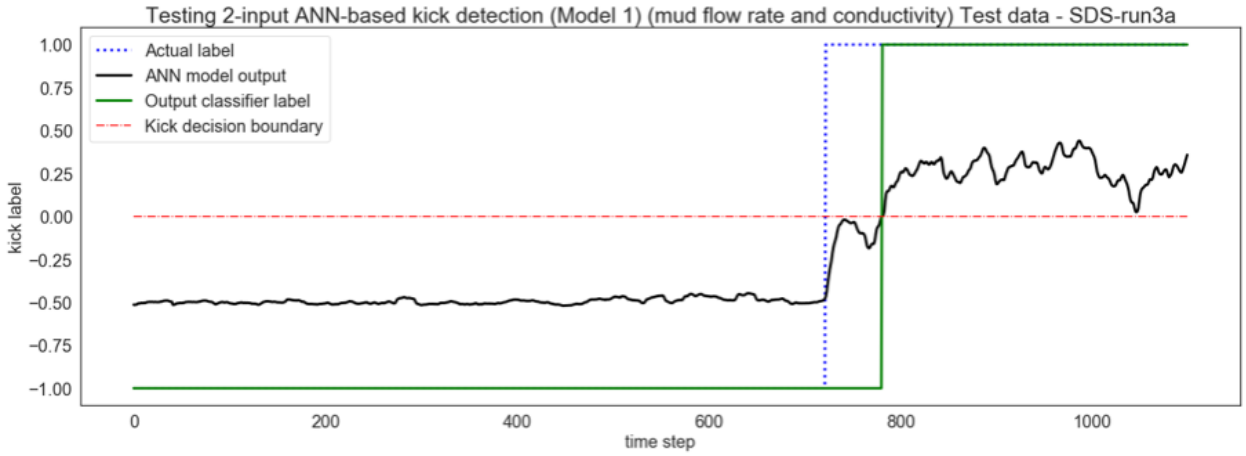

Figure 6-27: Plot from testing two-input ANN (model 1) with data from SDS system.

Table 6-16: Two-input ANN (model 1) performance metrics such as accuracy, recall, precision, F1-score, missed detection and false alarm rate for the three set of test data.

Model 1 (Two-input parameters)			
Input parameters	Mud flow rate and conductivity		
		Test data	
		SDS system SDS – different scenario	LDS system LDS Data
Classification accuracy		0.95	0.99
Confusion matrix	0,0	722	160
	0,1	0	0
	1,0	59	2
	1,1	319	43
Precision	No-Kick	0.92	0.99
	Kick	1.00	1.00
Recall	No-Kick	1.00	1.00
	Kick	0.84	0.96
F1-score	No-Kick	0.96	0.99
	Kick	0.92	0.98
Support	No-Kick	722	160
	Kick	378	45
False Alarm		No	No
Missed detection		No	No
Training data = SDS1-run1a Test data = SDS1-run3a			

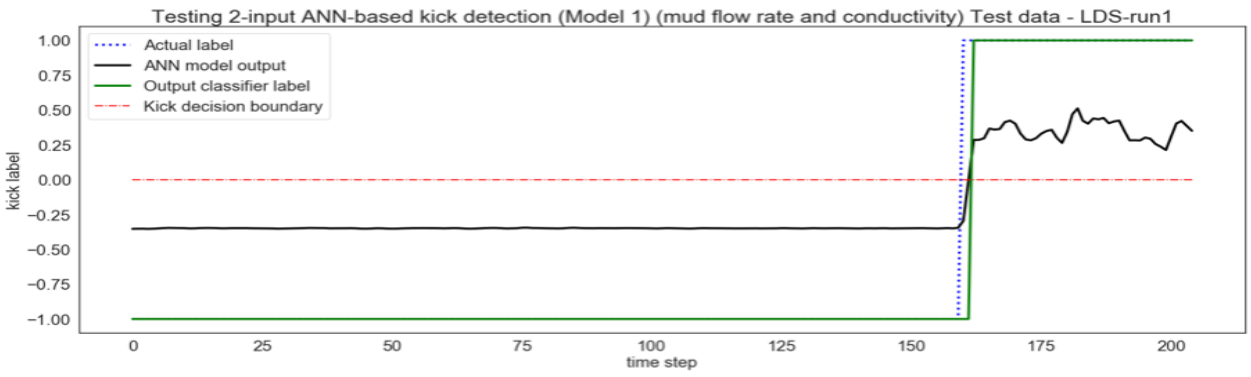

Figure 6-28: Plot from testing two-input ANN (model 1) with data from LDS system.

6.3.6 Density and conductivity

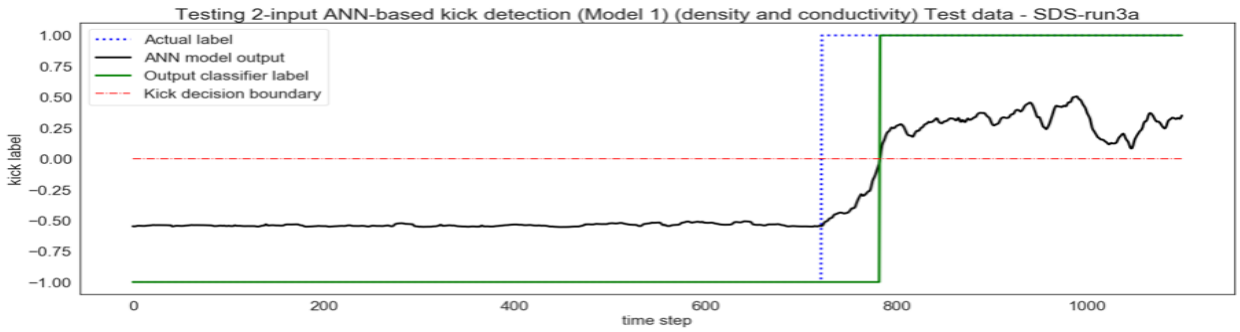

Figure 6-29: Plot from testing two-input ANN (model 1) with data from SDS system.

Table 6-17: Two-input ANN (model 1) performance metrics such as accuracy, recall, precision, F1-score, missed detection and false alarm rate for the three set of test data.

Model 1 (Two-input parameters)			
Input parameters	Density and conductivity		
		Test data	
		SDS system SDS – different scenario	LDS system LDS Data
Classification accuracy		0.94	0.99
Confusion matrix	0,0	722	160
	0,1	0	0
	1,0	61	3
	1,1	317	42
Precision	No-Kick	0.92	0.98
	Kick	1.00	1.00
Recall	No-Kick	1.00	1.00
	Kick	0.84	0.93
F1-score	No-Kick	0.96	0.99
	Kick	0.91	0.97
Support	No-Kick	722	160
	Kick	378	45
False Alarm		No	No
Missed detection		No	No
Training data = SDS1-run1a Test data = SDS1-run3a			

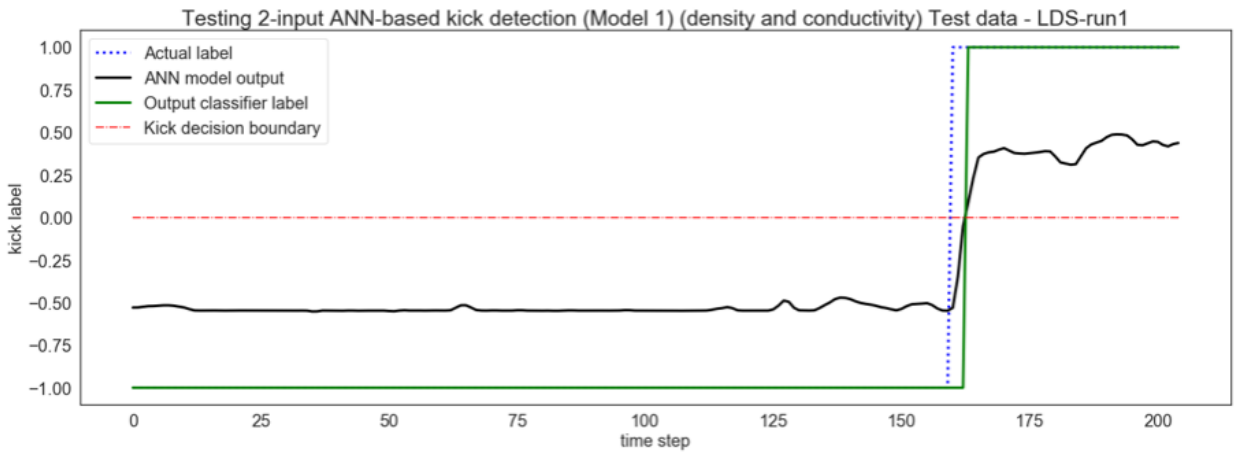

Figure 6-30: Plot from testing two-input ANN (model 1) with data from LDS system.

6.3.7 Discussion of two-input parameter ANN results

There were six possible combination of two parameters from the four parameters considered in this study. Model performance was similar as shown in *Table* 6-12, *Table* 6-13, *Table* 6-14, *Table* 6-15, *Table* 6-16 and *Table* 6-17. All but one combination showed success in detecting the kick event without a false alarm (FP = 0) for all test instances as seen in *Figure* 6-20. The combination of downhole pressure and mud flow rate detected successfully when tested with data from the SDS system but produced a false alarm (FP = 5) when tested with data from the LDS system. Such result is undesirable for a critical warning system because a reliable model should generalize well to new data.

6.4 Further discussion

Four-input and three-input parameter ANN model was observed to successfully detect kick events in all test cases. Two-input parameter ANN models may be prone to false alarm as observed in *Figure* 6-20 with downhole pressure and mud flow rate. This makes it less attractive. Single-input parameter-based models are usually not encouraged because of the susceptibility of recorded data to process and measurement noise, uncertainties, disturbances, and faults which could be catastrophic in the event of sensor failures. Single input parameter was not considered because in this thesis, we explore the use of ANNs (supervised learning) and it is not possible to train a network if there is only one input – as that input will have 100% weight. Relying on a single parameter to monitor a condition with very high consequence (blowout) is dangerous. The internal structure of the developed ANN model shows the weights. It helps us to determine which parameter is more significant to the goal of early kick detection. Even when one neuron is used, it is still not fully linear as we do use an activation function. In a general ANN (with more than one neuron), use of multiple nonlinear blocks would make such analysis not possible. The weight of each parameter for each model trained is shown in Table 6-7. The consistent positive-valued weights of downhole pressure and mud flow-out rate shows that they are more significant in identifying a kick event for all scenarios.

ANNs could be used to improve the system response in an MPD system. The proposed early kick detection method using an ANN would form an essential component of such a system. Generalizing this model to real drilling scenario necessitates collaboration with the industry to secure field data. In the absence of this, the model has been tested with drilling data from different laboratory scale drilling system.

7 Conclusions and Suggested Future Work

7.1 Conclusions

This research presented an experimental methodology that relied on collecting downhole data in a laboratory and a data processing methodology that uses machine learning to train and test data from two experimental drilling systems. It presented a detailed design of a new kick experiment setup that uses a Large Drilling Simulator (LDS) and synthetic rock samples. It also provides a detailed design of synthetic rock sample with geometrical capability to trap high-pressure formation fluid within. This generated new set of experimental data from kick caused by drilling into trapped high-pressure fluid zone using downhole parameter monitoring.

This study has focused on using supervised learning in facilitating early kick detection. From results obtained, we can conclude that supervised data-driven modelling, combined with downhole parameter monitoring, is effective in early kick detection. A data-driven model for early kick detection based on neural network-based supervised machine learning using historical drilling data from drilling systems with downhole monitoring capabilities has been developed. The model was tested and evaluated with data from the SDS system, SDS system with faulty conductivity data and different experimental drilling system.

The main strength of this work is the simplicity of the detection system presented. This work investigates the simplest ANN that would detect a kick. It demonstrates that a simple feedforward ANN with four input nodes, no (i.e. zero) hidden layers and one output neuron that employs a simple tanh activation function can model experimental drilling data to detect kicks. The study highlighted important factors such as missed detection, false detection, and detection time together with the associated tradeoffs to be considered when building a reliable kick

detection model. It showed that for a simple ANN structure, link weights could show the more significant parameters in achieving a learning goal. The parameters identified may not always be minimally sufficient to guarantee reliability. It also demonstrated how monitoring and modelling with multiple downhole parameters can reduce the susceptibility of the system to a false alarm.

This study led to a preliminary success in validating results of numerical analysis with laboratory experimentation. This study uses the parameters measured near the bottom of the drilled hole. We understand it is challenging to obtain downhole data from field; however, with advancement of sensor and communication technology this is becoming feasible.

7.2 Suggested future work

Further scope will include testing field data to validate these findings then training the model with other drilling parameters such as weight on bit, rate of penetration, torque etc. There exists the possibility of training a model that could distinguish among the different anomalous drilling events. To achieve this, a more complex neural network architecture will be required. A possible extension of this work is scaling the model to capture other types of drilling problems.

The next step from this effort after validating the model with field data is to leverage edge computing to perform sensor data processing downhole by implementing data-driven models as embedded software on a System-on-Chip (SoC). A simple data-driven model is particularly rewarding when data processing is done downhole. This will allow the design of optimized domain-specific hardware architecture. The hardware used is typically battery powered. Simpler and fewer software operations such as multiplication and addition (tanh can be implemented in a look-up table) will lead to less power consumption, smaller memory and simpler cooling requirements. This will lead to an increase battery run time, miniaturized designs/reduced bulk size, reduced maintenance frequency for such hardware, improved response time and lower

costs. The ability to deploy SoC modules downhole for real-time sensor data processing during critical monitoring is a key factor driving the research and application of simple computational models to drilling/subsea/underwater data.

References

[1] J. D. Brakel, B. A. Tarr, W. Cox, F. Jørgensen, and H. V. Straume, "SMART kick detection; first step on the well control automation journey," *SPE/IADC Drill. Conf. Proc.*, vol. 2015-Janua, no. September, pp. 725–741, 2015.

[2] X. Sun, B. Sun, S. Zhang, Z. Wang, Y. Gao, and H. Li, "A new pattern recognition model for gas kick diagnosis in deepwater drilling," *J. Pet. Sci. Eng.*, vol. 167, no. November 2017, pp. 418–425, 2018.

[3] J. Fu, Y. Su, W. Jiang, and L. Xu, "Development and testing of kick detection system at mud line in deepwater drilling," *J. Pet. Sci. Eng.*, 2015.

[4] M. A. Ahmed, O. A. Hegab, and A. Sabry, "Early detection enhancement of the kick and near-balance drilling using mud logging warning sign," *Egypt. J. Basic Appl. Sci.*, vol. 3, pp. 85–93, 2016.

[5] P. Griffin, "Early Kick Detection holds Kill Pressure lower," in *SPE Symposium on Mechanical Engineering aspects of Drilling and Production*, 1967.

[6] "Kick Detection: Information Technology Revolution Spurs New Research to Enhance Well Risk Management | Exploration & Production." [Online]. Available: https://www.ep.total.com/en/expertise/drilling-wells/kick-detection-information-technology-revolution-spurs-new-research-enhance. [Accessed: 17-Apr-2020].

[7] A. A. Nayeem, R. Venkatesan, and F. Khan, "Monitoring of down-hole parameters for early kick detection," *J. Loss Prev. Process Ind.*, vol. 40, pp. 43–54, 2016.

[8] R. Islam, F. Khan, and R. Venkatesan, "Real time risk analysis of kick detection: Testing and validation," *Reliab. Eng. Syst. Saf.*, vol. 161, no. May 2016, pp. 25–37, 2017.

[9] I. O. Sule, F. Khan, and S. Butt, "Experimental investigation of gas kick effects on dynamic

drilling parameters," *J. Pet. Explor. Prod. Technol.*, vol. 9, no. 1, pp. 605–616, 2019.

[10] H. Tang, S. Zhang, F. Zhang, and S. Venugopal, "Time series data analysis for automatic flow influx detection during drilling," *J. Pet. Sci. Eng.*, vol. 172, no. June 2018, pp. 1103–1111, 2019.

[11] Z. Zhang, Y. Xiong, L. Mao, J. Lu, M. Wang, and G. Peng, "Transient temperature prediction models of wellbore and formation in well-kick condition during circulation stage," *J. Pet. Sci. Eng.*, vol. 175, no. June 2018, pp. 266–279, 2019.

[12] C. S. Avelar, P. R. Ribeiro, and K. Sepehrnoori, "Deepwater gas kick simulation," *J. Pet. Sci. Eng.*, 2009.

[13] J. I. Hage and D. ter Avest, "Borehole acoustics applied to kick detection," *J. Pet. Sci. Eng.*, 1994.

[14] N. Tamim, D. M. Laboureur, A. R. Hasan, and M. S. Mannan, "Developing leading indicators-based decision support algorithms and probabilistic models using Bayesian network to predict kicks while drilling," *Process Saf. Environ. Prot.*, vol. 121, pp. 239–246, 2019.

[15] D. Hargreaves, S. Jardine, and B. Jeffryes, "Early Kick Detection for Deepwater Drilling : New Probabilistic Methods Applied in the Field," in *SPE Annual Technical Conference and Exhibition held in New Orleans, Louisiana, 30 September–3 October 2001*, 2001.

[16] S. A. Adedigba, O. Oloruntobi, F. Khan, and S. Butt, "Data-driven dynamic risk analysis of offshore drilling operations," *J. Pet. Sci. Eng.*, vol. 165, no. February, pp. 444–452, 2018.

[17] C. I. Ossai, "Modified spatio-temporal neural networks for failure risk prognosis and status forecasting of permanent downhole pressure gauge," *J. Pet. Sci. Eng.*, vol. 184, no. September 2019, p. 106496, 2020.

[18] W. Zhi, R. Senanayake, L. Ott, and F. Ramos, "Spatiotemporal Learning of Directional Uncertainty in Urban Environments," pp. 2–3.

[19] S. A. Adedigba, F. Khan, and M. Yang, "Dynamic failure analysis of process systems using neural

networks," *Process Saf. Environ. Prot.*, vol. 111, pp. 529–543, 2017.

[20] K. Chhantyal, M. Hoang, H. Viumdal, and S. Mylvaganam, "Flow Rate Estimation using Dynamic Arti?cial Neural Networks with Ultrasonic Level Measurements," *Proc. 9th EUROSIM Congr. Model. Simulation, EUROSIM 2016, 57th SIMS Conf. Simul. Model. SIMS 2016*, vol. 142, pp. 561–567, 2018.

[21] H. Jiang, G. Liu, J. Li, T. Zhang, C. Wang, and K. Ren, "Numerical simulation of a new early gas kick detection method using UKF estimation and GLRT," *J. Pet. Sci. Eng.*, vol. 173, no. July 2018, pp. 415–425, 2019.

[22] L. N. Hüffner, J. O. Trierweiler, and M. Farenzena, "Are complex black-box models for Permanent Downhole Gauge pressure estimation necessary?," *J. Pet. Sci. Eng.*, vol. 173, no. December 2017, pp. 715–732, 2019.

[23] M. Sabah, M. Talebkeikhah, F. Agin, F. Talebkeikhah, and E. Hasheminasab, "Application of decision tree, artificial neural networks, and adaptive neuro-fuzzy inference system on predicting lost circulation: A case study from Marun oil field," *J. Pet. Sci. Eng.*, vol. 177, no. February 2018, pp. 236–249, 2019.

[24] V. de J. da S. Ribeiro, G. F. de M. Oliveira, M. Cristian, A. L. Martins, L. D. Fernandes, and M. P. Vega, "Neural network based controllers for the oil well drilling process," *J. Pet. Sci. Eng.*, vol. 176, no. August 2018, pp. 573–583, 2019.

[25] F. Deregeh, M. Karimian, and H. Nezamabadi-Pour, "A New Method of Earlier Kick Assessment Using ANFIS," *Iran. J. Oil Gas Sci. Technol.*, vol. 1, no. 1, pp. 33–41, 2013.

[26] S. Unrau, P. Torrione, M. Hibbard, R. Smith, L. Olesen, and J. Watson, "Machine Learning Algorithms Applied to Detection of Well Control Events," in *SPE Kingdom of Saudi Arabia Annual Technical Symposium and Exhibition Dammam, Saudi Arabia, 24–27 April 2017*, 2017.

[27] A. Karimi Vajargah and E. van Oort, “Early kick detection and well control decision-making for managed pressure drilling automation,” *J. Nat. Gas Sci. Eng.*, vol. 27, pp. 354–366, 2015.

[28] H. Yang *et al.*, “A new method for early gas kick detection based on the consistencies and differences of bottomhole pressures at two measured points,” *J. Pet. Sci. Eng.*, vol. 176, no. November 2018, pp. 1095–1105, 2019.

[29] D. M. Nhat, R. Venkatesan, and F. Khan, “Data-driven Bayesian network model for early kick detection in industrial drilling process,” *Process Saf. Environ. Prot.*, vol. 138, pp. 130–138, Jun. 2020.

[30] J. A. Ajienka and O. O. Owolabi, “Application of mass balance of kick fluid in well control,” *J. Pet. Sci. Eng.*, 1991.

[31] Z. C. Lin and C. B. Yang, “Evaluation of machine selection by the AHP method,” *J. Mater. Process. Technol.*, vol. 57, no. 3–4, pp. 253–258, 1996.

[32] N. Tamim, D. M. Laboureur, R. A. Mentzer, A. R. Hasan, and M. S. Mannan, “A framework for developing leading indicators for offshore drillwell blowout incidents,” *Process Saf. Environ. Prot.*, vol. 106, pp. 256–262, 2017.

[33] M. Nait Amar, N. Zeraibi, and K. Redouane, “Bottom hole pressure estimation using hybridization neural networks and grey wolves optimization,” *Petroleum*, vol. 4, no. 4, pp. 419–429, 2018.

[34] P. Spesivtsev *et al.*, “Predictive model for bottomhole pressure based on machine learning,” *J. Pet. Sci. Eng.*, vol. 166, no. March, pp. 825–841, 2018.

[35] J. E. Udegbunam, “Improved Well Design with Risk and Uncertainty Analysis by,” University of Stavanger, 2014.

[36] M. A. Ojinnaka and J. J. Beaman, “Full-course drilling model for well monitoring and stochastic estimation of kick,” *J. Pet. Sci. Eng.*, vol. 166, no. March, pp. 33–43, 2018.

[37] Z. Zhang, “Development and Characterization of Portland Cement Based Rock Like Materials for Drilling Experiments,” 2016.

[38] U. Prasad, “Drillability of a Rock In Terms of Its Physico-Mechanical And Micro-Structural Properties,” *43rd U.S. Rock Mechanics Symposium & 4th U.S. - Canada Rock Mechanics Symposium*. American Rock Mechanics Association, Asheville, North Carolina, p. 7, 2009.

[39] M. B. Diaz, K. Y. Kim, H. S. Shin, and L. Zhuang, “Predicting rate of penetration during drilling of deep geothermal well in Korea using artificial neural networks and real-time data collection,” *J. Nat. Gas Sci. Eng.*, vol. 67, pp. 225–232, 2019.

[40] H. Fattahi and H. Bazdar, “Applying improved artificial neural network models to evaluate drilling rate index,” *Tunn. Undergr. Sp. Technol.*, vol. 70, pp. 114–124, 2017.

[41] S. B. Ashrafi, M. Anemangely, M. Sabah, and M. J. Ameri, “Application of hybrid artificial neural networks for predicting rate of penetration (ROP): A case study from Marun oil field,” *J. Pet. Sci. Eng.*, vol. 175, pp. 604–623, 2019.

[42] T. M. Mitchell, *McGrawHill,.Tom.Mitchell.-.Machine.Learning.pdf*. McGraw-Hill Science/Engineering/Math, 1997.

[43] J. W. Cooley and J. W. Tukey, “An Algorithm for the Machine Calculation of Complex Fourier Series,” *Math. Comput.*, vol. 19, no. 90, p. 297, 1965.

[44] D. P. Mandic and J. A. Chambers, *Recurrent Neural Networks for Prediction Authored (Hardback); 0-470-84535-X (Electronic) RECURRENT NEURAL NETWORKS FOR PREDICTION*, vol. 4. 2001.

[45] L. R. Medsker and L. C. Jain, “RECURRENT NEURAL NETWORKS Design and Applications,” *Book*, p. 389, 2001.

[46] J. Ivan and M. Gonzalez, “Deep Recurrent Neural Networks for Fault Detection and Classification

by," 2018.

[47] H. Sepp and S. J'urgen, "Long Short Term Memory," *Neural Comput.*, vol. 9, no. 8, pp. 1–32, 1997.

[48] K. Greff, R. K. Srivastava, J. Koutnik, B. R. Steunebrink, and J. Schmidhuber, "LSTM: A Search Space Odyssey," *IEEE Trans. Neural Networks Learn. Syst.*, vol. 28, no. 10, pp. 2222–2232, 2017.

[49] R. Dey and F. M. Salemt, "Gate-variants of Gated Recurrent Unit (GRU) neural networks," *Midwest Symp. Circuits Syst.*, vol. 2017-Augus, pp. 1597–1600, 2017.

[50] R. Fu, Z. Zhang, and L. Li, "Using LSTM and GRU neural network methods for traffic flow prediction," *Proc. - 2016 31st Youth Acad. Annu. Conf. Chinese Assoc. Autom. YAC 2016*, no. November 2016, pp. 324–328, 2017.

[51] J. Chorowski and J. M. Zurada, "Learning understandable neural networks with nonnegative weight constraints," *IEEE Trans. Neural Networks Learn. Syst.*, vol. 26, no. 1, pp. 62–69, 2015.

[52] C. Parisien, C. H. Anderson, and C. Eliasmith, "Solving the problem of negative synaptic weights in cortical models," *Neural Comput.*, vol. 20, no. 6, pp. 1473–1494, 2008.

[53] R. Fraczkiewicz, D. Zhuang, J. Zhang, D. Miller, W. S. Woltosz, and M. B. Bolger, "Busting the Black Box Myth: Designing Out Unwanted ADMET Properties with Machine Learning Approaches," *CICSJ Bull.*, vol. 27, no. 4, pp. 96–96, 2009.

[54] D. P. Kingma and J. Ba, "Adam: A Method for Stochastic Optimization," pp. 1–15, 2014.

[55] S. Muojeke, R. Venkatesan, and F. Khan, "Supervised data-driven approach to early kick detection during drilling operation," *J. Pet. Sci. Eng.*, vol. 192, no. April, p. 107324, 2020.

Appendix

Corresponding training features and labels of each trained model

Table 0-1: Corresponding training features and labels of model 1, Test data – SDS1-run3a.

Time (sec)	Downhole Pressure (psi g)	Mud Flow-out rate (lb/h)	Density (lb/ft3)	Conductivity (uS/cm)	Actual Label (Encoded)	Actual Label	Classified Label (from model)	Model Output
71.00	12.18	561.22	62.37	301.07	-1	No-Kick	No-Kick	-0.59
71.10	12.35	564.85	62.39	301.03	-1	No-Kick	No-Kick	-0.59
71.20	11.18	555.20	62.39	301.03	-1	No-Kick	No-Kick	-0.60
71.30	11.05	565.19	62.36	301.36	-1	No-Kick	No-Kick	-0.60
71.40	13.09	580.37	62.06	301.21	-1	No-Kick	No-Kick	-0.59
71.50	13.78	590.30	62.05	300.78	-1	No-Kick	No-Kick	-0.58
71.60	13.21	599.94	62.29	300.76	-1	No-Kick	No-Kick	-0.59
71.70	12.62	601.59	62.32	300.74	-1	No-Kick	No-Kick	-0.59
71.80	12.59	606.41	62.35	300.48	-1	No-Kick	No-Kick	-0.59
71.90	13.31	604.31	62.09	299.92	-1	No-Kick	No-Kick	-0.58
72.00	14.77	625.92	62.09	299.41	-1	No-Kick	No-Kick	-0.57
72.10	18.87	663.38	62.36	299.10	-1	No-Kick	No-Kick	-0.55
72.20	25.75	748.32	62.39	298.68	1	Kick	No-Kick	-0.51
72.30	28.27	894.97	62.39	295.82	1	Kick	No-Kick	-0.48
72.40	26.36	1062.24	62.39	289.89	1	Kick	No-Kick	-0.46
72.50	26.71	1238.30	62.39	285.06	1	Kick	No-Kick	-0.43
72.60	30.07	1424.80	62.39	283.04	1	Kick	No-Kick	-0.39
72.70	34.81	1602.60	62.39	282.26	1	Kick	No-Kick	-0.34
72.80	31.99	1751.95	62.39	280.42	1	Kick	No-Kick	-0.35
72.90	28.04	1909.02	62.39	276.33	1	Kick	No-Kick	-0.35
73.00	28.17	2028.42	62.39	272.92	1	Kick	No-Kick	-0.33
73.10	26.42	2127.35	62.39	271.67	1	Kick	No-Kick	-0.33
73.20	26.48	2228.03	62.39	271.06	1	Kick	No-Kick	-0.32
73.30	27.35	2296.22	62.39	268.83	1	Kick	No-Kick	-0.30
73.40	27.38	2351.34	62.39	264.14	1	Kick	No-Kick	-0.28
73.50	26.99	2390.90	62.39	260.30	1	Kick	No-Kick	-0.27
73.60	28.15	2433.29	62.39	258.91	1	Kick	No-Kick	-0.26
73.70	30.58	2454.66	62.39	258.35	1	Kick	No-Kick	-0.24
73.80	30.40	2463.49	62.39	257.33	1	Kick	No-Kick	-0.23
73.90	28.78	2481.38	62.39	255.58	1	Kick	No-Kick	-0.24
74.00	27.66	2491.51	62.39	254.32	1	Kick	No-Kick	-0.24
74.10	26.11	2502.12	62.39	253.91	1	Kick	No-Kick	-0.25
74.20	29.03	2497.17	62.39	253.84	1	Kick	No-Kick	-0.23

74.30	30.99	2495.44	62.39	254.23	1	Kick	No-Kick	-0.22
74.40	27.06	2499.73	62.39	255.39	1	Kick	No-Kick	-0.25
74.50	24.54	2504.19	62.39	256.52	1	Kick	No-Kick	-0.27
74.60	22.90	2501.47	62.32	256.93	1	Kick	No-Kick	-0.28
74.70	23.56	2472.69	62.06	257.09	1	Kick	No-Kick	-0.28
74.80	24.85	2459.02	61.94	257.06	1	Kick	No-Kick	-0.27
74.90	24.34	2463.35	61.89	256.91	1	Kick	No-Kick	-0.27
75.00	24.90	2475.46	61.46	256.85	1	Kick	No-Kick	-0.26
75.10	25.04	2493.69	60.93	256.77	1	Kick	No-Kick	-0.25
75.20	22.17	2485.55	60.26	256.84	1	Kick	No-Kick	-0.26
75.30	21.19	2459.21	59.27	258.08	1	Kick	No-Kick	-0.26
75.40	22.85	2436.94	58.47	261.06	1	Kick	No-Kick	-0.24
75.50	23.99	2409.08	58.08	263.56	1	Kick	No-Kick	-0.24
75.60	24.84	2368.45	57.71	264.42	1	Kick	No-Kick	-0.23
75.70	23.56	2321.01	56.97	264.54	1	Kick	No-Kick	-0.24
75.80	23.04	2276.45	55.72	263.66	1	Kick	No-Kick	-0.22
75.90	23.30	2225.74	54.68	261.62	1	Kick	No-Kick	-0.21
76.00	23.67	2186.82	53.86	259.86	1	Kick	No-Kick	-0.19
76.10	23.67	2158.11	53.01	259.20	1	Kick	No-Kick	-0.18
76.20	26.10	2117.90	52.17	258.99	1	Kick	No-Kick	-0.15
76.30	26.39	2085.09	51.00	260.77	1	Kick	No-Kick	-0.14
76.40	23.06	2034.93	50.41	265.18	1	Kick	No-Kick	-0.17
76.50	23.99	1971.24	50.37	268.70	1	Kick	No-Kick	-0.18
76.60	27.54	1928.89	50.03	269.95	1	Kick	No-Kick	-0.16
76.70	26.15	1908.82	49.66	269.95	1	Kick	No-Kick	-0.17
76.80	22.91	1916.84	49.35	269.18	1	Kick	No-Kick	-0.18
76.90	23.29	1940.66	49.12	267.44	1	Kick	No-Kick	-0.17
77.00	23.48	1954.55	48.87	265.78	1	Kick	No-Kick	-0.16
77.10	23.41	1944.06	48.69	265.11	1	Kick	No-Kick	-0.15
77.20	22.89	1921.84	48.66	264.56	1	Kick	No-Kick	-0.16
77.30	22.92	1921.02	48.41	261.09	1	Kick	No-Kick	-0.15
77.40	22.89	1946.82	47.82	253.55	1	Kick	No-Kick	-0.11
77.50	22.31	1981.77	46.96	247.51	1	Kick	No-Kick	-0.08
77.60	22.35	2010.62	46.16	245.32	1	Kick	No-Kick	-0.06
77.70	22.43	2021.81	45.55	244.35	1	Kick	No-Kick	-0.05
77.80	22.11	2027.88	44.91	241.85	1	Kick	No-Kick	-0.04
77.90	21.95	2048.58	44.33	237.51	1	Kick	No-Kick	-0.01
78.00	22.91	2068.23	43.64	234.31	1	Kick	Kick	0.02
78.10	22.27	2082.16	42.57	233.05	1	Kick	Kick	0.03
78.20	21.47	2074.91	41.36	232.09	1	Kick	Kick	0.05
78.30	23.42	2069.22	40.04	226.39	1	Kick	Kick	0.10
78.40	23.39	2083.12	38.89	213.67	1	Kick	Kick	0.15
78.50	19.64	2078.73	38.12	202.99	1	Kick	Kick	0.16
78.60	21.48	2047.85	37.54	198.93	1	Kick	Kick	0.19

78.70	24.58	2011.73	36.92	197.45	1	Kick	Kick	0.22
78.80	22.55	1987.21	36.10	195.52	1	Kick	Kick	0.22
78.90	22.11	1990.38	35.31	192.42	1	Kick	Kick	0.24
79.00	25.51	1998.29	34.65	189.99	1	Kick	Kick	0.28

Table 0-2: Corresponding training features and labels of model 2, Test data – SDS1-run1a.

Time (sec)	Downhole Pressure (psi g)	Mud Flow-out rate (lb/h)	Density (lb/ft3)	Conductivity (uS/cm)	Actual Label (Encoded)	Actual Label	Classified Label (from model)	Model Output
73.00	11.24	475.69	62.39	301.88	-1	No-Kick	No-Kick	-0.63
73.10	6.05	472.41	62.39	301.88	-1	No-Kick	No-Kick	-0.65
73.20	5.36	471.94	62.39	302.14	-1	No-Kick	No-Kick	-0.65
73.30	4.74	476.56	62.39	302.25	-1	No-Kick	No-Kick	-0.65
73.40	7.28	478.61	62.39	302.23	-1	No-Kick	No-Kick	-0.65
73.50	9.21	477.39	62.39	302.26	-1	No-Kick	No-Kick	-0.64
73.60	7.09	473.97	62.39	302.29	-1	No-Kick	No-Kick	-0.65
73.70	7.13	474.55	62.39	302.28	-1	No-Kick	No-Kick	-0.65
73.80	6.97	484.58	62.39	302.23	-1	No-Kick	No-Kick	-0.65
73.90	8.08	484.48	62.39	302.16	-1	No-Kick	No-Kick	-0.64
74.00	9.49	472.36	62.39	302.11	1	Kick	No-Kick	-0.64
74.10	10.01	479.27	62.39	302.17	1	Kick	No-Kick	-0.64
74.20	14.53	516.60	62.39	302.25	1	Kick	No-Kick	-0.61
74.30	26.52	571.90	62.39	302.26	1	Kick	No-Kick	-0.55
74.40	29.43	658.82	62.39	302.32	1	Kick	No-Kick	-0.53
74.50	23.40	791.36	62.39	302.36	1	Kick	No-Kick	-0.53
74.60	23.89	951.91	62.39	302.41	1	Kick	No-Kick	-0.51
74.70	26.11	1126.11	62.39	302.40	1	Kick	No-Kick	-0.47
74.80	25.36	1292.72	62.39	301.77	1	Kick	No-Kick	-0.44
74.90	26.03	1443.37	62.37	299.03	1	Kick	No-Kick	-0.40
75.00	29.06	1593.98	62.37	295.94	1	Kick	No-Kick	-0.35
75.10	29.46	1740.85	62.39	294.70	1	Kick	No-Kick	-0.32
75.20	30.17	1869.12	62.39	294.30	1	Kick	No-Kick	-0.29
75.30	37.48	1968.10	62.39	293.27	1	Kick	No-Kick	-0.22
75.40	36.86	2047.96	62.39	289.45	1	Kick	No-Kick	-0.20
75.50	29.13	2117.50	62.37	285.31	1	Kick	No-Kick	-0.22
75.60	29.77	2170.10	62.23	283.64	1	Kick	No-Kick	-0.20
75.70	30.30	2211.70	62.23	282.93	1	Kick	No-Kick	-0.19
75.80	29.76	2245.39	62.37	281.79	1	Kick	No-Kick	-0.18
75.90	29.45	2267.89	62.31	278.22	1	Kick	No-Kick	-0.17
76.00	28.94	2282.45	61.80	274.29	1	Kick	No-Kick	-0.16
76.10	29.02	2291.94	61.76	272.73	1	Kick	No-Kick	-0.15
76.20	28.65	2295.51	62.23	272.19	1	Kick	No-Kick	-0.16
76.30	29.46	2295.95	62.29	271.10	1	Kick	No-Kick	-0.15
76.40	29.20	2295.65	62.29	267.28	1	Kick	No-Kick	-0.14
76.50	27.37	2297.77	62.34	263.16	1	Kick	No-Kick	-0.15
76.60	27.50	2294.37	62.26	261.64	1	Kick	No-Kick	-0.14
76.70	28.45	2281.26	62.07	261.16	1	Kick	No-Kick	-0.13

76.80	29.88	2277.40	62.11	261.53	1	Kick	No-Kick	-0.13
76.90	30.29	2284.40	62.14	263.90	1	Kick	No-Kick	-0.13
77.00	27.33	2292.23	62.00	266.56	1	Kick	No-Kick	-0.15
77.10	24.79	2313.95	61.73	267.68	1	Kick	No-Kick	-0.16
77.20	26.34	2350.23	61.24	268.10	1	Kick	No-Kick	-0.14
77.30	26.69	2384.12	60.67	269.04	1	Kick	No-Kick	-0.12
77.40	25.53	2412.04	59.93	272.48	1	Kick	No-Kick	-0.12
77.50	25.72	2442.61	58.89	276.20	1	Kick	No-Kick	-0.11
77.60	26.86	2475.95	57.90	277.69	1	Kick	No-Kick	-0.08
77.70	29.96	2494.22	56.94	278.23	1	Kick	No-Kick	-0.05
77.80	31.36	2498.61	55.66	279.25	1	Kick	No-Kick	-0.02
77.90	27.67	2504.19	54.37	282.71	1	Kick	No-Kick	-0.03
78.00	24.70	2501.48	53.06	286.56	1	Kick	No-Kick	-0.04
78.10	24.96	2483.22	51.57	288.21	1	Kick	No-Kick	-0.03
78.20	32.90	2464.47	50.06	288.71	1	Kick	Kick	0.04
78.30	34.11	2427.82	48.64	289.50	1	Kick	Kick	0.05
78.40	24.22	2366.67	47.24	292.40	1	Kick	No-Kick	-0.01
78.50	22.14	2312.20	46.01	295.42	1	Kick	No-Kick	-0.03
78.60	23.56	2267.29	44.84	296.53	1	Kick	No-Kick	-0.01
78.70	21.92	2218.08	43.65	296.96	1	Kick	No-Kick	-0.02
78.80	18.34	2166.14	42.77	297.03	1	Kick	No-Kick	-0.04
78.90	19.22	2108.41	41.96	296.87	1	Kick	No-Kick	-0.04
79.00	22.68	2041.54	40.99	296.48	1	Kick	No-Kick	-0.01
79.10	22.93	1972.91	40.07	296.26	1	Kick	No-Kick	-0.02
79.20	19.70	1884.65	39.22	296.22	1	Kick	No-Kick	-0.04
79.30	18.61	1783.45	38.31	295.28	1	Kick	No-Kick	-0.06
79.40	21.58	1696.78	37.45	291.63	1	Kick	No-Kick	-0.04
79.50	22.47	1618.42	36.78	287.16	1	Kick	No-Kick	-0.03
79.60	21.61	1536.95	36.06	284.99	1	Kick	No-Kick	-0.04
79.70	21.73	1469.30	35.33	284.23	1	Kick	No-Kick	-0.04
79.80	21.57	1420.64	34.85	282.26	1	Kick	No-Kick	-0.04
79.90	19.70	1370.87	34.60	274.38	1	Kick	No-Kick	-0.04
80.00	20.13	1323.76	34.39	265.66	1	Kick	No-Kick	-0.03
80.10	21.68	1288.46	34.21	262.20	1	Kick	No-Kick	-0.02
80.20	19.85	1261.54	34.13	260.88	1	Kick	No-Kick	-0.03
80.30	18.33	1235.42	33.96	258.73	1	Kick	No-Kick	-0.04
80.40	19.12	1214.53	33.59	251.90	1	Kick	No-Kick	-0.02
80.50	20.22	1213.69	33.27	244.68	1	Kick	Kick	0.01
80.60	20.96	1229.98	33.12	241.82	1	Kick	Kick	0.03
80.70	22.14	1248.37	32.96	240.75	1	Kick	Kick	0.04
80.80	20.69	1262.73	32.74	238.31	1	Kick	Kick	0.05
80.90	17.93	1273.70	32.51	229.63	1	Kick	Kick	0.05
81.00	18.18	1282.49	32.32	220.21	1	Kick	Kick	0.08
81.10	18.53	1285.79	32.24	216.57	1	Kick	Kick	0.09

81.20	18.30	1277.27	32.14	215.31	1	Kick	Kick	0.10
81.30	18.78	1270.38	32.01	213.02	1	Kick	Kick	0.10
81.40	19.28	1272.92	32.00	205.75	1	Kick	Kick	0.12
81.50	18.95	1267.26	32.09	197.99	1	Kick	Kick	0.14
81.60	18.99	1250.63	31.98	194.83	1	Kick	Kick	0.14
81.70	17.22	1235.83	31.63	193.60	1	Kick	Kick	0.14
81.80	17.11	1220.00	31.24	191.50	1	Kick	Kick	0.14
81.90	19.29	1189.00	30.94	184.33	1	Kick	Kick	0.17
82.00	20.11	1158.96	30.69	176.40	1	Kick	Kick	0.19

Table 0-3: Corresponding training features and labels of model 3, Test data – SDS1-run2a.

Time (sec)	Downhole Pressure (psi g)	Mud Flow-out rate (lb/h)	Density (lb/ft3)	Conductivity (uS/cm)	Actual Label (Encoded)	Actual Label	Classified Label (from model)	Model Output
70.00	9.07	441.54	62.39	302.20	-1	No-Kick	No-Kick	-0.66
70.10	9.71	453.62	62.39	301.92	-1	No-Kick	No-Kick	-0.65
70.20	9.38	458.19	62.39	301.81	-1	No-Kick	No-Kick	-0.65
70.30	8.06	451.06	62.39	301.94	1	Kick	No-Kick	-0.66
70.40	6.91	444.22	62.39	302.11	1	Kick	No-Kick	-0.67
70.50	5.72	445.00	62.39	302.04	1	Kick	No-Kick	-0.67
70.60	9.06	450.39	62.39	301.80	1	Kick	No-Kick	-0.66
70.70	15.63	498.10	62.39	301.70	1	Kick	No-Kick	-0.62
70.80	19.14	617.96	62.38	301.56	1	Kick	No-Kick	-0.58
70.90	21.26	796.40	62.33	301.39	1	Kick	No-Kick	-0.54
71.00	16.53	998.02	62.33	300.01	1	Kick	No-Kick	-0.52
71.10	17.18	1197.01	62.38	297.63	1	Kick	No-Kick	-0.48
71.20	24.70	1386.44	62.39	296.00	1	Kick	No-Kick	-0.39
71.30	26.08	1563.90	62.37	295.51	1	Kick	No-Kick	-0.34
71.40	27.32	1733.91	62.37	295.06	1	Kick	No-Kick	-0.29
71.50	37.48	1899.68	62.39	289.89	1	Kick	No-Kick	-0.16
71.60	33.24	2034.88	62.39	281.55	1	Kick	No-Kick	-0.14
71.70	23.78	2135.11	62.39	276.34	1	Kick	No-Kick	-0.17
71.80	28.94	2215.35	62.37	274.50	1	Kick	No-Kick	-0.11
71.90	30.05	2288.64	62.20	273.69	1	Kick	No-Kick	-0.07
72.00	30.81	2363.93	62.20	270.11	1	Kick	No-Kick	-0.04
72.10	31.21	2420.82	62.37	264.56	1	Kick	No-Kick	-0.01
72.20	30.46	2452.84	62.39	261.46	1	Kick	Kick	0.00
72.30	30.52	2461.18	62.39	260.30	1	Kick	Kick	0.01
72.40	29.52	2469.70	62.38	259.65	1	Kick	Kick	0.00
72.50	29.11	2486.42	62.38	259.04	1	Kick	Kick	0.01
72.60	29.76	2504.19	62.39	258.22	1	Kick	Kick	0.02
72.70	29.94	2501.97	62.39	257.40	1	Kick	Kick	0.02
72.80	28.11	2471.11	62.39	257.20	1	Kick	No-Kick	0.00
72.90	26.45	2453.65	62.39	257.65	1	Kick	No-Kick	-0.02
73.00	25.94	2442.26	62.38	258.95	1	Kick	No-Kick	-0.03
73.10	26.41	2432.23	62.29	260.88	1	Kick	No-Kick	-0.03
73.20	25.58	2431.85	61.82	262.11	1	Kick	No-Kick	-0.04
73.30	23.52	2425.42	61.72	262.51	1	Kick	No-Kick	-0.05
73.40	23.69	2421.46	61.81	262.92	1	Kick	No-Kick	-0.06
73.50	23.18	2411.74	61.44	266.79	1	Kick	No-Kick	-0.07
73.60	21.46	2410.62	61.11	272.85	1	Kick	No-Kick	-0.09
73.70	21.60	2404.22	60.45	276.65	1	Kick	No-Kick	-0.10

73.80	21.85	2372.37	59.92	278.29	1	Kick	No-Kick	-0.10
73.90	21.73	2337.62	59.48	278.96	1	Kick	No-Kick	-0.11
74.00	20.78	2303.08	58.88	281.21	1	Kick	No-Kick	-0.12
74.10	21.58	2269.40	58.37	284.74	1	Kick	No-Kick	-0.13
74.20	22.14	2229.72	57.87	286.77	1	Kick	No-Kick	-0.13
74.30	20.93	2206.59	57.34	287.59	1	Kick	No-Kick	-0.15
74.40	21.76	2220.24	56.77	288.08	1	Kick	No-Kick	-0.13
74.50	21.59	2240.80	56.05	288.89	1	Kick	No-Kick	-0.12
74.60	21.89	2261.39	55.22	289.94	1	Kick	No-Kick	-0.11
74.70	22.50	2274.54	54.55	290.64	1	Kick	No-Kick	-0.09
74.80	21.59	2269.90	53.65	291.03	1	Kick	No-Kick	-0.09
74.90	20.98	2255.52	52.68	291.15	1	Kick	No-Kick	-0.09
75.00	19.32	2270.12	51.90	291.08	1	Kick	No-Kick	-0.09
75.10	18.80	2322.91	51.08	290.90	1	Kick	No-Kick	-0.07
75.20	21.23	2370.64	49.89	290.72	1	Kick	No-Kick	-0.03
75.30	21.89	2399.07	48.52	290.67	1	Kick	Kick	0.00
75.40	21.65	2426.45	47.25	290.55	1	Kick	Kick	0.02
75.50	23.25	2444.50	46.19	289.63	1	Kick	Kick	0.05
75.60	21.52	2425.66	45.21	288.33	1	Kick	Kick	0.05
75.70	20.05	2381.08	44.31	287.47	1	Kick	Kick	0.04
75.80	20.47	2351.94	43.81	287.08	1	Kick	Kick	0.04
75.90	17.18	2348.77	43.34	286.87	1	Kick	Kick	0.02
76.00	17.34	2329.75	42.79	284.72	1	Kick	Kick	0.03